cGMP signalling via CNP-Npr2-cGKI, and its role in axonal branching during embryonic development

Inaugural-Dissertation
to obtain the academic degree
Doctor rerum naturalium (Dr. rer. nat.)
submitted to the Department of Biology, Chemistry and Pharmacy
of the Freie Universität Berlin

by

Agne Stonkute
from Vilnius

January, 2010

The present thesis was prepared between October 2005 and January 2010 at the Max-Delbrück-Centrum for Molecular Medicine, Department of Developmental Neurobiology, under the supervision of Prof. Dr. Fritz G.Rathjen

1. **Reviewer: Prof. Dr. Fritz G. Rathjen**
2. **Reviewer: Prof. Dr. Petra Knaus**

Disputation on 5.7.2010

CONTENTS

1 INTRODUCTION

The vertebrate nervous system is composed of a giant array of neural circuits, many of which are established during embryonic development when axon trajectories and functional connections between neurons and their targets are elaborated. Growing axons are guided to their targets by at least four mechanisms: contact attraction, chemoattraction, contact repulsion, and chemorepulsion (Tessier-Lavigne and Goodman, 1996). Many neuronal connections are made by collateral branches of axons rather then by primary axonal growth cones. The same forces that guide axonal growth cones, appear to regulate axonal branching (Dent et al., 2003;Tessier-Lavigne and Goodman, 1996). Axonal branching enables innervation of multiple targets by the same neuron, leading to the formation of a complex neural network. There are different modes of axonal branching: a) branching which is a result of the growth cone activity, i.e. growth cone splitting/bifurcation and delayed branching and b) interstitial branching which is independent of the growth cone (Acebes and Ferrus, 2000). Whereas guidance of a growth cone is a quite well studied phenomenon, axonal branching is less understood. Sensory axons in spinal cord which display both modes of branching is an excelent model to investigate molecular mechanisms underlying this phenomenon.

1.1 Navigation and branching of axons

Axons reach their targets through growth cone navigation and through establishment of axonal branches (Gallo and Letourneau, 1999;Huber et al., 2003;Kornack and Giger, 2005). These processes can be studied in regard to environmental cues, which give an impulse to axon to grow in a particular direction or to send branches to particular targets. Another aspect of this directed growth is understanding, how neuron translates signals received from environment into commands that result in an organized growth or branching in a specific direction.

Environmental cues that can steer growth cone include netrins and their receptors DCC/UNC5, Slits and their receptor Robo, semaphorins with their receptors plexins and neuropilins, ephrins and their receptors Eph tyrosine kinases (Brose and Tessier-Lavigne, 2000;Chisholm and Tessier-Lavigne, 1999;Huber et al., 2003;Imondi and Kaprielian, 2001). In addition to these groups of guidance cues, cell adhesion molecules can guide growth cone by modulating its adhesion to extracellular matrix and other cells (Castellani et al.,

2000;Chilton, 2006;Maness and Schachner, 2007;Shimada et al., 2008;Suter and Forscher, 1998). Neurotrophic growth factors induce localized directional changes in growth cones (Akiyama et al., 2009;Gallo et al., 1997;Song and Poo, 1999). Guidance cues have influence not only on growth direction but also on branching of axon. Vertebrate Slit2 promotes branching of DRG neurons in vitro (Brose and Tessier-Lavigne, 2000;Van and Flanagan, 1999;Wang et al., 1999) while SemaphorinA supresses it (Dent et al., 2004). Netrin promotes branching from the axon shaft, without involving growth cone while FGF-2 promotes branching by inducing growth cone arrest and enlargement which gives time for growth cone cytoskeleton reorganization (Dent et al., 2004). Not only a signal received from environment determines whether the axon will branch. The signal should be interpreted by the axon and the outcome of interpretation depends on the neuron type, e.g. NGF is necessary for collateral sprouting from pain sensory neurons (Acebes and Ferrus, 2000), but it does not affect branching of central trigeminal axons in brainstem (Ozdinler and Erzurumlu, 2001).

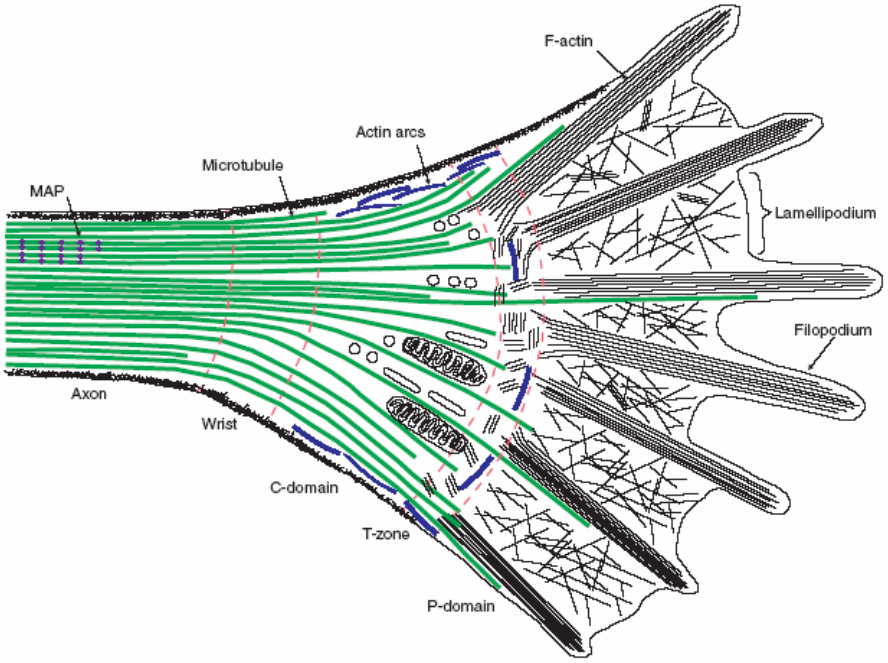

Fig.1.1: Schematic representation of growth cone cytoskeleton (Geraldo and Gordon-Weeks, 2009). Microtubules (in green) are organised into parallel bundles by microtubule-associated proteins (MAPS) in axon shaft but in central domain (C-domain) they become defasciculated and extend through the transition zone (T-zone) or even intrude into peripheral domain (P-domain). Most of microtubules are kept away from the P-domain by retrograde actin flow, and those few that intrude are aligned alongside bundles of actin filaments (F-actin). Actin filaments predominate in P-domain where they are organized into a branched dendritic network and form lamellipodia or into parallel bundles and form filopodia. In the T-zone actin is severed. Actin arcs (in blue), composed of F-actin and myosin II transport growing microtubules from the sides of the growth cone into the central domain and facilitates their bundling in the growth cone wrist.

Extension of growth cone, navigation, initiation of branches require coordinated and controlled assembly and dissasembly of the neuronal cytoskeleton (Kornack and Giger, 2005) The neuronal growth cone is organized into peripheral (the leading edge) and central (central area of growth cone) domains. Actin filaments predominate in peripheral domain whereas microtubules are abundant in central domain where they project from the axon shaft (Fig. 1.1). Microtubules are kept away from peripheral domain by a retrograde actin flow. Some highly dynamic microtubules, that rapidly assemble, intrude deep into peripheral domain. They use actin bundles as guides along which they grow towards the leading edge. When actin bundles are disrupted on one side of the growth cone, microtubules cannot penetrate into this area of peripheral domain anymore and axon ceases to grow in this direction which leads to axon turning (Kornack and Giger, 2005;Rodriguez et al., 2003;Zhou et al., 2002;Zhou and Cohan, 2004).

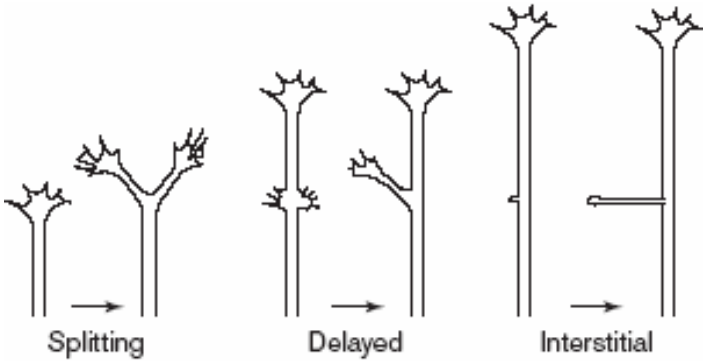

Fig.1.2: The modes of neural branching: bifurcation, delayed and interstitial (Acebes, 2000)**.** In the bifurcation mode an active growth cone divides into two smaller growth cones generating two branches. In the delayed mode, a branch develops from an unstable region of the cell membrane left behind by a previous growth cone. In the interstitial mode the branch emerges from an apparently stable membrane region, usually in an orthogonal direction.

Branching of axons involves rearrangement of cytoskeleton. When repulsive cue is applied in the middle of the growth cone surface, it disrupts the actin bundle structure or microtubule polymerization there. When actin bundles are lost in the middle of the peripheral domain of a growth cone microtubules in this area are lost as well and the same happens when microtubuli are lost. Attenuation of microtubule or F-actin dynamics also inhibits polymerization of the other cytoskeletal element (Dent and Kalil, 2001). Remaining actin bundles on both sides of the growth cone extend further and microtubules follow them. As a result of such growth in two directions, the growth cone splits and bifurcation of growth cone occurs (Zhou et al., 2002). Axon does not grow in a steady pace - its growth cone can pause,

enlarge while the cytoskeleton of the growth cone reorganizes. After the pause growth cone proceeds growing but it leaves filopodial and lammelipodial protrusions on the axon shaft, where new growth cone is formed and delayed (interstitial) branching appears (Acebes and Ferrus, 2000;Dent et al., 1999;Kalil et al., 2000;Szebenyi et al., 1998). Interstitial branching which is independent of growth cone develops all along axon shaft from an apparently stable membrane and not immediately behind the growth cone where filopodial remnants are visible; usually in an orthogonal orientation (Fig. 1.2) (Acebes and Ferrus, 2000;O'Leary and Terashima, 1988;Portera-Cailliau et al., 2005).

Not only cytoskeleton remodelling is important in growth cone navigation and axon branching. Local protein synthesis (Farrar et al., 2009;Lin and Holt, 2007;Van Horck and Holt, 2008;Wu et al., 2005), asymetric vesicle transport, membrane exocytosis (Kamiguchi and Lemmon, 2000;Tojima et al., 2007), substrate adhesion (Chilton, 2006) also play a role in directional axon growth and branching.

1.2 Cyclic GMP and its role in axonal guidance

Cyclic GMP (cGMP) is a cyclic nucleotide which serves as a second messenger in the cells and regulates variety of cellular processes including cellular growth and contractility, cardiovascular hoemostasis, inflamation, visual signal transduction, neuronal plasticity and learning (Feil and Kemp-Harper, 2006). It is produced from guanosine triphosphate (GTP) upon activation of guanylyl cyclases. Guanylyl cyclases that convert synthesis of cGMP from GTP can be either membrane bound particulate guanylyl cyclases or soluble guanylyl cyclases. Homodimer or homotetramer membrane bound guanylyl cyclases are activated upon binding of natriuretic peptides, guanylin/uroguanylin, toxins (thermostable enterotoxins) or guanylyl cyclase activating proteins, whereas heterodimers soluble guanylyl cyclases are activated by nitric oxide (NO) and NO donors, less efficiently by carbon monoxide (CO) (Feil and Kemp-Harper, 2006;Kobialka and Gorczyca, 2000;Koesling and Friebe, 1999;Lucas et al., 2000).

cGMP has several targets: cyclic nucleotide gated ion channels (CNG), phosphodiesterases and cGMP dependent kinases (cGK) (Fig. 1.3). The principal family of CNG channels regulates influx of Na^+ and Ca^{2+} into cells, they are important in phototransduction, in Na^+ reabsorbtion in kidney (Lucas et al., 2000). Phosphodiesterases activated by cyclic nucleotides hydrolize cyclic nucleotides. They can be stimulated by cGMP (e.g. PDE2), inhibited by cGMP (e.g. PDE3), inhibited by cAMP (e.g. PDE10) and hydrolyse either

cAMP (e.g. PDE4), or cGMP (e.g. PDE5) or both (e.g. PDE2). In this way cGMP elevating agents can change level of cAMP and vice versa (Feil and Kemp-Harper, 2006;Lucas et al., 2000;Omori and Kotera, 2007). cGMP dependent protein kinases represent the pricipal intracellular mediator of cGMP actions and will be discussed separately in the next chapter.

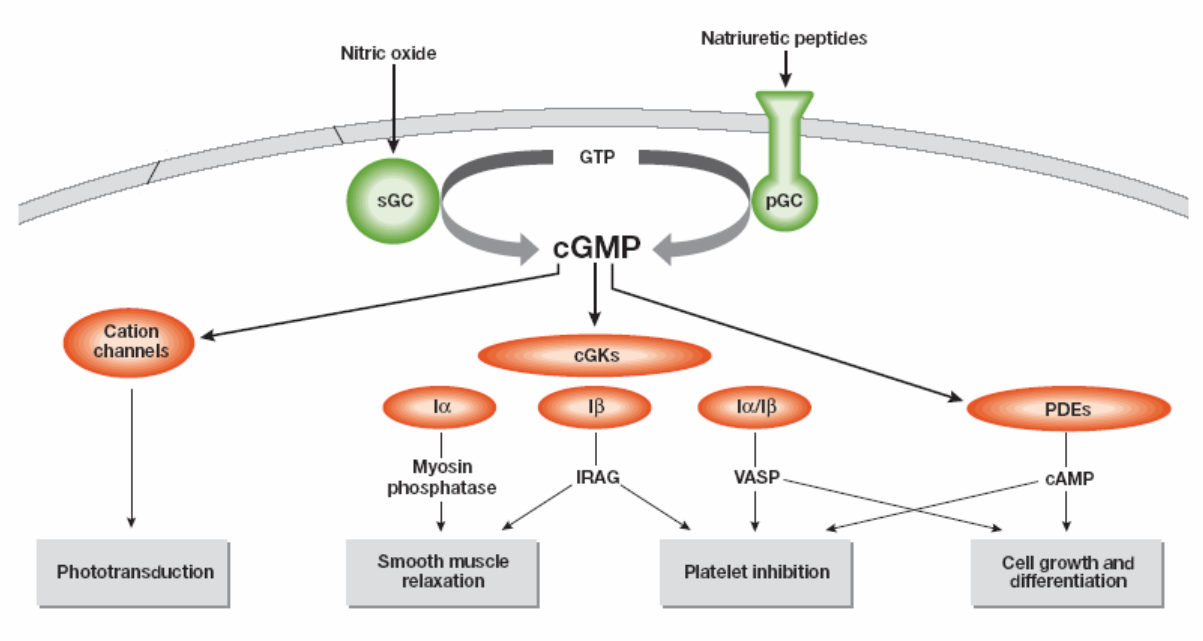

Fig.1.3: cGMP signalling (adapted from (Feil and Kemp-Harper, 2006)). Green coloured cGMP generators - soluble guanylyl cyclases (sGC) and particulate guanylyl cyclases (pGC) - produce cGMP which stimulates three main red coloured targets: cyclic nucleotide gated ion channels, cGMP dependent kinases (cGKs) and phosphodiesterases (PDEs). cGK has two genes: cGKI and cGKII. cGKI has two splice variants: cGKIα and cGKIβ. Some cellular functions of cGMP effectors (red) are indicated in grey boxes and above them - phosphorylation targets of cGKI underlying these cellular functions.

Cyclic nucleotides, including cGMP, received attention of scientists working in the field of axonal growth when Poo and colleagues demonstrated that these second messengers are capable of modulating the response of growth cones to guidance cues. They showed that increased cGMP signalling changed growth cone repulsion, induced by Sema III, into attraction, and decreased cGMP signal changed attraction, induced by neurotrophin-3 (NT-3), into repulsion. Change of growth cone response to guidance cues was shown to be mediated by cGMP dependent kinase (Song et al., 1998;Song and Poo, 1999).

1.3 cGMP dependent kinases

cGMP dependent protein kinases are serine/threonine kinases activated by cGMP. In mammals two genes *prkg1* and *prkg2* encode soluble cGKI and membrane-associated cGKII. cGKI protein has α and β isoforms that are splice variants and differ in the N-terminal dimerization domain. cGK has dimerization mediating domain and inhibitory region supressing kinase activity in the absence of cGMP at the N-terminus, regulatory domain where cGMP is bound and C-terminal catalytic domain which has kinase activity and binding sites for ATP and phosphorylation substrates (Fig. 1.4) (Domek-Lopacinska and Strosznajder, 2005;Feil et al., 2005a;Hofmann et al., 2000;Hofmann, 2005;Lohmann et al., 1997;Wang and Robinson, 1997).

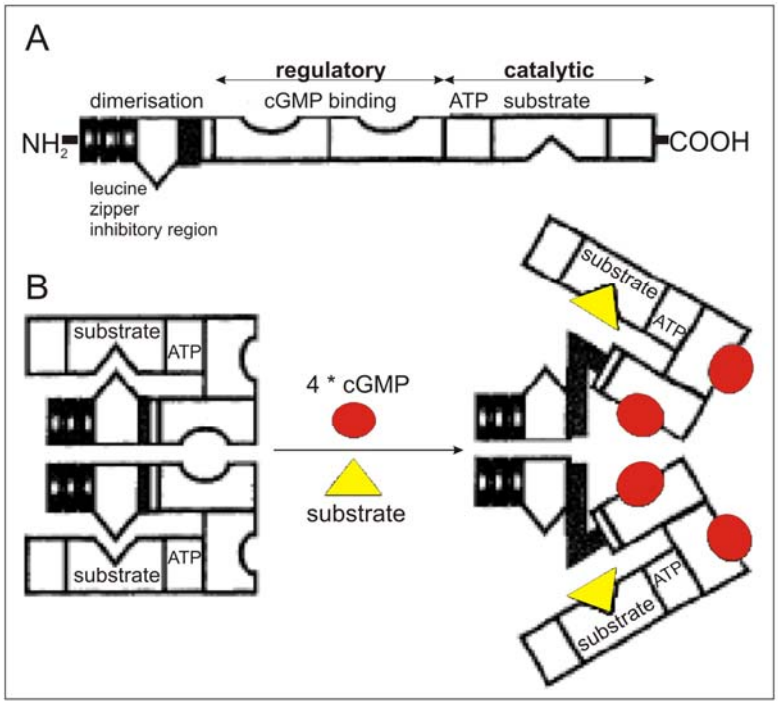

Fig.1.4: Schematic representation of cGK structure and its activation by cGMP (Feil et al., 2005a). (A) cGKI subunit consists of: an amino terminal domain mediating dimerization, regulatory domain containing two cGMP binding sites and catalytic domain with a kinase activity comprising binding sites for ATP and cGKI substrates. Amino terminal domain includes an inhibitory region supressing kinase activity in the absence of cGMP. (B) Binding of four cGMP molecules to a cGK homodimer induces a conformational change. As a result kinase activity is no longer inhibited by the amino terminal domain and can phosphorylate substrate proteins.

cGK mediates signal of cGMP by phosphorylating its downstream targets. Protein kinases often exhibit specificities for the specific amino acids around the phosphorylation sites. The motif around the phosphorylation site that is recognized by cGK is K/R K/R X S/T. cGKI is

closely related with cAMP dependent kinase (PKA) and some downstream targets are even shared by both kinases. However, cGK kinase prefers RKXS/T consensus motif while PKA prefers RRXS/T motif (Dostmann et al., 1999;Glass and Krebs, 1979;Schlossmann and Desch, 2009;Tegge et al., 1995).

Most of cGK substrates are phosphorylated by either cGKI or cGKII but not by both. cGKI isozymes often share their substrates, however, some substrates are regulated specifically by cGKIα (e.g. regulating myosin phosphatase targeting subunit) or by cGKIβ (e.g. IP_3RI-associated cGMP kinase substrate - IRAG). cGKI relaxes smooth muscle tone. Loss of cGKI results in severe vascular and intestinal dysfunctions (Pfeifer et al., 1998). cGKI also plays a role in generation of long term potentiation (LTP) in hippocampus and long term depression (LTD) in cerebellum, as well as in nociception. cGKII is involved in endochondrial oscifications. cGKII knock-out mice are dwarfs (Hofmann et al., 2006;Vaandrager et al., 2005).

One of the best known targets of cGKI is VASP. Phosphorylation of this protein makes a size shift from 46 to 50 kDa in SDS-PAGE under reducing conditions, and VASP is widely used as a marker of cGK phosphorylation. VASP phosphorylation in platellets is a well studied phenomenon. VASP is directly involved in accelerating actin filament elongation by delivering monomeric actin to the growing barbed end and by restricting actin filaments capping. Capping of barbed ends by capping proteins prevents continued polymerisation. Phosphorylation of VASP brings loss of its anticapping activity (Aszodi et al., 1999;Breitsprecher et al., 2008;Lebrand et al., 2004). Other known cGK target that plays a role in actin regulation is RhoA (Hofmann et al., 2009;Schlossmann and Desch, 2009).

cGKI can change intracellular Ca^{2+} level by phosphorylating and activating large-conductance Ca^{2+}-activated maxi-K^+ (BK_{Ca}) channels. Opening of BK_{Ca} channels results in hyperpolarisation of cell membrane and closing of voltage-dependent Ca^{2+} channels, thereby reducing Ca^{2+} influx. It can phosphorylate IP3 receptor I associated cGMP kinase substrate (IRAG), thereby inhibiting IP3 induced Ca^{2+} release from intracellular stores.

There are over ten cGKI substrates identified in vivo and a much larger number shown to be phosphorylated in vitro (Hofmann et al., 2009).

1.4 Spinal cord

The brain and spinal cord together make up the central nervous system. The spinal cord functions in the transmission of sensory and motor signals between the brain and the rest of

the body. In cross-section, neuronal axonal tracts forming white matter and nerve cell bodies forming the gray, butterfly shaped central region, are observed. The cell bodies of the primary sensory neurons that innervate receptors, sensing pressure, vibration, temperature, pain, muscle tension are located in the dorsal root ganglia (DRG). DRG are attached parallel on both sides of the spinal cord. DRG neurons give rise to axons that grow to spinal cord within dorsal roots. After reaching the dorsolateral wall of spinal cord, the dorsal root entry zone, axons bifurcate and grow rostrocaudally without penetrating the dorsal mantle layer (Fig. 1.5). The first axon reach the dorsal root entry zone (DREZ) and bifurcate at embryonic day 10.5 (E10.5) in the mouse. After 48 hours of "waiting period" collateral branches sprout from sensory axons and extend into the dorsal mantle layer (Ozaki and Snider, 1997).

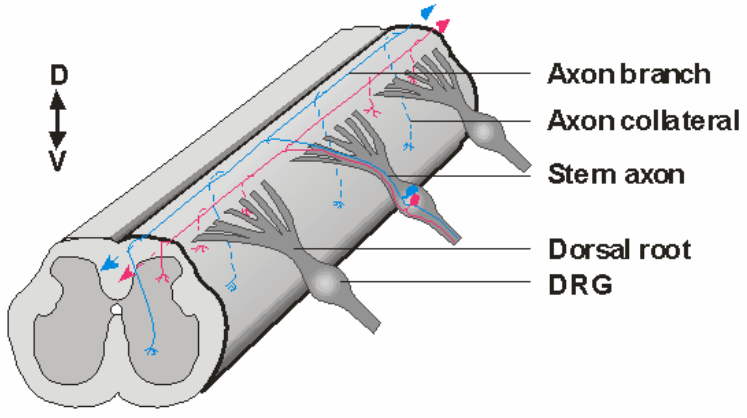

Fig.1.5: Schematic representation of spinal cord and dorsal root ganglia (Schmidt et al., 2007). Cell bodies of sensory neurons assembled at dorsal root ganglia (DRG) give rise to axons that reach the spinal cord via dorsal roots. Axons bifurcate upon arrival at the dorsal root entry zone and grow in rostrocaudal direction. Later collateral branches sprout from the stem axon and grow into the gray matter. Different classes of sensory axons have different growth trajectories in the gray matter: proprioceptive afferents (in blue) expressing trkC, which are involved in the muscle stretch reflex, grow directly ventrally whereas cutaneous afferents (in red), expressing trkA, enter the dorsal horn and stay here in superficial regions (Ozaki and Snider, 1997;Sharma and Frank, 1998).

There are several axon guidance molecules expressed in the spinal cord that are known to control sensory axon growth. Netrin-1 is expressed in the ventral spinal cord and also transiently, in E12.5 mouse embryos, in the dorsolateral spinal cord where it prevents DRG axon from entering mantle layer prematurely (Masuda et al., 2008;Watanabe et al., 2006). Sema 3A contributes to regulation of developing sensory projections. It is expressed during early developmental stages in the chick spinal cord but its expression stops at the dorsal horn

when collateral branches of sensory axons penetrate the mantle layer (Fu, 2000;Shepherd, 1997). At the early developmental stages all sensory axons at the spinal cord are repelled by Sema 3A (Fu et al., 2000;Puschel et al., 1996). However, sensory trajectories towards the spinal cord are not affected in the Sema 3A knock-out mice (Masuda et al., 2007) suggesting that Sema 3A is not crucial in sensory axon guidance. Slit1 and Slit2 are expressed in the dorsal spinal cord at the time when sensory axons reach the spinal cord, whereas, Robo1 and Robo2, receptors for Slit, are expressed in the DRG. In vitro it was shown that Slit2 stimulates elongation and branching of sensory axons (Brose and Tessier-Lavigne, 2000;Ma and Tessier-Lavigne, 2007;Nguyen Ba-Charvet et al., 2001;Nguyen-Ba-Charvet et al., 2001;Wang et al., 1999). Finally, three neurotrophins: nerve growth factor (NGF), brain-derived neurotrophic factor (BDNF) and neurotrophin-3 (NT-3) are chemoattractants to DRG axons (Masuda et al., 2007).

1.5 cGMP signalling in spinal cord

The group of Fritz Rathjen found that cGMP signal mediated by cGKI is required for sensory axon bifurcation at the spinal cord. Investigation of DiI stained whole mounts and anti-trkA stained transverse sections of the spinal cord revealed defect of the cGKI knock-out sensory axon growth suggesting that bifurcation of sensory axons is impaired. Anti-trkA staining in transverse spinal cord sections of cGKI mutant mice is decreased compared to normal mice, showing that cGKI knock-out mice have less trkA-positive collateral branches due to the reduced axon number available for the production of collaterals from the stem axon within the dorsal funiculus. This anatomical feature correlates with finding that functional connectivity of sensory afferents in mice is reduced (Schmidt et al., 2002).

Susanne Schäffer from the same group identified VASP as a phosphorylation target of cGKI in sensory neurons. However, pathfinding of DRG axons was not disturbed in VASP knock-out mouse, suggesting that VASP is not involved in bifurcation error found in cGKI knock-out mouse (Schäffer, 2006).

Katharina Seiferth, a member of Fritz Rathjen's group, showed that expression of PDE2A correlates with expression of cGKI and expression of cGMP producing Npr2 receptor in spinal cord. PDE2A is activated by cGMP and hydrolizes both cGMP and cAMP. PDE2A is observed in cell bodies of DRG neurons and their axons. This suggests that PDE2A might play a role in bifurcation of sensory axons as a part of cGMP signalling pathway (Seiferth, 2008).

1.6 The aims of this study

The purpose of this study was to extend the knowledge about cGMP signalling cascade regulating sensory axon bifurcation, first of all by detailed analysis of the bifurcation error which was detected in the previous study but was not unequivocally proved (Schmidt et al., 2002). This goal required improvement of the DiI labelling technique enabling labelling of single sensory axons. Improved DiI labelling technique allowed to set further aims:

- to study sensory axon branching at the DREZ in mice mutant for the components of cGMP signalling cascade, including cGKI, Npr2, CNP, using the improved DiI tracing;
- to analyse the formation of collaterals of sensory axons within the spinal cord by DiI labelling;
- to search for bifurcation errors outside the spinal cord, first of all by analysing central branch of trigeminal sensory axon using DiI tracing,
- to study downstream phosphorylation targets of cGKI by DiI tracing and biochemical methods. The latter aim could be divided into two smaller ones:
    - to study known/putative downstream targets of cGKI (VASP, Mena, myosin IIB, GSK3β, RhoA) regarding their role in sensory axon bifurcation;
    - to identify novel targets of cGKI in DRG neurons.

2 MATERIALS AND METHODS

2.1 Materials

2.1.1 Chemical reagents and enzymes

Component	Producer
Acetic acid	Sigma Aldrich, Deisenhofen
Acrylamide	Bio-Rad, München
Agarose	Invitrogen, Karlsruhe
Aliuminium hydroxide ($Al(OH)_3$)	Sigma Aldrich, Deisenhofen
Ammonium persulfate (APS)	GE Healthcare, München
Ampholytes	Bio-Rad, München
5-bromo-4-chloro-3-indolyl phosphate para-toluidine salt (BCIP)	Carl Roth, Karlsruhe
Bovine serum albumin (BSA) fraction V	Biomol, Hamburg
Calyculin A	Enzo Life Sciences, Lörrach (formerly Alexis)
Coomassie Brilliant Blue R250	Bio-Rad, München
Dithiothreitol (DTT)	Sigma Aldrich, Deisenhofen
DMEM	Invitrogen, Karlsruhe
dNTP-Mix	Invitrogen, Karlsruhe
Ethanol	Sigma Aldrich, Deisenhofen
Ethidium bromide	Sigma Aldrich, Deisenhofen
Ethylene diamine tetraacetic acid (EDTA)	Merc, Darmstadt
Glycine	Merck, Darmstadt
Isopropanol	Sigma Aldrich, Deisenhofen
Hydrogen peroxyde	Sigma Aldrich, Deisenhofen
Lambda protein phosphatase	New England Biolabs, Frankfurt am Main
Magnesium chloride	Sigma Aldrich, Deisenhofen
β-mercaptoethanol	Sigma Aldrich, Deisenhofen
Methanol	Sigma Aldrich, Deisenhofen

$MnCl_2$	New England Biolabs, Frankfurt am Main
Mowiol	Carl Roth, Karlsruhe
Nitro blue tetrazolium (NBT)	Carl Roth, Karlsruhe
O.C.T. Tissue Tec	Sakura Finetec, USA
Okadaic acid	Enzo Life Sciences, Lörrach (formerly Alexis)
Paraformaldehyde	Sigma Aldrich, Deisenhofen
PBS (Dulbecco), calcium and magnesium free	Biochrom, Hamburg
8-pCPT-cGMP	Biolog, Bremen
Protein A-sepharose, CL 4B	GE Healthcare Life Sciences, München (formerly Amersham)
Protein phosphatase buffer	New England Biolabs, Frankfurt am Main
Restriction enzyme AflIII	New England Biolabs, Frankfurt am Main
Restriction enzyme AvaII (Eco47I)	Fermentas, St. Leon-Rot
Sucrose	Sigma Aldrich, Deisenhofen
Silver nitrate, $AgNO_3$	Merck, Darmstadt
Sodium chloride (NaCl)	Carl Roth, Karlsruhe
Sodium dodecyl sulfate (SDS)	BioRad, München
Taq DNA Polymerase, recombinant	Invitrogen, Karlsruhe
N',N'-tetramethylendiamine (TEMED)	GE Healthcare, München
Tris(hydroxymethyl)-aminomethan (Tris)	Merck, Darmstadt
Triton X-100	Sigma Aldrich, Deisenhofen
Tween 20	Sigma Aldrich, Deisenhofen
Urea	Sigma Aldrich, Deisenhofen
Molecular mass standards for SDS-PAGE	BioRad, München

All the chemicals that were used but are not listed above, were bought from Merck, Roth or Sigma.

2.1.2 Buffers and solutions

• **5 x Laemmli buffer**	60mM Tris/HCl (pH 6.8); 10% SDS; 10% β-mercaptoethanol; 50% glycerine; 1.5% bromophenol blue
• **Antibody solution for immunohistochemistry**	5% goat serum in wash buffer for immunohistochemistry
• **AP (alkaline phosphatase) buffer**	100mM Tris-HCl pH 9.7; 5mM $MgCl_2$; 0.01mM $ZnCl_2$
• **AP (alkaline phosphatase) developer**	0.165 mg/ml NBT; 0.825 mg/ml BCIP in AP buffer
• **Blocking buffer for Western blot**	4 % BSA (w/v) in wash buffer for Western blot
• **Blocking buffer for immunohistochemistry**	10 % goat serum in wash buffer for immunohistochemistry
• **Coomassie destain**	500 ml methanol; 100 ml acetic acid; 500ml water
• **Coomassie stain**	500 ml methanol; 100 ml acetic acid; 500 ml water; 2.5 g coomassie briliant blue R250
• **Destain solution (for Pro-Q Diamond stain)**	50 ml 1M sodium acetate ($C_2H_3NaO_2$), pH 4; 200 ml acetonitrile; water up to 1 l.
• **Elution buffer for phosphoprotein enrichment**	8M uera; 100mM potassium pyrophosphate, pH 9 (with phosphoric acid)
• **Equilibration buffer I for 2D gel electrophoresis**	0.375 M Tris HCl pH 8.8; 6 M urea; 20% (v/v) glycerol; 2% (w/v) SDS. Immediately before usage 35mg/10ml DTT are added.
• **Equilibration buffer II for 2D gel electrophoresis**	0.375 M Tris HCl pH 8.8; 6 M urea; 20% (v/v) glycerol; 2% (w/v) SDS. Immediately before usage 250mg/10ml iodocetamide and some grains of bromophenol blue are added.

• **Fixation solution (for silver staining)**	50% (v/v) methanol, 12% (w/v) trichloroacetic acid (TCA), 2% (w/v) $CuCl_2$
• **Incubation buffer for phosphoprotein enrichment**	8M urea; 30mM MES; 0.2M potassium glutamate; 0.2M sodium aspartate; 0.5%CHAPS; pH 6.0 (with HCl)
• **Lysis buffer for 2D gel electrophoresis**	8 M urea; 2M thiourea; 4 % (w/v) CHAPS; 6.5mM DTT; 0.5% ampholytes. Immediately before usage 8 mM PMSF is added.
• **Mowiol (10% solution)**	2.4 g Mowiol (Calbiochem); 15.6 ml water; 2.4 ml 1 M Tris pH 8.5 combined and left overnight; next day 6 ml glycerine added.
• **PFA (paraformaldehyde) solution, 4%**	4% PFA (w/v) in 1x PBS. PFA is first dissolved in water and heated under constant stirring to 60°C. 10 N NaOH is added until solution becomes clear. PBS is added; pH adjusted to 7.2.
• **Protease inhibitor coctail**	5 mM pepstatin A; 5 mM leupeptin; 20 u/µl aprotonin; 100 mM PMSF
• **Ponceau stain**	2% (w/v) Ponceau S; 3% (v/v) perchloretic acid
• **Rehydration buffer for 2D gel electrophoresis**	8M urea; 2M thiourea; 1% (w/v) CHAPS. Immediately before usage 5.2µl/ml ampholytes; 12µl/ml destreak and several grains of bromophenol blue are added.
• **SDS-PAGE electrophoresis buffer**	25 mM Tris; 192 mM glycine; 0.1% (w/v) SDS
• **Solution W**	10% (v/v) ethanol; 5% (v/v) acetic acid
• **TAE Buffer (50X)**	40 mM Tris base; 20 mM glacial acetic acid; 1 mM EDTA (pH 8.0)
• **Transfer buffer**	20% (v/v) methanol in SDS-PAGE electrophoresis buffer without SDS
• **Wash solution (PBS/Tween 20) for**	0.5 % (v/v) Tween 20 in 1xPBS

Western blot

- **Wash solution (PBS/Triton X-100) for immunohistochemistry** 0.25% Triton X-100 in 1xPBS

2.1.3 Special reagents and kits

Kit/reagent	Producer
DAB kit	Vector laboratories, Burlingame, CA.USA
High Pure Plasmid Isolation Kit for small-scale (mini) preparations	Roche, Mannheim
Pierce ECL Western blotting substrate	Pierce, Rockford (USA)
Readystrip, IPG strips; 7 cm, 17 cm; pH 3-10, 4.7-5.9	BioRad, München

2.1.4 Cell culture media

Medium	Producer
Nutrient mixture F-12 + GlutaMAX	Gibco, Eggenstein

2.1.5 Additional components of cell culture media

Component	Producer	Concentration
Fetal calf serum (FCS)	Gibco, Eggenstein Biochrom, Hamburg	15 % (v/v)
HAT media supplement	Invitrogen, Karlsruhe	2 % (v/v)
Penicillin/streptomycin	Gibco, Eggenstein	100 U/µl

2.1.6 Primers/Oligonucleotides for genotyping

Gene	Label of primer	Primer sequence (Direction 5'-3')	Product size, bp
CNP	GT_lbab_UP2 GT_lbab_LP	AGCTGGTGGCAATCAGAAAA CTCTTGGGTGCAGAGCTAGG	318

Npr2	GC_B1	TTCACAGCGCTGTCAGCTGAG	348
	GC_B2	ACTTAGGGAGCGCTGACTGTGG	
cGKI	RF 125	GTCAAGTGACCACTATG	338 (KO)
	RF53	CCTGGCTGTGATTTCACTCCA	284 (WT)
	RF118	AAATTATAACTTGTCAAATTCTTG	250
VASP	GIK 273	CGAATAGCCTCTCCACCCAAGCGGCCGGAGAAC	700
	GIK 274	GGCCAGCAGAACAGTATTGGAGAACATCCAGG	
	GIK 269	TTAGCTTGGTTTGGGGACTGAACCAGCCTCCTTTC	450
	GIK 270	CAGCCACTCCCTGGTACTTCCTTACCTTGCTCAC	
Mena	Me_F3	TGGGCAGAAAGATTCAAGACC	
	Me_in2_R2	CCAGTTTCAATGCCCATTCCTT	1123
	pGT0Lxf_R2	CGGATCTCAAACTCTCCTCC	824
GFP, YFP	oIMR0872	AAGTTCATCTGCACCACC	173
	oIMR1416	TCCTTGAAGAAGATGGTGCG	
Interleukin	oIMR0042	CTAGGCCACAGAATTGAAAGATCT	324
	oIMR0043	GTAGGTGGAAATTCTAGCATCATCC	

2.1.7 Antibodies

2.1.7.1 Primary antibodies

Antibody	**Concentration** (WB) – Western blot (IH) – immunohistochemistry (WH) – „whole mount“	**Company/donating lab**
Rabbit anti VASP	1:5 000 (WB)	Frank B.Gertler
Rabbit anti Mena Mouse anti Mena	1:5 000 (WB) 1:10 (WB)	Frank B.Gertler
Mouse anti 2H3 (165kDa neurofilament-protein)	0.1µg/ml (WH)	Dev. Studies Hybridoma Bank, Iowa
Mouse anti γ-tubulin	1:10 000 (WB)	Fa. Sigma
Mouse anti RhoA (clone 26C4)	1:200 (WB)	Santa Cruz
Rabbit anti phospho-RhoA	1:1000 (WB)	Calbiochem

(ST1035)		
Rabbit anti RKVpS (against peptide sequence CGGLRKVpSK)	1:2000 (WB)	GenScript
Mouse anti GSK3β (clone 4G-1E)	1:1000 (WB) 1:25 (IH)	Upstate
Rabbit anti phospho-GSK-3β (Ser9) (clone 5B3)	1:1000 (WB) 1:100 (IH)	Cell signalling
Rabbit anti Phospho-PKA Substrate (RRXS/T) (100G7E)	1 :5000 (WB)	Cell signalling
Rabbit anti phospho-threonine	1:1000 (WB)	Cell signalling
Mouse anti phospho-threonine (clone PTR8)	1:50 (WB)	Sigma
Mouse anti phospho-serine	1:2500 (WB)	BD Biosciences
Rabbit anti trkA	1:1000 (IH)	Fa. Chemicon
Rabbit anti L1	2.5µg/ml (IH)	AG Rathjen
Rabbit anti IP3R type I	1:1000 (WB)	Calbiochem

2.1.7.2 Secondary antibodies

Antibody	Concentration	Company/donating lab
Goat anti Rabbit –cy3	1:400 (IH)	Dianova
Goat anti Rabbit -HRP	1 :25000 (WB) 1:400 (WH)	Dianova
Goat anti Mouse -HRP	1:25000 (WB)	Dianova
Goat anti Rabbit -AP	1:10000 (WB)	Dianova
Goat anti Mouse -AP	1:10000 (WB)	Dianova

2.1.8 Cell lines

- F11 cell line, a fusion product of cells of mouse neuroblastoma cell line N18TG-2 and embryonic rat dorsal-root ganglion (DRG) neurons

2.1.9 Experimental animals

- C57Bl6 (bred at MDC)
- cGKI knock-out mice (received from Franz Hofmann; München (Wegener et al., 2002))
- VASP knock-out mice (received from Reinhard Fässler; München (Aszodi et al., 1999))
- Mena/VASP double knock-out mice (received from Thomas Renee; (Menzies et al., 2004))
- Thy1-YFP-H mice (received from Joshua R. Sanes; (Feng et al., 2000))
- Thy-GFP-M (received from Joshua R. Sanes; (Feng et al., 2000))
- cn/cn mice (obtained from Jackson ImmunoResearch Laboratories)
- lbab mice (obtained from Jackson ImmunoResearch Laboratories)
- GSK3 knock-in mice (Ser21 in GSK3-α and Ser9 in GSK3-β are changed to Ala) (fixed E12 embryos used for analyses were received from Dario R. Alessi and Kei Sakamoto (McManus, 2005)

2.1.10 Equipment

Type of equipment	**Label**	**Producer**
Cell culture hood	Kelvitron	Heraeus, Hanau
Centrifuge	Centrifuge 5415C	Eppendorf, Hamburg
Centrifuge	Biofuge 13	Heraeus, Hanau
Centrifuge	RC M150GX	Sorvall, Bad Homburg
Cryostat	Jung CM 3000	Leica, Wetzlar
Magnetic stirrer	Ilkamag Reo	WTW, Weilheim
Molecular imager system	ChemiDoc	BioRad, München
Micropipette Puller	Flaming/Brown, model P-97	Sutter Instrument Co.
Microscope	Telaval 31	Zeiss, Jena
Microscope	Axiovert 135	Zeiss, Jena
Microscope	Axiovert 200M	Zeiss, Jena
pH-meter	pH525	WTW, Weilheim

Photodevelopment machine	Curix 60	Agfa, Mortsel, Belgium
Photometer	Biophotometer 6131	Eppendorf, Hamburg
SDS-PAGE cell	Protean II	BioRad, München
SDS-PAGE cell	Protean II xi	BioRad, München
Thermocycler	PCR-Mastercycler gradient	Eppendorf, Hamburg
Thermomixer		Eppendorf, Hamburg
Universal image system	Universal Hood II	BioRad, München
Vortex mixer	CERTOMAT MV	WTW, Weilheim
Western Blot cell	Protean II	BioRad, München
Western Blot cell	Criterion	BioRad, München

2.2 Methods

2.2.1 DiI labelling

DiI belongs to fluorescent lipophilic carbocyanine dyes. It labels both fixed and living cells. DiI becomes incorporated into the plasma membranes of neurons exposed to it and then diffuses within the plane of the membrane. There is no evidence of passive diffusion from labelled neurons to other neurons or glia (Godement et al., 1987;Vercelli et al., 2000).

Spinal cords with attached DRG were isolated from E12-E14 aged mice embryos and left in 4% paraformaldehyde in PBS overnight. On the next day DRG labelling was carried out. Needle pulled from borosilicate glass capillary was dipped in 200 µM DiI solution in ethanol. Ethanol evaporated leaving tiny DiI crystals on the glass needle. DRG were touched with the tip of the needle, thereby leaving some of DiI crystals on DRG cell bodies. Neurons that incorporated the dye become labelled and can be observed after one day.

The needles are made using a micropipet puller. We use Kwik-Fil borosilicate glass capillaries 1B150F-4 (World precision Instruments) with the following program to create a fine tip: heat = 640, pull = 0, velocity = 44, time = 136.

For N.trigeminus labelling heads of E12-E14 mice were fixed in 4% paraformaldehyde in PBS for one week. After fixation heads were sagittally sectioned on vibratome into 140 µm thick slices. The slices were examined under the light microscope to locate trigeminal ganglion. Observed trigeminal ganglia were labelled with DiI by touching the ganglion with a glass needle tip coated with tiny DiI crystals. Labelled slices were mounted in Mowiol solution between two cover slips and examined under fluorescence microscope next day.

2.2.2 Histological methods

2.2.2.1 Preparation of tissue sections

Spinal cords dissected from E12-E14 embryos were fixed at 4°C in freshly prepared 4% paraformaldehyde with 0.32 M sucrose on a shaker for 4 hours and afterwards left overnight under the same conditions in 30 % sucrose in PBS. On the next day spinal cords were embedded in Tissue Tek (Sakura) and immediately frozen on dry ice. Frozen spinal cords were stored at -80°C until they were cut on cryostat in 16 µm thick transverse sections. Spinal cord slices were collected on microscope slides coated with gelatine and stored at -20°C.

2.2.2.2 Tissue sections of stimulated and unstimulated spinal cords

Heads of E12 embryos were cut providing better accessibility to the spinal cord. Spinal cords were exposed from the dorsal side by stripping the thin dermis layer. Embryos with exposed spinal cords were left for 5 min in 37°C warm 1 mM 8-pCPTcGMP solution with phosphatase inhibitors calyculin A (1 µM) and okadaic acid (1 µM). Control embryos with stripped spinal cord were incubated in PBS with phosphatase inhibitors. After incubation embryos were immediately fixed at 4°C in freshly prepared 4 % paraformaldehyde with 0.32 M sucrose. Further steps are described in section 2.2.2.1 “Preparation of tissue sections”.

2.2.2.3 Immunohistochemistry of tissue sections

Spinal cord sections were thawed for 1 h at room temperature. They were blocked with blocking solution for 1 hour followed by 5 wash steps à 5 min. First antibody in antibody solution was added and sections incubated overnight at 4°C. Next day slices were washed 5 times à 5 min and second antibody in antibody solution was added. Slices were incubated in darkness at room temperature for 2 hours. Then slices were washed 3 times à 3 min and mounted in Mowiol on microscope slide covered with cover slip. Immunostained slices of spinal cord were examined under fluorescence microscope Axiovert 135 equipped with Neofluar/Acroplan objectives, a charged-coupled device camera (Axiocam HRC), and acquisition software (Axiovision 3.1).

2.2.2.4 Whole-mount staining of embryos

Whole-mount staining of Mena/VASP double knock-out embryos with anti-neurofilament was performed in order to confirm their phenotype described by Menzies et al. (Menzies et al., 2004). E10.5 embryos were dissected from uterus and left rocking in 4% paraformaldehyde solution in PBS at 4^{o}C overnight. Next day embryos were immersed in Dent's fixative and left rocking at 4^{o}C overnight. Afterwards Dent's fixative was replaced by fresh Dent's fixative with 10% H_2O_2 and embryos left rocking at room temperature for 5-6 hours until they become bleached. At this point it is possible to store embryos in methanol at -20^{o}C for longer period. After the bleaching step embryos were blocked overnight at 4^{o}C in blocking solution for Western blots containing 5% (v/v) DMSO. Incubation with neurofilament 2H3 (Devlp. Studies Hybridoma Bank; Iowa) in blocking solution with 5% (v/v) DMSO was carried out at 4^{o}C overnight. Next day 5 wash steps with PBS à 1 hour and incubation with the secondary antibody RbαM HRP in blocking solution with 5% (v/v) DMSO overnight at 4^{o}C followed. Embryos were washed 5 times à 1 hour in PBS. Neurofilament staining was developed using DAB reaction with DAB kit according to manufacturer's instructions. Stained embryos were immersed into benzylalcohol/benzylbenzoat mix (1:3) and stored in eppendorf tubes. It should be taken into account that benzylalcohol/benzylbenzoat mix is an organic solvent and most plastics will melt upon a contact with it, therefore only organic solvent stable eppendorf tubes and dishes should be used.

2.2.3 Biochemical methods

2.2.3.1 Preparation of protein lysate from unstimulated and 8-pCPTcGMP stimulated DRG

Embryonic mouse DRG were isolated from E12-E13 embryos. In average 40 DRG were obtained from one embryo and kept on ice in PBS until further processing. Half of DRG (20 DRG from one embryo) were treated as unstimulated control, another half was stimulated with cGMP analogue 8-pCPTcGMP. After centrifugation (5 min 3000 rpm on microfuge) PBS was removed, 50 µl fresh PBS or 50 µl PBS with 1 mM 8-pCPTcGMP were added to 20 DRG. DRG were left for 5 min at 37^{o}C for stimulation. The lysate was prepared by

homogenisation with Eppendorf-homogeniser in PBS; followed by addition of 12.5 µl 5 x Laemmli buffer (50 mM Tris -HCl pH 6.8; 12.5 % glycerol; 1 % SDS; 0.01 % bromophenol blue) and boiling for 5 min. Lysates were stored at -20°C. When DRG were isolated from mutant mouse strain, tail or leg from each embryo was taken for further genotyping.

2.2.3.2 Preparation of protein lysate from unstimulated and 8-pCPTcGMP stimulated F11 cells

F11 cells were serum-starved over night. The next day cells were collected. They detach easily from a cell culture plate after using shear stress by pipeting cell culture medium up and down in the plate. F11 cells together with cell culture medium collected from one 10 ml cell culture plate were divided between two Falcon tubes and centrifuged for 5 min at 800 rpm in Heraeus floor centrifuge. After removal of supernatant 500 µl or 450 µl previously removed cell culture medium was taken back to cell pellet. Cells were homogenized in cell culture medium by passing them several times through syringe and needle (0.40 x 20 mm). After homogenization 50 µl 10 mM 8-pCPTcGMP was added to the sample with volume of 450 µl. Cells were left for 5 min at 37°C for stimulation. Afterwards 125 µl 5 x Laemmli buffer was added and lysate was boiled for 5 min at 95 °C. Lysates were stored at minus 20°C.

Homogenisation of F11 cells was performed before stimulation with 8-pCPTcGMP because it was noticed that the 51 kDa band becomes completely dephosphorylated under these conditions. In case F11 cell lysates were not prepared immediately after stimulation with 8-pCPTcGMP; homogenisation was carried out following stimulation of F11 cells. After the stimulation step F11 cells were again centrifuged (5 min 800 rpm in Heraeus floor centrifuge), supernatant containing 8-pCPTcGMP removed and fresh PBS added. Then further processing of cells proceeded.

2.2.3.3 Subcellular fractionation of DRG and F11 cell lysates

About 300 DRG were isolated from 10 embryos. They were divided into two parts and kept in PBS. One part was stimulated with 10 mM 8-pCPTcGMP at 37°C for 5 min, another part served as an unstimulated control. Both samples were then centrifuged (in an Eppendorf-centrifuge at 3000 rpm for 3 min) and after removal of supernatant pellets were resuspended in 300 µl PBS. After homogenization (syringes with needle ø 0.4 mm, Braun) lysates were centrifuged at 1000 g for 5 min. Supernatant (defined as postnuclear supernatant) was

transferred to another eppendorf tube and centrifuged at 100,000 g for 15 min in ultracentrifuge. Resulting supernatant was defined as cytoplasmic fraction and pellet – as membrane fraction. After each step sample aliquots were taken for further analysis. They were prepared for SDS-PAGE analysis by boiling at 95^{o}C for 5 min with addition of 5xLaemmli buffer.

2.2.3.4 Dephosphorylation with lambda protein-phosphatase

2.2.3.4.1 Dephosphorylation of cell lysates (prior to electrophoresis)

Protein phosphatase buffer, $MnCl_2$ (final concentration 2mM and protease inhibitor cocktail were added to cell lysate. After addition of 1µl (=400 units) of lambda protein phosphatase to 50µl of lysate it was incubated at 30°C for 20 min. The reaction was stopped by adding 5x Laemmli buffer and boiling lysate for 5 min at 95°C.

2.2.3.4.2 Dephosphorylation on the nitrocellulose membrane (after SDS-PAGE and blot)

Blotted nitrocellulose membrane was blocked in blocking buffer for Western blot for 1 hour with constant agitation and incubated in blocking buffer containing 2 mM $MnCl_2$ and 400 U/ml of lambda protein phosphatase overnight at 4°C. The membrane was washed in washing buffer for Western blot for 3-4 min, rinsed in 4-5 changes of water. Then the Western blotting assay was continued as usually.

2.2.3.5 SDS-PAGE

To separate proteins by size sodium dodecyl sulfate polyacrylamide gel electrophoresis (SDS-PAGE) was performed in a vertical gel chamber "Mini Protean II" (BioRad). This method is based on a discontinous gel system: a stacking gel and a separating gel (Laemmli, 1970). Separating gel containing different percentages of acrylamide according to the molecular mass of protein of interest was made using solutions for polyacrylamide gel, listed below. The separating gel solution was applied into the gel cassette up to ± 6.5 cm, and the last ± 2.5 cm of the cassette was filled with isopropanol. The gel was polymerized for at least 30 minutes, and the isopropanol was carefully removed. The stacking gel solution was directly poured into the gel cassette, and the gel comb was placed to form the slots. The stacking gel was polymerized for at least 60 minutes.

Table 2.1: Preparation of separating and stacking gels

Contents	Separating gel 7.5 %	Separating gel 10 %	Stacking gel
30 % acrylamide/bisacrylamide	2.5 ml	3.3 ml	0.65 ml
1M Tris; pH 8.8	3.75 ml	3.75 ml	-
1M Tris; pH 6.8	-	-	0.65 ml
H_2O	3.6 ml	2.8 ml	3.7 ml
10 % SDS	100 µl	100 µl	50 µl
10 % APS	50 µl	50 µl	25 µl
TEMED	10 µl	10 µl	10 µl

Electrophoresis was carried out in Tris-glycine electrophoresis buffer. The electrophoresis was divided in two steps. During the first step, proteins were run in the stacking gel for 10 min at 100 V. During the second step, proteins were separated by size running through the pores of the separating gel at 200 V. SDS-PAGE standards (BioRad) were used to assess apparent molecular masses of proteins.

2.2.3.6 Western blot

Then proteins separated on the polyacrylamide gel were transferred with "Mini-Transblot" rig (BioRad) in transfer buffer on a nitrocellulose membrane (at 100 V for 1 h, 4°C). After transfer, the membrane was immersed for 5 min in Ponceau stain, washed with distilled water and scanned. Bands of SDS-PAGE standard were marked with a pencil.

Afterwards, nitrocellulose membrane was immersed in blocking buffer for 30 min at room temperature and incubated with primary antibody diluted in blocking buffer overnight at 4°C. After three washings for 10 min, membrane was incubated with secondary antibody, either coupled to HRP (1:25000 in washing buffer) or to AP (1:10000 in washing buffer) for 1 h at room temperature. Then the membrane was washed five times for 5 min in washing buffer and once for 10 min either in PBS or in AP-buffer. In case of antibodies coupled to HRP; chemiluminescence signal was produced by the "SuperSignal West Dura Extended Duration Substrate" (Pierce) according to Pierce's instructions and developed either on "Lumi-Film Chemiluminescent Detection Film" (Roche) with a photodevelopment-machine Curix 60

(Agfa) or image of the signal was obtained in a BioRad Universal Hood II equipped with a ChemiDoc documentation system. In case of antibodies coupled to AP the membrane was developed in AP-buffer with 165 µg/ml NBT-solution and 82.5 µg/ml BCIP-solution.
Intensity of the bands in Western blots was assessed using software programme ImageJ.

2.2.3.7 Coomassie staining

Coomassie Blue staining is based on the binding of the dye Coomassie Brilliant Blue R250, which binds nonspecifically to virtually all proteins. Although Coomassie Blue staining is less sensitive than silver staining, it is widely used due to its convenience.
Gel was immersed into Coomassie staining solution immediately after SDS-PAGE. It was left there shaking for 1 hour. Afterwards followed destaining with destain solution as long, as sharp blue bands of proteins became visible.

2.2.3.8 Silver staining

In silver staining protein detection depends on the binding of silver ions to glutamin, asparagine and cysteine amino acid chains of proteins, followed by reduction to free metallic silver. The protein bands are visualized as spots where the reduction occurs.
Immediately after SDS-PAGE, gel was fixed in fixation solution for 20 min, followed by washing in solution W for 10 min and incubation in 0.01% (w/v) $KMnO_4$ solution for 10 min. Gel was washed twice à 5 min in solution W. Then it was shaken in 10% ethanol for 10 min, washed for 10 min in water and shaken in 0.2 % $AgNO_3$ for 10 min. Finally, it was washed with water for 20 sec, and incubated in 10% (w/v) K_2CO_3. Protein bands were developed by shaking gel in developing solution as long as desired intensity of protein band staining was achieved (usually 3-15 min). In the end gel was immersed in solution W for 10 min followed by water. Afterwards gel was scanned and dried for 45 min between two transparent cellophane sheets on heating block under vacuum conditions.

2.2.3.9 Phosphoprotein staining

To visualize phosphoproteins gels were stained with Pro-Q Diamond phosphoprotein gel stain (Invitrogen). Immediately after SDS-PAGE gels were fixed in 50% methanol (v/v) and 10% (v/v) acetic acid solution for 30 min. Afterwards gel was incubated in water for 10 min

with gentle agitation. This step was repeated twice in order to remove all methanol and acetic acid. Then gel was incubated in diluted Pro-Q Diamond Stain for 90 minutes with gentle agitation. Finally gel was incubated in destain solution for 90 minutes in total, changing destain solution every 30 minutes, and washed with water.
Pro-Q Diamond phosphoprotein stain has an excitation maximum at 555 nm and an emission maximum at 580 nm. It was imaged with Molecular Imager FX (BioRad) using 532 nm laser as excitation source and 555 nm longpass emission filter.

2.2.3.10 Phosphoprotein enrichment with aliuminium hydroxide

F11 cells were serum-starved over night. The next day F11 cells were collected from three 10 ml cell culture plates and centrifuged for 5 min at 800 rpm in Heraeus floor centrifuge. After removal of supernatant F11 cells remained in pellet. The pellet was resuspended in 2 ml incubation buffer. Cells were homogenized by passing them several times through syringe and needle (0.40 x 20 mm). Homogenized cells were centrifuged in Heraeus "Biofuge 13" at 4,000 rpm for 10 minutes. Supernatant was taken to eppendorf tubes and centrifuged at 13,000 rpm in an Eppendorf centrifuge for 20 min. An aliquot of supernatant was taken for further analysis. 5x Laemmli buffer was added to it and the sample was boiled for 5 min.

$Al(OH)_3$ was prewashed with incubation buffer. 1ml incubation buffer was added to 80 mg $Al(OH)_3$, solution was vortexed and centrifuged at maximum speed in table centrifuge for 1 min. Supernatant was removed. The procedure was repeated four times.

About 700 µl supernatant left after centrifugation of F11 cells homogenate in incubation buffer was added to 80 mg of prewashed $Al(OH)_3$. The mixture was left rotating at 4^oC overnight. The incubation overnight was followed by five washing steps with incubation buffer. Finally, proteins were eluted from the $Al(OH)_3$ matrix by incubation with 800 µl of elution buffer for 30 min at room temperature. Proteins were precipitated with methanol/chloroform precipitation (described in detail in 2.2.5.1 "Sample preparation") prior to gel loading.

2.2.3.11 Immunoprecipitation

About 300 DRG were isolated from 10 embryos. They were divided into two parts and kept in PBS. One part was stimulated with 10 mM 8-pCPTcGMP at 37^oC for 5 min, another part

served as an unstimulated control. Both samples were then centrifuged (in an Eppendorf-centrifuge at 3,000 rpm for 3 min) and after removal of supernatant diluted in 500µl PBS with 0.5% Triton-X-100. After homogenization (syringes with needle ø 0.4 mm, Braun) and centrifugation (at 13,000 rpm in an Eppendorf centrifuge for 15 min) supernatants were taken to new tubes and pellets were discarded. Supernatants were diluted in 500 µl PBS with protease inhibitor coctail and preincubated with 50 µl of protein A-sepharose-slurry for 30 min with constant agitation. After centrifugation (at 2,000 rpm in an Eppendorf centrifuge for 10 min) supernatants were taken to new tubes and incubated with antibodies (end volume 1 ml, for antibody against RRXpS/pT - end concentration 7.5 µg/ml) overnight at 4°C with constant agitation. Then, both samples were incubated for 1 h at room temperature with 50 µl of protein A-sepahrose-slurry for the immunoprecipitation. After centrifugation (at 2,000 rpm in table centrifuge for 1 min) precipitates were taken into 2 Ultra-free-MC tubes, washed three times in 200 µl PBS with 0.2% Triton-X-100 and once in 200 µl PBS. Precipitates were eluted in 50 µl 1x Laemmli buffer at 95°C for 5 min. After centrifugation (at 13,000 rpm in an Eppendorf centrifuge for 5 min) eluates were ready to be analysed by SDS-PAGE and Western blotting.

2.2.4 Methods of molecular biology

2.2.4.1 Genotyping

2.2.4.1.1 Isolation of genomic DNA

Genomic DNA for genotyping was isolated from murine tissues with “High Pure PCR Isolation Kit” (Roche Molecular Biochemicals) according to instructions of manufacturer.

2.2.4.1.2 PCR

PCR was performed with PCR device “Mastercycler Gradient” (Eppendorf) and documented with “ChemiDoc” (BioRad).

<u>25µl reaction volume for cGKI</u>

2.5µl 10xPCR buffer, minus Mg^{2+} (Invitrogen)

1.5µl 50mM $MgCl_2$ (Invitrogen)

2µl 2.5 mM dNTP mix (Invitrogen)

0.3µl RF125 (10 pmol/µl) - primer

0.3µl RF53 (20 pmol/µl) - primer
0.4µl RF118 (25 pmol/µl) - primer
75ng DNA
0.25 µl Taq DNA polymerase

PCR program for cGKI
94°C/5min
94°C/10sec, 55°C/45sec, 72°C/30sec, 35 cycles
72°C/5min
4°C/∞

25µl reaction volume for Npr2
2.5µl 10xPCR buffer, minus Mg^{2+} (Invitrogen)
0.75µl 50mM $MgCl_2$ (Invitrogen)
2µl 2.5mM dNTP mix (Invitrogen)
GC_B1 2µl (10 pmol/µl) - primer
GC_B2 2µl (10 pmol/µl) - primer
75ng DNA
0.25 µl Taq DNA polymerase

PCR program for Npr2
94°C/5min
94°C/30sec, 62°C/20sec, 72°C/30sec, 35 cycles
72°C/5min
4°C/∞

PCR product was restricted with AflIII (NEB) at 37°C and electrophoresed on 3% agarose gel. Recognition site of AflIII ACRYGT is present in mutant cn allele, therefore, PCR product is restricted. In wild type Npr2 allele ACLYGT sequence cannot be cut by AflIII.

25µl reaction volume for CNP
2.5µl 10xPCR buffer, minus Mg^{2+} (Invitrogen)
0.75µl 50mM $MgCl_2$ (Invitrogen)
2µl 2.5mM dNTP mix (Invitrogen)

GT_lbab_UP2 0.2µl (100 pmol/µl) - primer
GT_lbab_LP2 0.2µl (100 pmol/µl) - primer
75ng DNA
0.25 µl Taq DNA polymerase

PCR program for CNP
95°C/3min
94.5°C/35sec, 60°C/20sec, 72°C/20sec, 35 cycles
72°C/10min
4°C/∞

PCR product was restricted with Eco47I (Fermentas) at 37°C and electrophoresed on 3% agarose gel. Recognition site of Eco47I GGWCC is present in wild type CNP allele, therefore, PCR product is restricted. In mutant lbab allele GGWCG sequence cannot be cut by Eco47I.

25µl reaction volume for VASP wild type
2.5µl 10xPCR buffer, minus Mg^{2+} (Invitrogen)
0.75µl 50mM $MgCl_2$ (Invitrogen)
0.5µl 2.5mM dNTP mix (Invitrogen)
GIK 269 0.75µl (10 pmol/µl) - primer
GIK 270 0.75µl (10 pmol/µl) - primer
75ng DNA
0.25 µl Taq DNA polymerase

25µl reaction volume for VASP knock-out
2.5µl 10xPCR buffer, minus Mg^{2+} (Invitrogen)
0.75µl 50mM $MgCl_2$ (Invitrogen)
0.5µl 2.5mM dNTP mix (Invitrogen)
GIK 273 0.5µl (10 pmol/µl) - primer
GIK 274 0.5µl (10 pmol/µl) - primer
75ng DNA
0.25 µl Taq DNA polymerase

PCR program for VASP (wild type and knock-out)
94°C/3min
94°C/45sec, 60°C/35sec, 72°C/1min, 35 cycles
72°C/10min
4°C/∞

25µl reaction volume for Mena wild type

2.5µl 10xPCR buffer, minus Mg^{2+} (Invitrogen)

0.75µl 50mM $MgCl_2$ (Invitrogen)

0.5µl 2.5mM dNTP mix (Invitrogen)

me_F3 0.75µl (10 pmol/µl) - primer

me_in2_R2 0.75µl (10 pmol/µl) - primer

75ng DNA

0.25 µl Taq DNA polymerase

25µl reaction volume for Mena knock-out

2.5µl 10xPCR buffer, minus Mg^{2+} (Invitrogen)

0.75µl 50mM $MgCl_2$ (Invitrogen)

0.5µl 2.5mM dNTP mix (Invitrogen)

pGT0Lxf_R2 0.5µl (10 pmol/µl) - primer

me_F3 0.75µl (10 pmol/µl) - primer

75ng DNA

0.25 µl Taq DNA polymerase

PCR program for Mena (wild type and knock-out)

94^oC/3min

94^oC/45sec; 56^oC/35sec; 72^oC/90sec; 32 cycles

72^oC/10min

$4^oC/\infty$

25µl reaction volume for GFP/YFP

2.5µl 10xPCR buffer, minus Mg^{2+} (Invitrogen)

1.5µl 50mM $MgCl_2$ (Invitrogen)

1µl 2.5mM dNTP mix (Invitrogen)

2.5µl oIMR0872 (10 pmol/µl) - primer

2.5µl oIMR1416 (10 pmol/µl) - primer

1.25µl oIMR0042 (10 pmol/µl) - primer

1.25µl oIMR0043 (10 pmol/µl) - primer

75ng DNA

0.25 µl Taq DNA polymerase

PCR program for GFP/YFP

94^oC/1.5min

94^oC/30sec, 60^oC/1min, 72^oC/1min, 35 cycles

72^oC/2min

$4^oC/\infty$

2.2.5 2D electrophoresis

2-D electrophoresis is a powerful and widely used method for the analysis of complex protein mixtures. The technique sorts proteins according to two independent properties in two discrete steps: the first-dimension step, isoelectric focusing (IEF), separates proteins according to their isoelectric points (pI). The second-dimension step, SDS-PAGE, separates proteins according to their subunit molecular masses (MW). Each spot on the resulting two-dimensional array corresponds to a single protein species in the sample. Single spots eluted or transferred from 2-D gels can be rapidly identified.

2.2.5.1 Sample preparation

The protein fraction to be loaded on a 2-D gel must be present in a low ionic strength denaturing buffer that maintains the native charges of proteins and keeps them soluble. Salt is the major cause of poor focusing in isoelectric focusing (IEF) and increases focusing time, as proteins will migrate to their pI only after the ions have moved out of the strips. Proteins were concentrated and desalted by methanol chloroform precipitation (Wessel and Flugge, 1984). Four volumes of methanol, four volumes of chloroform and three volumes of water are added to one volume of protein solution. Mixture is vortexed after addition of each component and centrifuged at 4,000 rpm in Heraeus centrifuge for 5 min. Upper phase is removed. Three volumes of methanol are added to lower phase and interphase, mixture is vortexed and again centrifuged at 4,000 rpm in Heraeus centrifuge to pellet protein. Supernatant is removed and pelletted protein is air-dried. It can be stored at -20^{o}C. Pellet is resuspended in lysis buffer before resolving it by 2D gel electrophoresis.

2.2.5.2 First–dimension isoelectric focusing (IEF)

For 7 cm IPG strip 125 µl sample volume, for 17 cm strip – 300 µl sample volume are loaded, respectively. In case protein sample is too concentrated it can be diluted with rehydration buffer. Sample is pippeted as a line along the back edge of a channel in rehydration tray. ReadyStrip IPG strip is gently placed, gel side down, onto the sample. It is left for approximately 30 min until most of the liquid has been absorbed by the strip. Then it is overlaid with 0.5-1 ml mineral oil to prevent evaporation during the rehydration process. Rehydration tray is covered with the plastic lid provided and left in the Protean IEF Cell

(BioRad) overnight (11-16 h) on passive rehydration program. After rehydration wet wicks are placed at both ends of wire electrodes and focusing program is started.

Focusing program for 7 cm strip

1) 250V for 30 min
2) slow ramp from 250V to 400 V in 30min
3) slow ramp from 400V to 3500 V in 1 hour 50 min
4) 3500 V for 1 hours 30 min

Focusing program for 17 cm strip

1) slow ramp from 0V to 300V in 30 min
2) 300V for 30 min
3) slow ramp from 300V to 500 V in 1 hour
4) 500 V for 1 hour
5) slow ramp from 500V to 3500 V in 1 hour 30 min
6) 3500 V for 4 hours 30 min

The current was maintained at 50μA/IPG strip. Focusing was performed at 20^{o}C.

2.2.5.3 Second-dimension SDS-PAGE

Prior to running the second dimension, it is necessary to equilibrate the IPG strip in a buffer that contains SDS. Mineral oil is removed from IPG strip by placing it (gel side up) onto a piece of dry filter paper. IPG strip (gel side up) is placed to the equilibration tray containing 10 ml equilibration buffer I containing DTT. The tray is placed on a shaker and gently shacked for 15 min. Afterwards IPG strip is immersed in 10 ml equilibration buffer II containing iodoacetamide. The tray is again shaken for 15 min. IPG strip is dipped briefly into the 1x SDS electrode buffer laid onto the back of the SDS-PAGE gel using a spatula to push carefully the IPG strip into the well. To ensure good contact between the gel and the IPG strip, it is overlaid with separating gel with the same acrylamide concentration but four times more APS and Temed as it was used preparing the SDS-PAGE gel. The gel is loaded into the electrophoresis cell and the electrophoresis is begun as usually. After second dimension SDS-PAGE gels were either blotted or stained with silver staining.

3 RESULTS

3.1 Analysis of the role of the cGMP signalling components acting upstream of the cGKI in the bifurcation of sensory axons

3.1.1 Branching of sensory axons in cGKI knock-out mice analysed by DiI tracing

3.1.1.1 Bifurcation of sensory axons is impaired in the absence of cGKI

Previous studies based on whole-mount anti-neurofilament staining (Schaffer, 2005) and injection of the lipophilic tracer DiI into DRG neurons (Schmidt et al., 2002) have shown that the guidance of sensory axons at the dorsal root entry zone of the spinal is impaired in cGKI knock-out mice – most likely by a lack of bifurcations. Both studies have investigated the erroneous growth of sensory axons by a bulk labelling method which did not allow the analysis of axonal pathfinding on the level of a single axon.

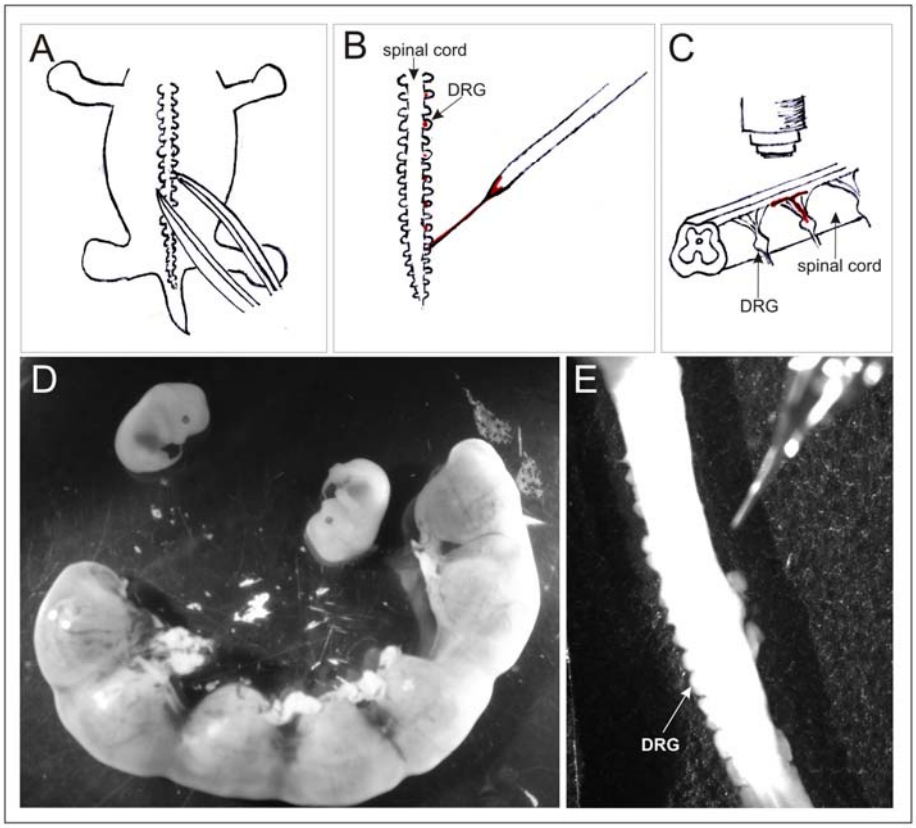

Fig. 3.1: Single axon tracing by DiI labelling at the DREZ. (A) spinal cord with attached DRG is dissected from E12-E13 mouse embryo. (B) A tip of a pipette pulled from a capillary is coated with DiI - it is soaked in DiI solution and then it is kept under a bulb light until ethanol evaporates and DiI crystals are left on the tip of the pipette. Dissected spinal cord is placed under binocular microscope und every second or third DRG is touched by a DiI coated pipette thereby leaving some DiI crystals on DRG. (C) After 24 hours, when DiI diffused along the membranes of labelled cells, spinal cord is examined under the microscope. Labelled cells

can be observed all the way from the cell body in DRG up to axonal bifurcation at the dorsal root entry zone. (D) E12 embryos in uterus and two embryos which are already dissected from the uterus. (E) Spinal cord with attached DRG and tip of the pipette coated with DiI under binocular microscope.

In order to examine the bifurcation error on a single axon level I improved the DiI labelling method. I tried to inject DiI solution in ethanol into embryonic DRG cells observed under the microscope using the pipette pulled from a capillary which was navigated by a micromanipulator. This was a labour consuming method which did not result in desired quality of sensory axon staining. Another approach – to label embryonic DRG with crystals left on the needle tip, pulled from a glass capillary, after evaporation of the ethanol proved to be much better (Fig. 3.1). Glass needle was soaked in DiI solution in ethanol and was rotated under a lamp for several minutes until the ethanol has evaporated. DRG hanging on both sides of dissected embryonic spinal cord were touched with the tip of the needle and thereby minute DiI crystals (usually not visible with naked eye) were left on DRG. This method allowed to observe single axons labelled by DiI.

Application of minute DiI crystals at the DRG surface resulted in a labelling of small number of sensory neurons (Fig.3.2) allowing the analysis of single axons. DiI labelling of DRG in wild-type mouse embryos revealed axons extending through the dorsal root and forming regular T- or Y-shaped branches (Fig.3.2 B,D,F,H) at the dorsal root entry zone. In contrast, in cGKI knock-out mouse embryos only turns in either rostral or caudal direction are observed instead (Fig.3.2 C,E,G,I). Sensory axons of heterozygous mice bifurcate in a pattern indistinguishable from wild-type mice.

Single bifurcations and turns observed in a dorso-lateral view of whole mount spinal cord preparations were quantified. In wild-type and heterozygous mice 95% of all quantified sensory axons bifurcate whereas in cGKI knock-out mice only 3% are bifurcating, the rest 97% turn either rostrally or caudally. Figure 3.3 summarizes quantification results of turns and bifurcations at cervical, thoracal, lumbar and caudal levels of spinal cord. No statistically significant difference in axonal behaviour was observed at these different spinal levels.

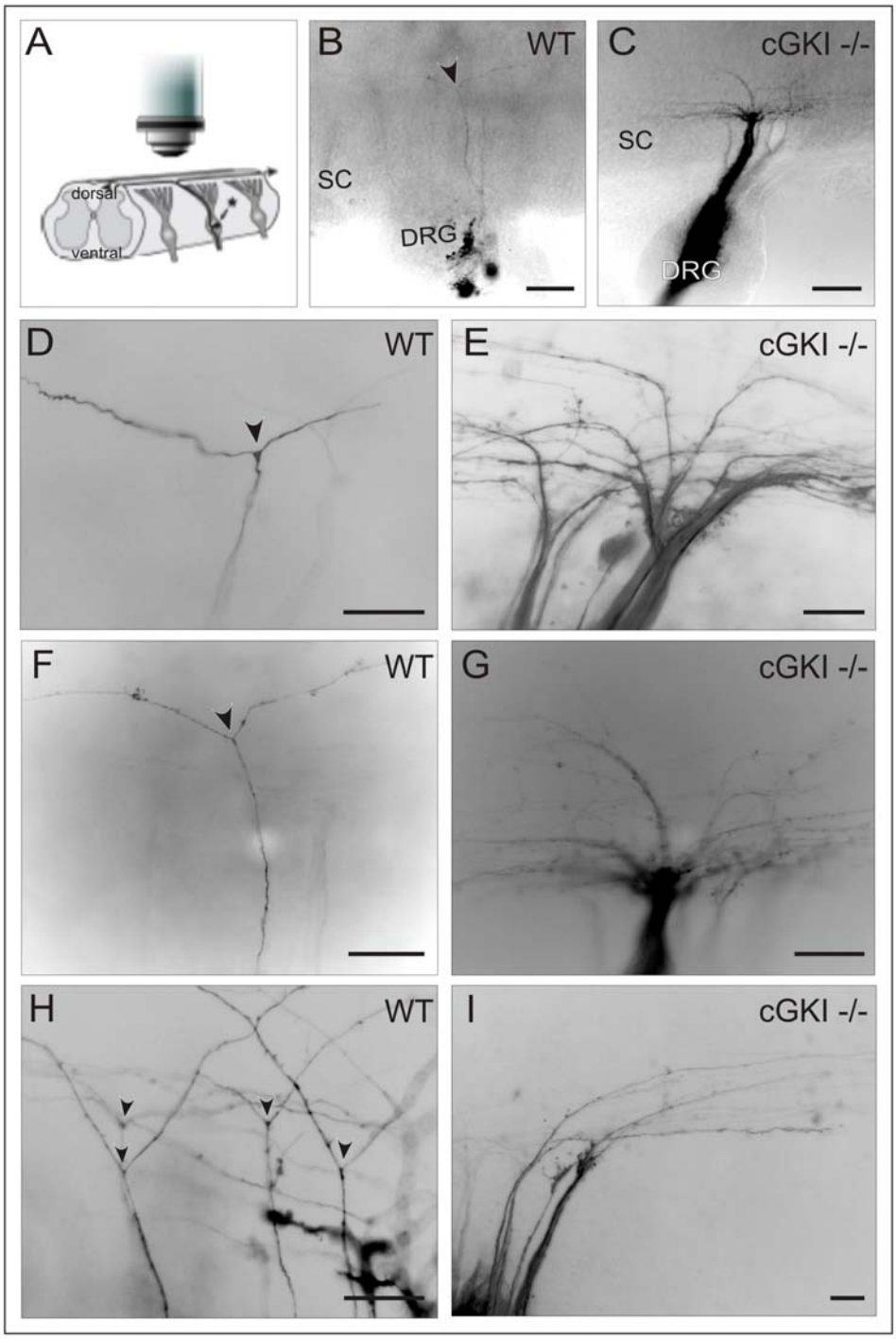

Fig. 3.2: Bifurcation error in cGKI knock-out mice on the single axon level. (A) Schematic illustration of microscopic analysis of sensory axons. Spinal cord is flattened between two cover slips and observed under the microscope from the dorsal side. At the border where sensory axons reach dorsal root entry zone bifurcations are observed. (B,D,F,H) Sensory axons labelled in wild-type embryos bifurcate at the DREZ. (C,E,G,I) Sensory axons labelled in cGKI knock-out embryos fail to bifurcate. (B-C) are overview pictures showing DRG with the cell bodies of sensory neurons and axons extending towards the spinal cord and finally bifurcating or turning either caudally or rostrally at the dorsal root entry zone. Lateral diffusion of the lipophilic tracer DiI after local application allows the visualization of axonal trajectories. Scale bar: (B-C) 100 µm; (D-I) 50 µm. SC – spinal

cord; DRG – dorsal root ganglion. Arrowheads indicate bifurcation points. In all pictures dorsal side is to the top and ventral to the bottom. E12-E14 mouse embryos were analysed.

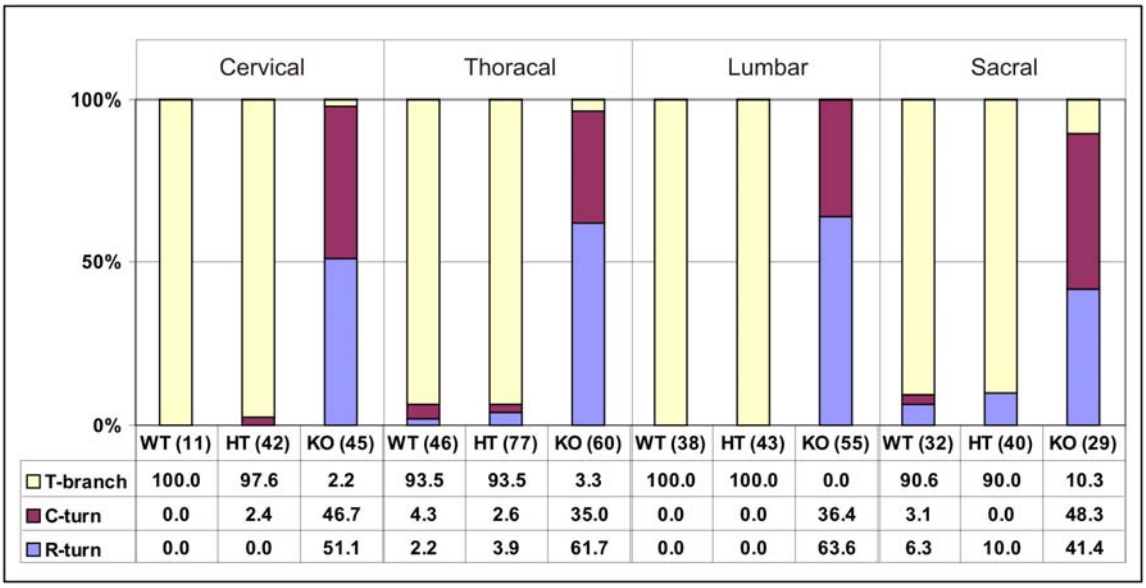

	WT (11)	HT (42)	KO (45)	WT (46)	HT (77)	KO (60)	WT (38)	HT (43)	KO (55)	WT (32)	HT (40)	KO (29)
T-branch	100.0	97.6	2.2	93.5	93.5	3.3	100.0	100.0	0.0	90.6	90.0	10.3
C-turn	0.0	2.4	46.7	4.3	2.6	35.0	0.0	0.0	36.4	3.1	0.0	48.3
R-turn	0.0	0.0	51.1	2.2	3.9	61.7	0.0	0.0	63.6	6.3	10.0	41.4

Fig. 3.3: Quantification of DiI-labelled bifurcations and caudal or rostral turns at different levels of the spinal cord in wild-type (WT), heterozygous (HT), or cGKI knock-out (KO) mice. The numbers of counted single axons are given in brackets for different trunk levels for each genotype. Percentage values of axonal bifurcations and turns are shown in the graph and indicated in the table. The quantification was performed blind with regard to the genotype. 25 wild-type, 17 cGKI knock-out and 33 heterozygous embryos, E12-E14, were analysed.

Sensory axons in cGKI knock-out mice turn only in caudal or rostral direction. Quantification of the turning behaviour indicated a slight preference for rostral turns (Table 3.1.). 58.5% of all turning axons in cGKI knock-out mice turn to the rostral side and 41.5 % - to the caudal side. This difference in turning direction is statistically significant at p value of 0.05 (binomial test).

Table 3.1: Quantification of axonal turn directions in E12-E14 cGKI knock-out mouse embryos.

Caudal turns	Rostral turns	Total
76	107	183

3.1.1.2 Sensory axons are still able to generate collateral branches in the absence of cGKI

Sensory axons display several modes of branching. They bifurcate rostrocaudally thereby generating two branches. After this each of the branches extends collateral branches into the spinal grey matter: nociceptive collaterals stay in the superficial region of the dorsal horn while proprioceptive collaterals grow ventrally to the ventral horn (Ozaki and Snider, 1997). Interestingly, in contrast to the almost complete inability to bifurcate, sensory axons of cGKI knock-out mice are still able to generate collateral branches as detected in DiI labelled sensory axons (Fig. 3.4).

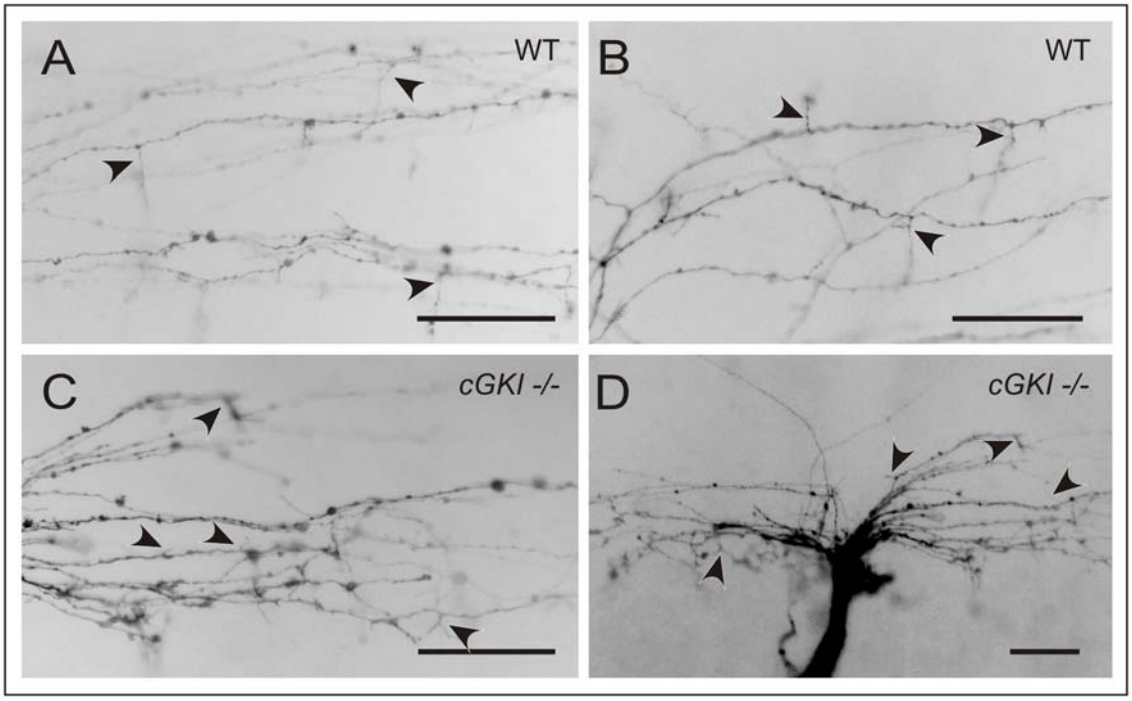

Fig. 3.4: Collateral branches are generated in cGKI knock-out mice. (A-B) Collateral branches (arrowheads) observed on DiI labelled axons of wild-type mouse embryos. (C-D) Collateral branches (arrowheads) in cGKI knock-out mouse embryos. Scale bar: (A-D) 50 μm.

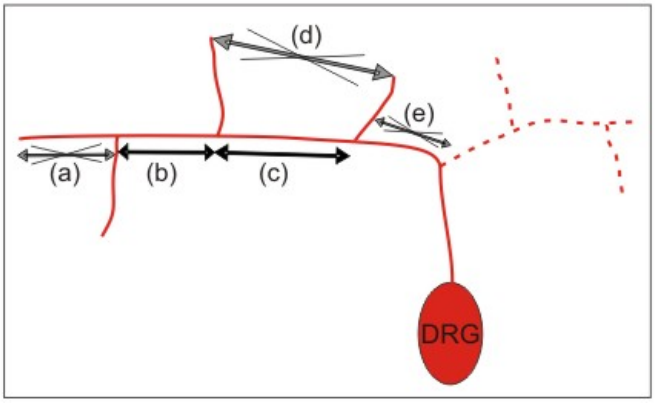

Fig. 3.5: Schematic illustration of measurement of distances between adjacent collaterals. Sensory neuron is coloured in red. A red continuous line represents turning axon in cGKI knock-out mouse whereas continuous line together with dashed red line represent bifurcated sensory axon in wild type mouse. Distances between the origin points of two adjacent collaterals, (b) and (c), were measured. Based on such definition measurement of distance (d) would be wrong, because it is a distance between the distal parts of adjacent collaterals and not their origin points. Distances (a) and (e) do not meet the definition because they are not distances between two adjacent collaterals - (a) is a distance between the end point of the axon and the collateral, (e) is a distance between the turning/bifurcation point of the axon and the collateral. Swellings on the stem axon were not considered as collaterals, although there is an opinion that swelling shows where collateral will sprout (Ozaki and Snider, 1997). Measurements were carried out manually using magnification microscope objective lens with a ruler model partition eyepiece. Even adjacent collaterals are not always on the same plane as observed under the microscope and different focus is necessary for each of them, therefore, manual measurement, rather than processing of pictures with software was chosen. Distances between adjacent collaterals were measured in E14 embryos.

In the cGKI knock-out mice a DRG neuron develops only one longitudinal axon stem instead of two. Since collaterals are generated from the longitudinal axon stems and there is only half of them in the cGKI knock-out mouse compared to the wild-type mouse, there should be also twice less collateral branches in the cGKI knock-out mouse. Indeed, reduced amount of sensory collaterals in cGKI deficient mouse embryo compared to wild type mouse embryo was shown by anti-trkA (trkA is expressed by nociceptive neurons) staining in transverse spinal cord sections (Schmidt et al., 2002). To analyse whether the impairment of sensory axon bifurcation in the cGKI knock-out mouse leads to less collateral branches generated from longitudinal axon stems or there is some compensation mechanism turned on, I quantified the distance between collateral origin points in the cGKI knock-out and their sibling wild type E14 mouse embryos and compared the results (Table 3.2).

Table 3.2: Measurement of distances between origin points of neighbouring collateral branches in cGKI knock-out and wild-type mouse embryos.

	Number of examined embryos	Number of examined axons	Number of measured distances	Average distance, µm
cGKI KO animals	5	18	54	29.5
WT animals	5	14	48	46.6

The distances between the collateral origins on the longitudinal stem axon were reduced in cGKI deficient mouse embryos compared to their wild type littermates (Fig. 3.4). This reduction was statistically significant at p value 0.001 (Mann-Whitney U test).

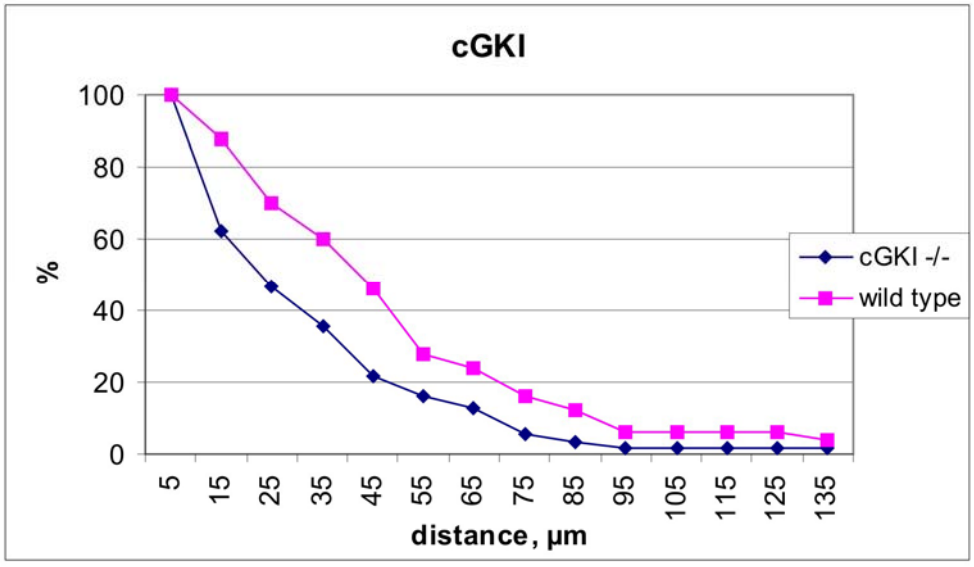

Fig. 3.6: Frequency cumulation plot for distances between adjacent collaterals in cGKI knock-out and wild-type mouse embryos. Only distances >5 µm are included. Distances between two collateral origin points were quantified in microscopic view fields of E14 mouse embryos.

3.1.2 Branching of sensory axons in mice lacking functional Npr2 (*cn/cn*) analysed by DiI tracing

3.1.2.1 Bifurcation of sensory axons is impaired in mice lacking functional Npr2

cGMP is generated from GTP by guanylyl cyclases. There are two forms of guanylyl cyclases: plasma membrane guanylyl cyclases from which 7 genes are known in mammals and soluble guanylyl cyclases that are activated by nitric oxide. The latter is a heterodimer composed of two different subunits α and β (Lucas et al., 2000). H. Schmidt showed by RT-PCR that guanylyl cyclase E and natriuretic peptide receptor 2 (Npr2, also known as NprB or GC-B) are expressed in DRG, however, in situ hybridisation confirmed presence of Npr2

only in DRG (Schmidt et al., 2007). Interestingly, it is expressed in a pattern overlapping with that of cGKIα in embryonic DRG. Therefore, Npr2 looked like a most likely candidate to produce cGMP in DRG.

To test whether Npr2 is involved in sensory axon bifurcation I labelled DRG of the spontaneous Npr2 loss of function mutant cn/cn with the lipopihilic tracer DiI, as described for cGKI knock-out mice. Due to a point mutation that leads to the substitution of a highly conserved hydrophobic residue leucine with the hydrophylic residue arginine in the guanylyl cyclase domain of Npr2, Npr2 is no longer able to generate cGMP (Tsuji and Kunieda, 2005).

DiI labelling of sensory axons in cn/cn mouse embryos revealed the same bifurcation error that was observed in cGKI knock-out mouse embryos. Sensory axons in the wild-type mouse embryos bifurcated after reaching the dorsal root entry zone, whereas in cn/cn mouse embryos they turned either rostrally or caudally (Fig. 3.7). Sensory axons of heterozygous mouse embryos bifurcated and looked like axons of wild-type mouse embryos. Quantification of all detected bifurcations and turns confirmed initial observations – 99 % of sensory axons observed in wild-type mice and only 4 % - in cn/cn mice were bifurcating (Fig. 3.8).

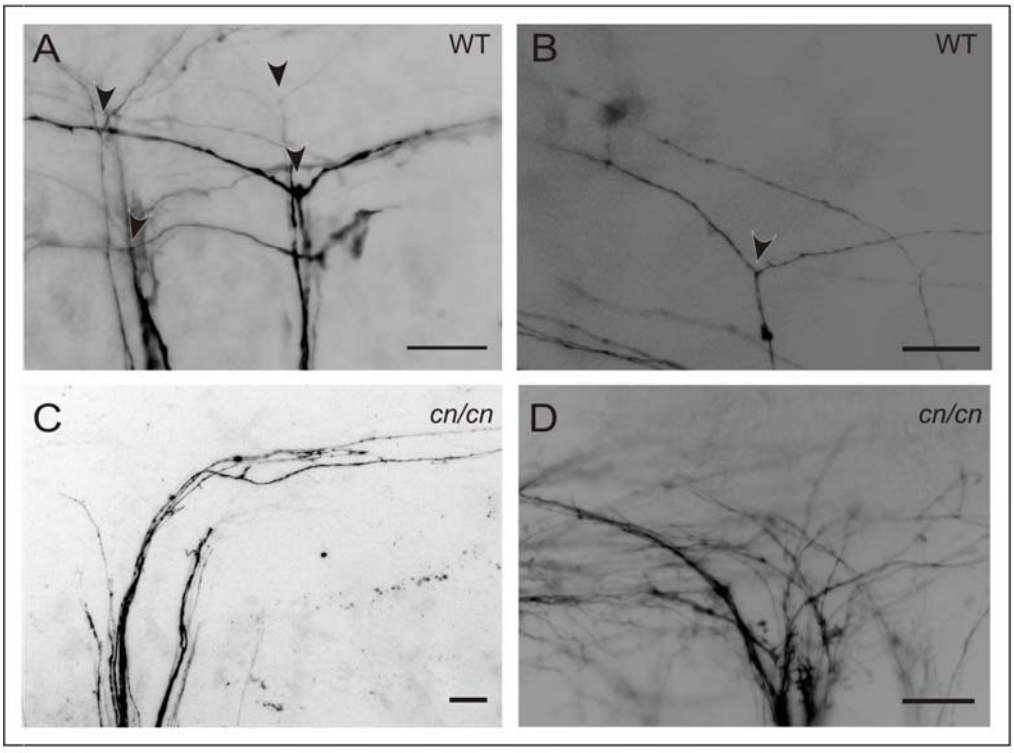

Fig. 3.7: Bifurcation error in cn/cn mice shown on a single axon level. (A-B) Sensory axons labelled with DiI bifurcate at the DREZ of wild type embryos. Arrowheads point at the bifurcation points. (C-D) Sensory

axons labelled in cn/cn embryos fail to bifurcate and turn either in rostral or caudal direction. Scale bar: (A-D) 50 µm. E12-E14 mouse embryos were analysed.

As in cGKI knock-out mice a preference for rostral turns was observed in cn/cn mice (table 3.3). While 57 % of all turns were directed rostrally only 43 % were in caudal direction. However, in contrast to cGKI knock-out mice, the difference between amount of axons turning caudally and rostrally in cn/cn mice is not statistically significant ($p>0.05$, binomial test), therefore, the results should be treated cautiously.

Taken together, the identical quantitative and qualitative phenotypes of cGKI knock-out and cn/cn mice suggests that both cGKI and Npr2 act in the same cGMP signalling cascade.

Table 3.3: Quantification of turn directions in cn/cn mice

	Caudal turns	**Rostral turns**	**Total**
cn/cn	78	104	182

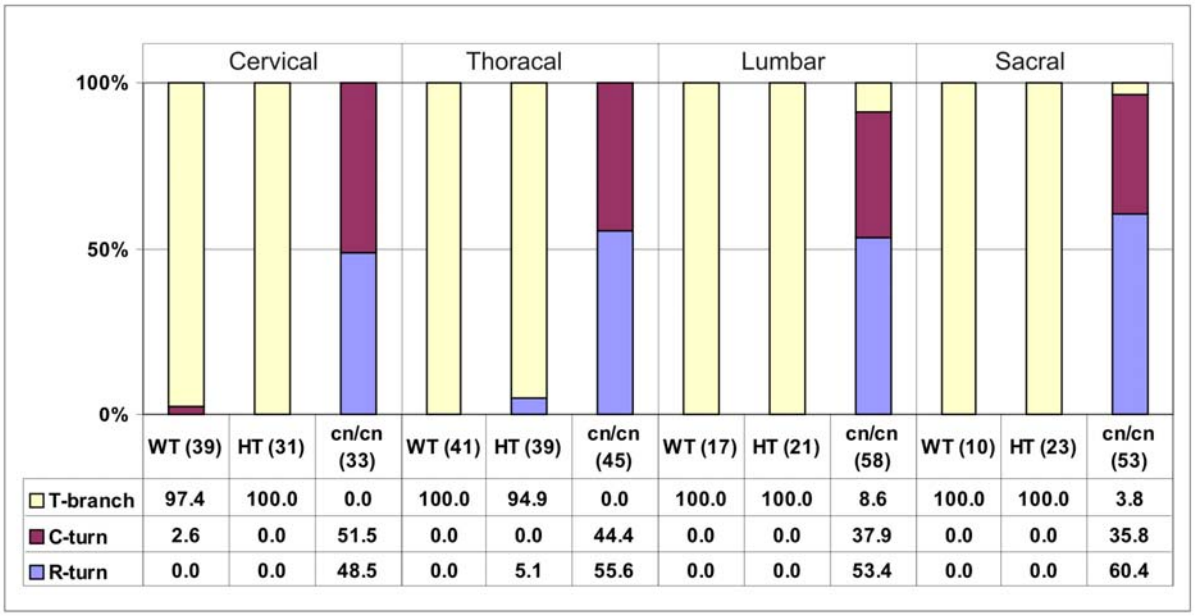

	WT (39)	HT (31)	cn/cn (33)	WT (41)	HT (39)	cn/cn (45)	WT (17)	HT (21)	cn/cn (58)	WT (10)	HT (23)	cn/cn (53)
T-branch	97.4	100.0	0.0	100.0	94.9	0.0	100.0	100.0	8.6	100.0	100.0	3.8
C-turn	2.6	0.0	51.5	0.0	0.0	44.4	0.0	0.0	37.9	0.0	0.0	35.8
R-turn	0.0	0.0	48.5	0.0	5.1	55.6	0.0	0.0	53.4	0.0	0.0	60.4

Fig. 3.8: Quantification of DiI-labelled bifurcations and caudal or rostral turns at different levels of the spinal cord in wild-type (WT), heterozygous (HT), or cn/cn mice. The numbers of counted single axons are given in brackets for different trunk levels for each genotype. Percentage values of bifurcations and turns which are schown in the form of percentage graph are given in the table below the graph. The quantification was performed blind with regard to the genotype. 13 wild-type, 8 cn/cn and 13 heterozygous embryos E12-E14 were analysed.

3.1.2.2 Double heterozygous mice for cGKI and Npr2 do not show any defect in sensory axon bifurcation

Analysis of mice lacking cGKI or mutant for Npr2 led to the conclusion that both proteins are a part of the same signalling cascade. Mice heterozygous for cGKI allele or for functional Npr2 allele do not show defects in sensory axon bifurcation, mutations are recessive. If recessive mutations occur in two genes whose products interact, it is conceivable that a double heterozygote for the two mutations might show a phenotype, whereas heterozygotes for either mutation alone would be wild-type (Lawrence S.B., 1994).

Npr2 receptor is a dimer. Mouse heterozygous for Npr2 would produce only 50% of wild-type Npr2 monomers, but only half of them will dimerize with another wild-type monomer, so heterozygous mouse will have only 25% of functional Npr2 receptors. Respectively, less cGMP will be produced by a reduced number of functional Npr2. In double heterozygous mice, in addition to restricted amount of cGMP, reduced amount of cGKI is available for activation by cGMP. This double restriction could lead to insufficient cGMP signalling resulting in errors of sensory axon bifurcation, which would confirm that Npr2 and cGKI act in the same pathway regulating sensory axon bifurcation.

To determine whether double heterozygous mice for both cGKI and functional Npr2 show any defects in sensory axon bifurcation I analysed these axons by DiI labelling, as described for cGKI mice. Analysis revealed no difference between wild type and double heterozygous mice in respect to axonal bifurcation. As figure 3.9 demonstrates, sensory axons in these mice bifurcate. Quantification of bifurcations and turns indicates that 93 % of all observed axons bifurcate. Quantification was carried out at different trunk levels and no significant differences were observed (Fig. 3.10). Comparison with heterozygous mice Npr2/cn and cGKI+/- shows that double heterozygous mice do not differ from heterozygous mice in regard to sensory axon bifurcation (Fig. 3.11).

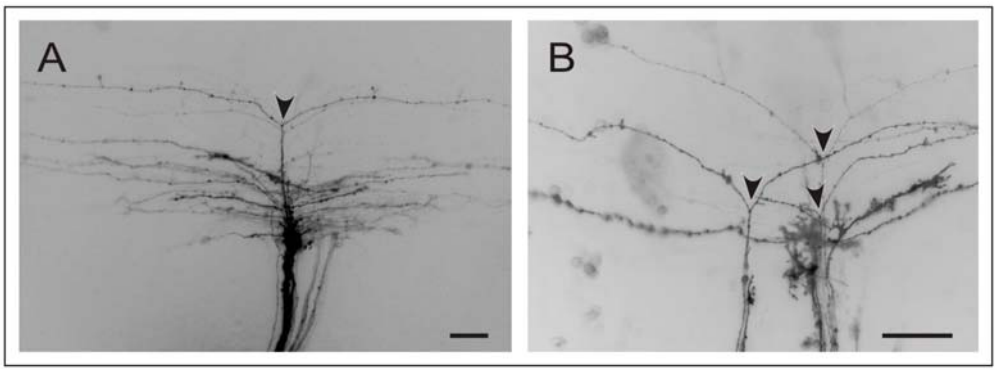

Fig. 3.9: Sensory axons of mice heterozygous for both cGKI and Npr2 alleles do not have the bifurcation error. (A-B) sensory axons labelled with DiI in double heterozygous embryos bifurcate and do not differ from single heterozygous mice or wild type mice. Scale bar: (A-B) 50 µm. E12-E13 mouse embryos were analysed.

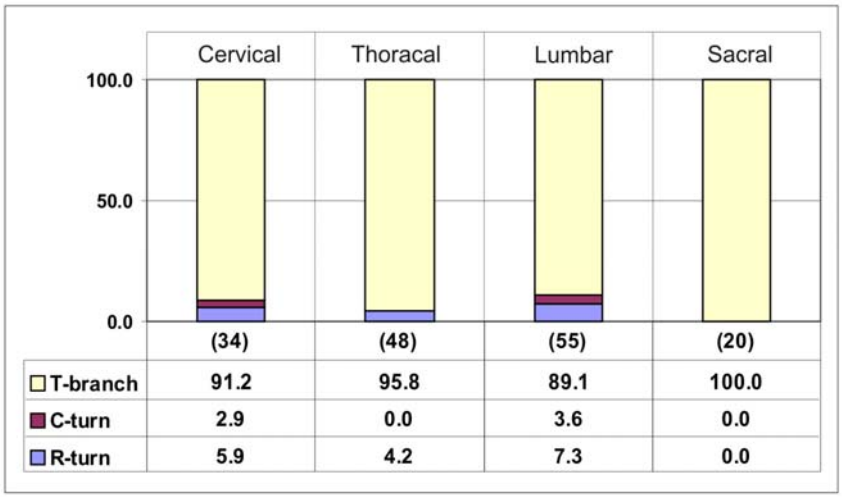

	Cervical	Thoracal	Lumbar	Sacral
	(34)	(48)	(55)	(20)
T-branch	91.2	95.8	89.1	100.0
C-turn	2.9	0.0	3.6	0.0
R-turn	5.9	4.2	7.3	0.0

Fig. 3.10: Quantification of DiI-labelled bifurcations and caudal or rostral turns at different levels of the spinal cord in double heterozygous mouse (cGKI +/- / Npr2/cn). The numbers of counted single axons are given in brackets for different trunk levels. The table shows the percentage values for bifurcations and turns at different trunk levels. There are no differences between different trunk levels, almost all of observed sensory axons bifurcate. 12 double heterozygous embryos (cGKI +/- / Npr2/cn), E12-E13, were analysed.

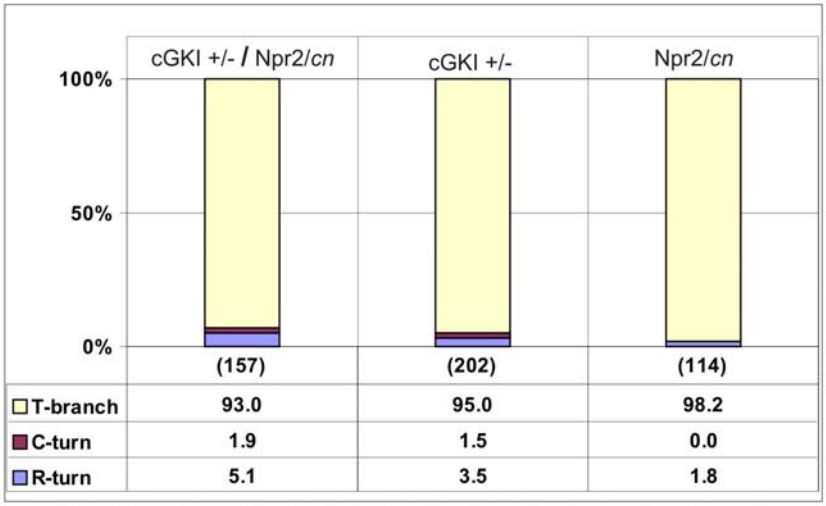

	cGKI +/- / Npr2/*cn*	cGKI +/-	Npr2/*cn*
	(157)	(202)	(114)
T-branch	93.0	95.0	98.2
C-turn	1.9	1.5	0.0
R-turn	5.1	3.5	1.8

Fig. 3.11: Quantification of DiI-labelled bifurcations and caudal or rostral turns in double heterozygous embryos (cGKI +/- / Npr2/cn) and in embryos heterozygous either for cGKI or for functional Npr2 does not reveal any significant difference. The numbers of counted single axons are given in brackets for different trunk levels. The table shows the percentage values for bifurcations and turns for different genotypes.

This analysis shows that double heterozygous mice for cGKI and functional Npr2 genes do not differ from single heterozygous mutant and have a wild type phenotype, suggesting that cGMP signalling constricted both on cGMP generation level and cGKI level is still sufficient to elicit axonal bifurcation.

Hypothetically, if cGMP generated by reduced number of functional Npr2 in mutant mice activates less than a half of wild-type amount of cGKI then amount of cGMP is a restricting factor in cGMP signalling. However, this number of cGKI activated by a reduced number of cGMP molecules is sufficient to elicit bifurcation, as it is evident from Npr2/cn mouse. If cGMP generated by a reduced number of Npr2 is able to activate more than half of wild-type amount of cGKI, then amount of cGKI becomes a restricting factor. However, half of wild-type amount of cGKI molecules are enough for sensory axon bifurcation, as it is apparent from cGKI heterozygous mouse. Thus, a double heterozygous mouse most likely has the same restricting factor as either of the two single heterozygous mice. The situation would be aggravated if one of the heterozygotes would have a mutant cGKI molecule which binds cGMP but does not become activated and thereby confines cGMP molecules. In this case double heterozygous would have a lower cGMP concentration compared to Npr2 mutant mouse.

3.1.2.3 Absence of functional Npr2 does not effect generation of collateral branches

In cn/cn mouse absence of sensory axon bifurcations, as in cGKI knock-out mouse, has been observed. Although bifurcation of sensory axons is impaired in cn/cn mice but their interstitial branching is not affected (Fig. 3.12). I measured the distances between the origin points of adjacent collaterals to find out whether there is some compensation mechanism triggered in cn/cn mice to overcome reduced number of longitudinal stem axons from which collaterals sprout. The distance between collateral origin points is reduced in cn/cn mice and this reduction is statistically significant ($p < 0.02$, Mann-Whitney U test) – the same phenomenon that was oberved in the cGKI knock-out mouse (Table 3.4). Reduced distance between collaterals is also shown by the frequency cumulation plot of distance lenghts (Fig. 3.13)

The average distance between adjacent collaterals between cGKI knock-out and cn/cn mice differs substantially. Both mutant mice have different genetic background - cGKI mice are on a 129/Sv while cn/cn mice on an AKR/J genetic background. Distances between adjacent collaterals in wild type mice on these two background differ substantially as well, therefore, results for both mouse strains (cGKI knock-out and cn/cn) should be considereded separately and should not be compared.

Table 3.4: Measurement of distances between neighbouring collateral branches in cn/cn and littermate wild-type mice

	Number of examined embryos	Number of examined axons	Number of measured distances	Average distance, µm
cn/cn animals	4	23	63	51.9
WT animals	11	35	78	64.9

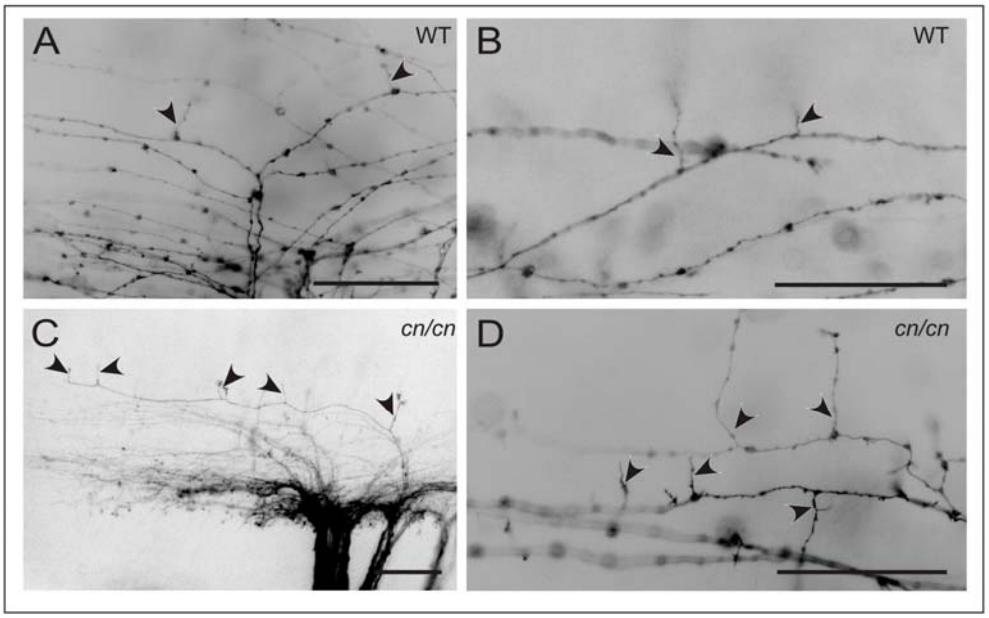

Fig. 3.12: Collateral branches are generated in cn/cn mice. (A-B) Collateral branches (arrowheads) originating from DiI labelled axons of wild-type mice. (C-D) Collateral branches sprout (arrowheads) in cn/cn mice as well, although bifurcation in these mice is impaired. (A,C) Overview pictures. (B,D) Magnified collateral branches. Scale bar: (A-D) 50µm.

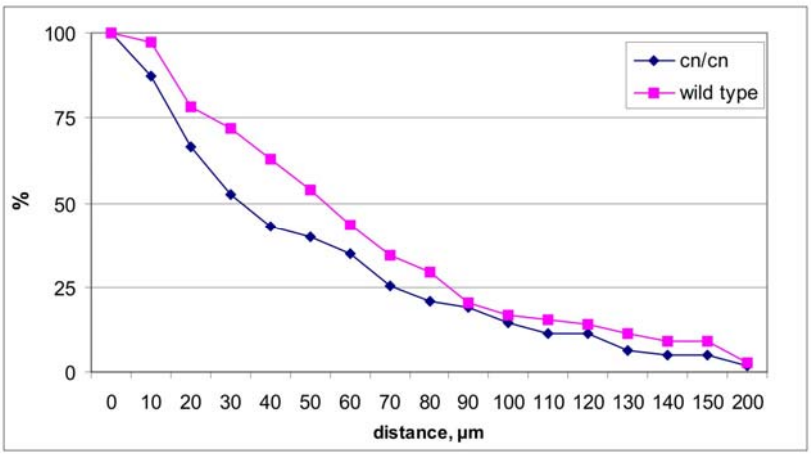

Fig. 3.13: Frequency cumulation plot for distances between two origin points of adjacent collaterals in cn/cn and wild-type mice. Only distances >5 µm are included. Distances between origin points of adjacent collaterals were measured in microscopic view fields of E14 mouse embryos.

3.1.3 Branching of sensory axons in mice lacking functional CNP (lbab) analysed by DiI tracing

3.1.3.1 Sensory axons of mice lacking functional CNP have the same bifurcation error as mice lacking cGKI or functional Npr2

Npr2 is activated by C-type natriuretic peptide (Koller et al., 1991), which suggests that CNP might play a role in the bifurcation of sensory axons acting upstream in the cGMP signalling cascade. I analysed an lbab/lbab (long bone abnormality) mouse to explore this hypothesis. This mouse has a point mutation in a gene encoding CNP leading to the amino acid substitution from arginine to glycine in a highly conserved ring structure of the peptide. Mutated CNP has a reduced ability to bind and activate Npr2 and as a result has reduced effect on increase of cGMP level (Tsuji et al., 2008;Yoder et al., 2008).

Indeed, our presumption about the role of CNP on the bifurcation of sensory axons has been confirmed after the analysis of sensory axons labelled with DiI. As Figure 3.14 shows wild-type mice have bifurcating sensory axons growing both in rostral and caudal directions whereas their littermates lbab/lbab mice lacking functional CNP have sensory axons which are unable to bifurcate, instead they choose only one direction to grow further after a turn – either rostral or caudal.

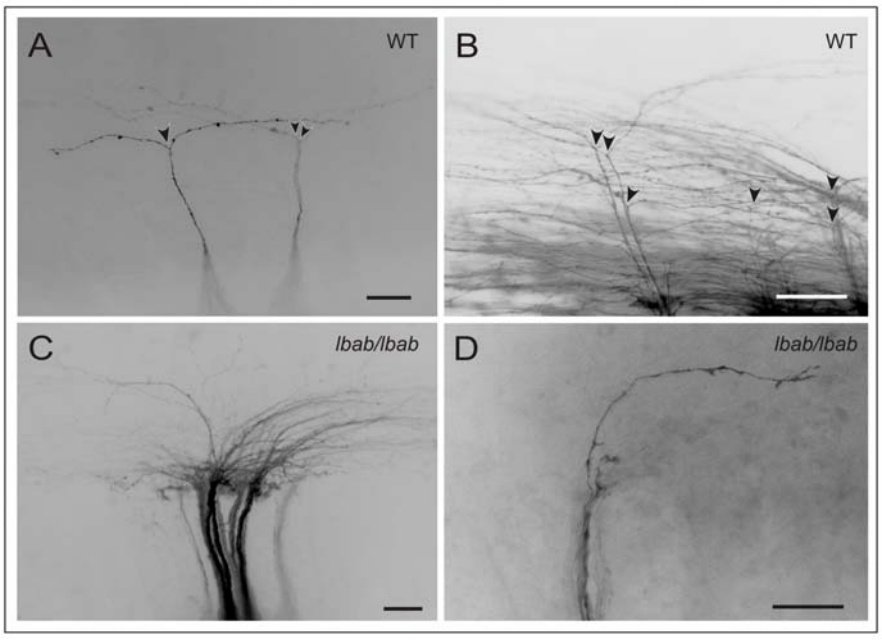

Fig. 3.14: Bifurcation error in lbab/lbab mice shown on a single axon level. (A-B) DiI labelled sensory axons in wild-type embryos bifurcate at the DREZ. (C-D) Sensory axons in lbab/lbab embryos fail to bifurcate and turn either in rostral or caudal direction. Scale bar: (A-D) 50 μm. E12-E13 mouse embryos were analysed.

Quantification of observed turns and bifurcations gives similar results as in the case of the cGKI knock-out and cn/cn mice. The vast majority of sensory axons, 95%, are bifurcating in wild-type mice whereas only 0.3% are bifurcating in lbab/lbab mice. There are no significant differences observed between different levels of the spinal cord (Fig. 3.15).

Again a preference for rostral turns was observed in lbab/lbab mice, as it was in other mice lacking a component of the cGMP pathway and accordingly having almost no bifurcating sensory axons (Table 3.5). However, difference in numbers of rostrally and caudally turning axons was not statistically significant ($p<0,05$, binomial test).

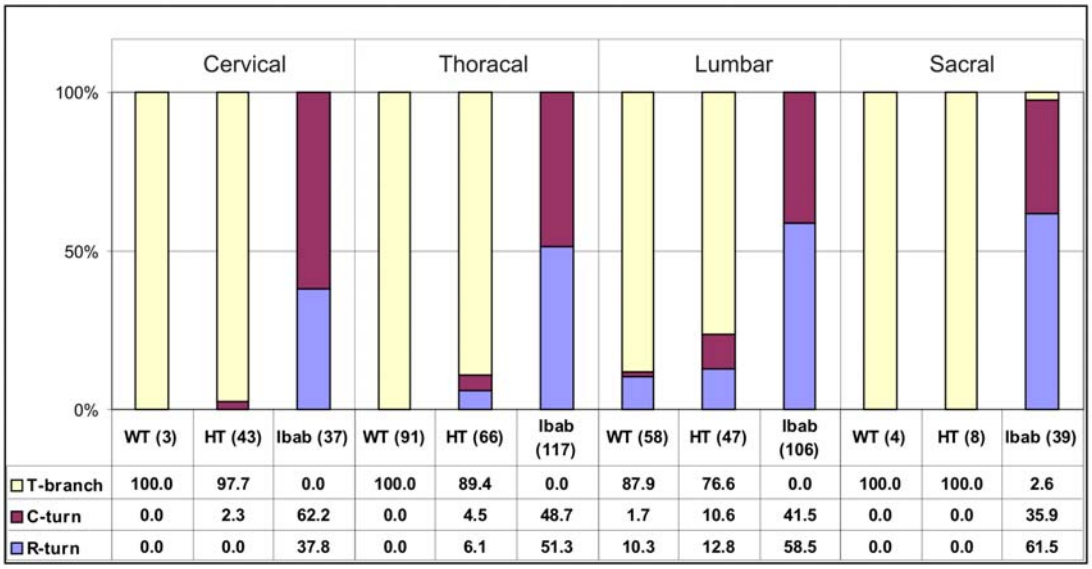

	WT (3)	HT (43)	lbab (37)	WT (91)	HT (66)	lbab (117)	WT (58)	HT (47)	lbab (106)	WT (4)	HT (8)	lbab (39)
T-branch	100.0	97.7	0.0	100.0	89.4	0.0	87.9	76.6	0.0	100.0	100.0	2.6
C-turn	0.0	2.3	62.2	0.0	4.5	48.7	1.7	10.6	41.5	0.0	0.0	35.9
R-turn	0.0	0.0	37.8	0.0	6.1	51.3	10.3	12.8	58.5	0.0	0.0	61.5

Fig. 3.15: Quantification of DiI-labelled bifurcations and turns at different levels of the spinal cord in wild-type (WT), heterozygous (HT), or lbab/lbab (lbab) mice. The numbers of counted single axons are given in brackets for different trunk levels for each genotype. Percentage values are given in the table below the percentage graph. The quantification was performed blind with regard to the genotype. 9 wild-type, 8 lbab/lbab and 11 heterozygous embryos E12-E13 were analysed.

Table 3.5: Quantification of turn directions in cn/cn mice

	Caudal turns	Rostral turns	Total
lbab/lbab	138	160	298

DiI labelling revealed failure to bifurcate in cGMP signalling mutant embryos. Analysis of adult (2 months old) mice revealed whether the bifurcation defect recovers in postnatal stage. For this analysis a Thy-1-EYFP allele crossed into lbab/lbab mouse was used. A part of sensory neurons express EGFP in these mice which allows to follow their trajectories. Failure

to bifurcate persists in mature stage (Fig. 3.16). Graphic in figure 3.17 summarises results of quantified bifurcations and turns observed in 2 month old mice.

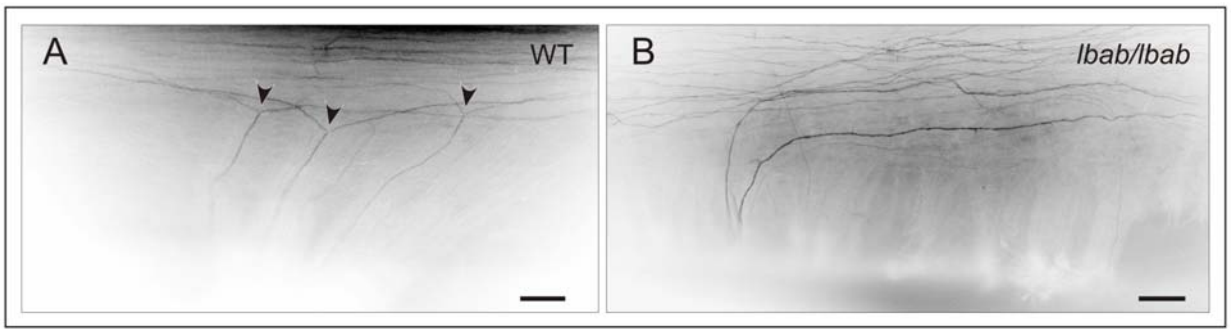

Fig. 3.16: Turns instead of bifurcations are observed in mature lbab/lbab mouse. (A) Bifurcating sensory axons expressing YFP in adult wild-type mouse crossed with Thy-1-YFP-H line. (B) Turns of sensory axons observed in Thy-1-YFP-H x lbab/lbab mouse. Scale bar: (A-B) 100µm.

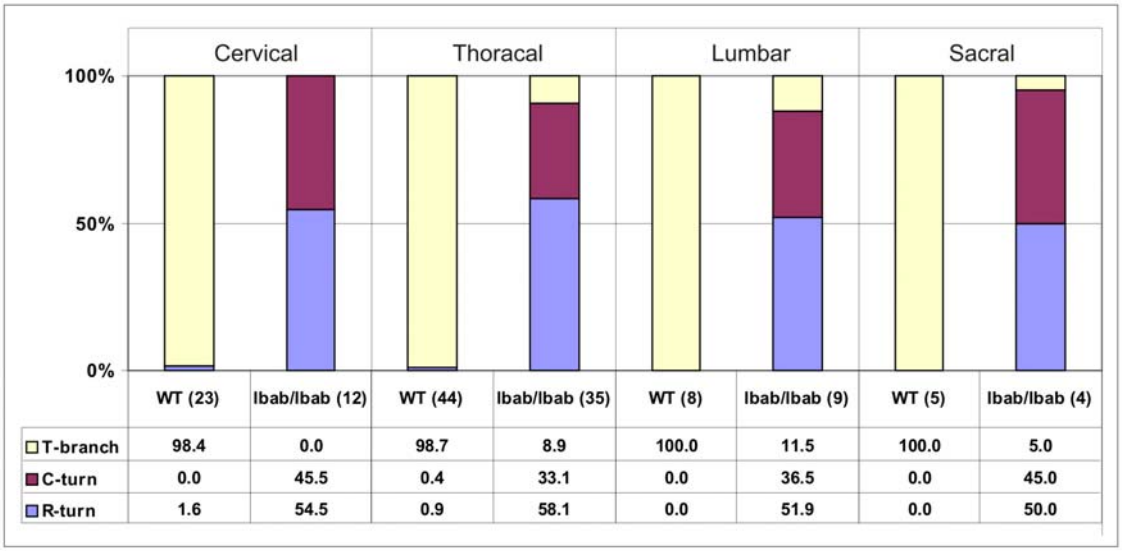

	WT (23)	lbab/lbab (12)	WT (44)	lbab/lbab (35)	WT (8)	lbab/lbab (9)	WT (5)	lbab/lbab (4)
T-branch	98.4	0.0	98.7	8.9	100.0	11.5	100.0	5.0
C-turn	0.0	45.5	0.4	33.1	0.0	36.5	0.0	45.0
R-turn	1.6	54.5	0.9	58.1	0.0	51.9	0.0	50.0

Fig. 3.17: Bifurcation defect is found in postnatal stage of lbab/lbab mouse as well. The numbers of counted single axons are given in brackets for different trunk levels for each. Percentage values are given in the table below the percentage graph. 2 wild type and 3 lbab/lbab 2 month old animals crossed with Thy-1-YFP-H mice were analysed.

3.1.3.2 Generation of collateral branches is not impaired in the absence of functional CNP

As it was detected in other cGMP signalling mutant mice, only bifurcation of sensory axons is affected when a component of cGMP pathway is missing. Collateral branching is observed even in mice with defect cGMP signalling. Analysis of lbab/lbab mouse confirms this. Although sensory axons in these mice do not bifurcate collateral branching is not impaired. (Fig. 3.18)

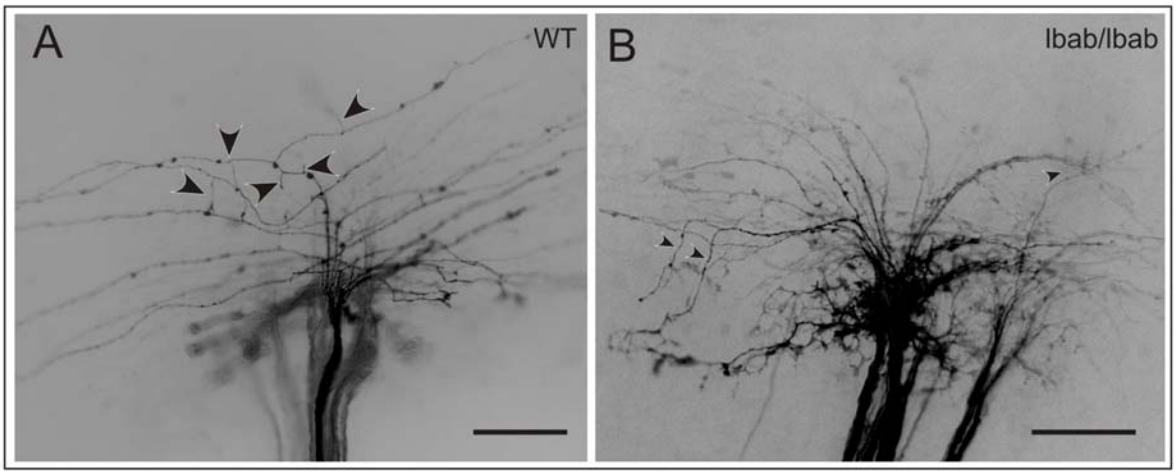

Fig. 3.18: Collateral branches are generated in lbab/lbab mice. (A) Collateral branches (arrowheads) sprout from DiI labelled axons of wild-type mice. (B) Collateral branches (arrowheads) in lbab/lbab mice. Scale bar: (A-B) 50µm.

3.2 Search for bifurcating neurons outside the spinal cord

cGKI, a crucial protein for sensory axon bifurcation at the dorsal root entry zone, is expressed outside the spinal cord as well. Expression of cGKI was confirmed in cerebellar Purkinje cells, the hippocampus, dorsomedial hypothalamus, deep cerebellar nuclei, cerebral cortex, subcommissural organ, several cranial nerves including N. trigeminus, olfactory bulb, pituitary gland, and retina (Feil, 2005;Schäffer, 2006). Another component of the cGMP signalling pathway involved in sensory axon bifurcation, Npr2, is expressed in hippocampus (granule and pyramidal cells), in pyramidal cells of V and VI layer in the neocortex, principal sensory and motor nuclei of the trigeminal nerve, in the cerebellum (Purkinje cell layer), in pituitary and pineal glands (Herman et al., 1996). However, distribution of mRNA encoding Npr2 has been described in the adult brain. CNP was detected in the embryonic cerebral cortex and pons (Cameron et al., 1996). Overlapping expression of cGMP signalling cascade components outside the spinal cord, in the cerebral cortex or hippocampus, suggests a possibility that cGMP signalling pathway might regulate neuronal bifurcation not only in the spinal cord but also in other regions of the nervous system. Therefore, I looked for bifurcating neuron populations outside the spinal cord and analysed them in wild-type and cGKI knock-out mice.

3.2.1 Dendrites of pyramidal neurons

Bifurcation is most often exhibited by dendrites (Acebes and Ferrus, 2000). Pyramidal neurons, abundant in most mammalian forebrain structures, including the cerebral cortex, the hippocampus and the amygdala, have basal and apical dendrites that bifurcate. Apical dendrites of pyramidal neurons bifurcate, sometimes several times, before building a tuft of branches at a variable distance from the soma. Basal dendrites are short and branch close to the soma (Fig. 3.19 A) (Bannister and Larkman, 1995;Larkman, 1991;Spruston, 2008). Although branching of pyramidal dendrites is often called bifurcation, it is used as a synonyme for branching rather than a definition of a special branching mode. Indeed, dendrites of pyramidal neurons split into two branches that remind Y-shaped bifurcation but there is no study describing whether such form of branching arises due to a growth cone splitting or due to collateral branching. Moreover, dendrites do not have such stereotyped branching behaviour like sensory axons: they split at a different distance to soma, sometimes several times, sometimes they do not split at all. On the one hand Y-shaped branches of dendrites and expression of cGKI and Npr2 by pyramidal cells in the cortex and the

hippocampus leads to an assumption that cGMP pathway might regulate bifurcation of pyramidal dendrites, but on the other hand branching behaviour of dendrites is not identical to bifurcation of sensory axons. I analysed the role of cGMP signalling in dendritic branching of pyramidal cells in the cortex and the hippocampus.

3.2.1.1 Apical dendrites of pyramidal neurons in cortex branch in the absence of cGKI

The bifurcation of apical dendrites of layer V pyramidal cells was analysed by crossing Thy-1-GFPM mice with cGKI knock-out mice. Only a small fraction of pyramidal cells is labelled in the Thy-1-GFPM mouse line, which allows to visualize single dendrites.

In contrast to sensory axon branching, the branching pattern of apical dendrites varied. First of all, not all apical dendrites bifurcated, secondly, bifurcations did not occur at the same level. Most apical dendrites bifurcated close to layer 2/3, but there were apical dendrites that bifurcated close to soma (Fig.3.19 B). Some apical dendrites were lacking any bifurcation and apical tuft at all. In his detailed analysis of cortical pyramidal cell dendrites Larkman describes slender layer V pyramidal cells that have an apical dendrite which tapers to a fine diameter and terminates without forming a terminal arbour, before reaching layer 1 (Larkman, 1991). There were cells with an apical dendrite which tapered off without branching, but it was difficult to detect whether the tuft of the dendrite was removed by slicing cryosections or whether a dendrite did not form a tuft.

The most important finding from the analysis of P21 mice coronal cortex sections was that apical dendrites form Y-shaped branches both in cGKI knock-out and in wild-type mice (Fig. 3.19 C-D), suggesting that cGMP signalling does not regulate branching of apical dendrites in layer V pyramidal cells. Since optical observations did not reveal any changes in branching behaviour of apical dendrites of cortical pyramidal neurons in the absence of cGKI further detailed analysis of dendritic branching was not carried out.

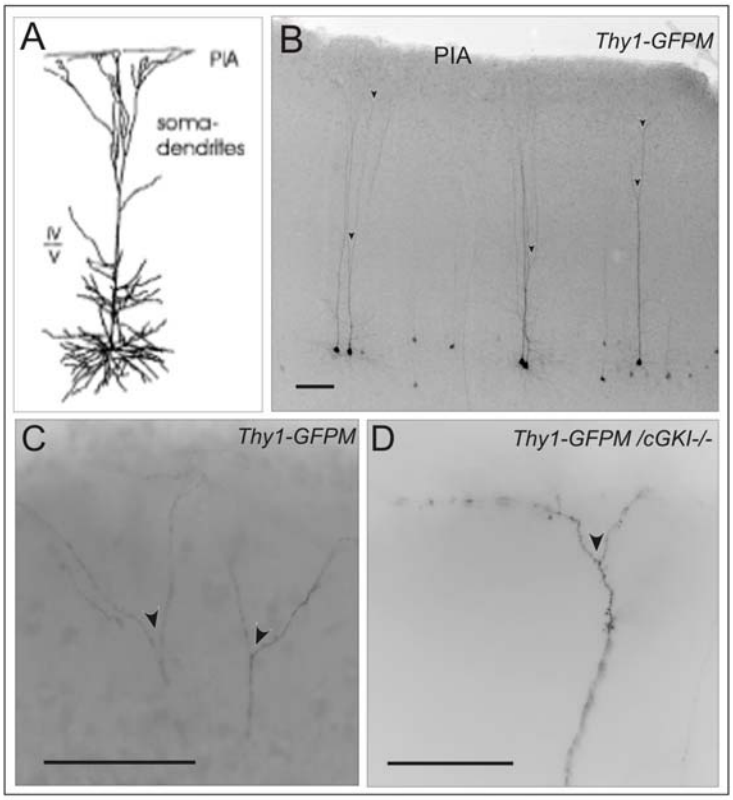

Fig. 3.19: Apical dendrites of layer V pyramidal neurons in the cortex do not differ in cGKI knock-out and wild type mice. Mouse line Thy-1-GFPM was crossed with cGKI knock-out mouse. In coronal sections some of large pyramidal neurons expressing EGFP are observed. (A) Camera lucida drawing from a layer V neuron (Salin et al., 1995) (B) An overview picture of layer V pyramidal neurons in the cortex. (C) Magnified view of several bifurcations in pyramidal neuron apical dendrites of wild type mouse. (D) Magnified view of bifurcation in pyramidal neuron apical dendrite of cGKI knock-out mouse. Bars: (B-D) 100µm. PIA, pial surface. Three wild type and three cGKI knock out mice were analysed

3.2.1.2 Apical and basal dendrites of pyramidal neurons in hippocampus branch in the absence of cGKI

The same Thy-1-GFPM mouse line was crossed with cGKI knock-out mouse line enabling analysis of pyramidal neuron dendrites in the hippocampus. Here, both apical and basal dendrites were analysed.

As in the cortex, apical dendrites of pyramidal neurons in the hippocampus do not branch in a stereotyped pattern. Some of them were observed to bifurcate closer to the soma than others. CA3 pyramidal neurons are reported to bifurcate within stratum radiatum whereas most of CA1 pyramidal neurons usually traverse stratum radiatum, giving off oblique branches, before bifurcating to form an apical tuft (Bannister and Larkman, 1995;Spruston, 2008).

Bifurcations of apical dendrites were observed both in wild-type as well as in cGKI knock-out mice (Fig. 3.20 A-B)

Branching of basal dendrites occurs close to the soma forming shorter processes than apical dendrites. There are several basal dendritic trees emanating from the soma. Therefore, it is more difficult to observe their branching pattern compared to a single apical dendrite. Not all dendrites were observed to bifurcate. However, bifurcations of basal dendrites were observed both in wild-type and cGKI knock-out mice (Fig. 3.20 B-C). Though not quantitatively analysed, these results consolidate my previous assumption that bifurcation of pyramidal cell dendrites is not regulated by cGKI and most likely not by the other known components of the cGMP signalling cascade.

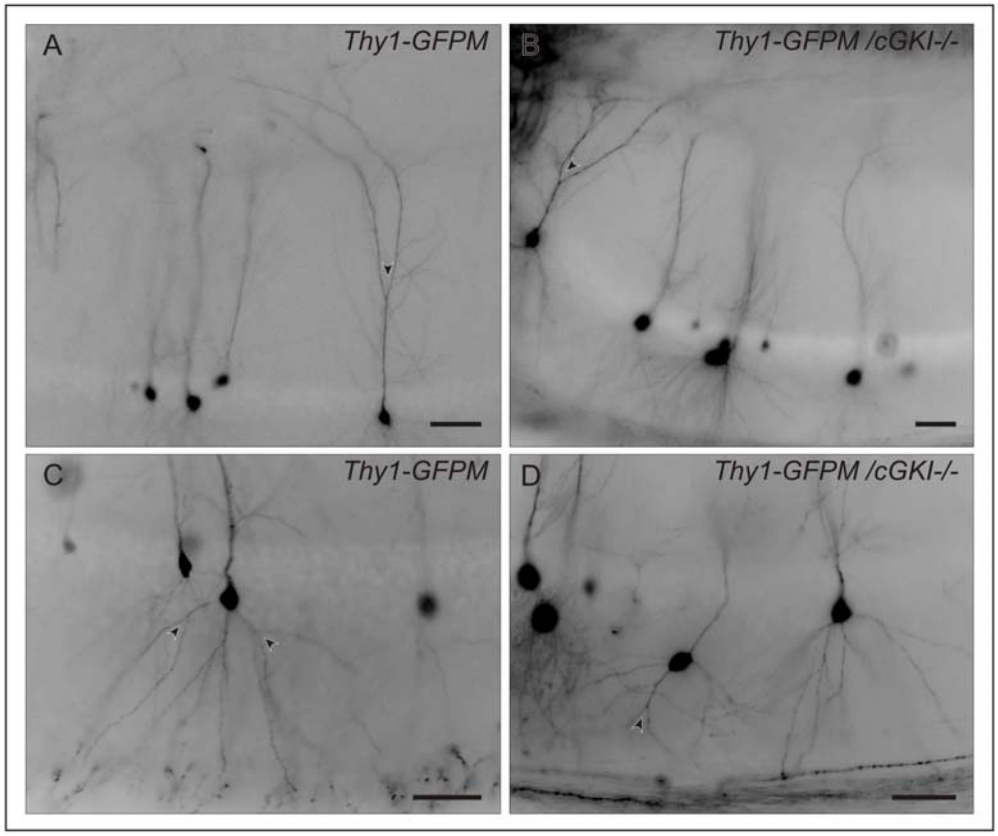

Fig. 3.20: Apical and basal dendrites in hippocampal pyramidal cells bifurcate both in cGKI knock-out and wild type mice. Coronal sections of hippocampus of GFP expressing wild-type and cGKI knock-out mice. In coronal sections GFP under Thy1 promotor expressing pyramidal cells in CA3 region of hippocampus are observed. (A) Apical dendrites in wild-type mouse bifurcate (bifurcation indicated by arrow). (B) Apical dendrites bifurcate in cGKI knock-out mouse as well. (C) Bifurcation of basal dendrites occurs in wild-type mouse. (D) Bifurcation pattern of basal dendrites in cGKI knock-out mouse does not differ from that in wild-type mouse. Bars: (A-D) 100µm.

3.2.2 Central projections of trigeminal ganglion

The trigeminal nerve is the largest of the cranial nerves. Its name derives from the fact that it has three major branches: the ophthalmic nerve, the maxillary nerve, and the mandibular nerve. The three branches converge on the trigeminal ganglion that contains the cell bodies of incoming sensory nerve fibers. The trigeminal ganglion is analogueous to the dorsal root ganglia of the spinal cord, which contain the cell bodies of incoming sensory fibers from the rest of the body. From the trigeminal ganglion, a single large sensory root enters the brainstem at the level of the pons (Fig. 3.21 A-C). Central trigeminal axons fasciculated into one sensory root bifurcate upon entry into brainstem and lay down the ascending and descending components of the trigeminal tract (Fig. 3.21 A). This happens around embryonic day 13 in mouse. Between E13 and E16, central trigeminal axons grow without any collateral formation which starts later (Erzurumlu and Jhaveri, 1995;Hasegawa et al., 2007;Ulupinar et al., 1999;Ulupinar et al., 2000).

Since sensory axons extending from dorsal root ganglia and from trigeminal ganglion have functional similarities (both transmit sensory information to the brain), anatomical similarities (cell bodies are located in ganglia, axons enter spinal cord or brainstem where they bifurcate and after a waiting period send collaterals deeper into spinal cord or brainstem) and both express cGKI one could expect that bifurcation of trigeminal sensory axons is also regulated by cGMP dependent pathway. To test this hypothesis, I analysed DiI labelled trigeminal sensory axons of E13 cGKI knock-out and wild-type mice.

In wild type mice sensory axons bifurcate after reaching the pons and two branches formed by bifurcation grow in opposite directions forming ascending and descending trigeminal tracts (Fig. 3.21 D). In cGKI knock-out mice sensory axons do not bifurcate in the lateral pons region, they turn either towards spinal cord and form descending trigeminal tract or turn towards cortex and form ascending trigeminal tract (Fig. 321 E). Quantification of observed bifurcations and turns is presented in the table 3.6.

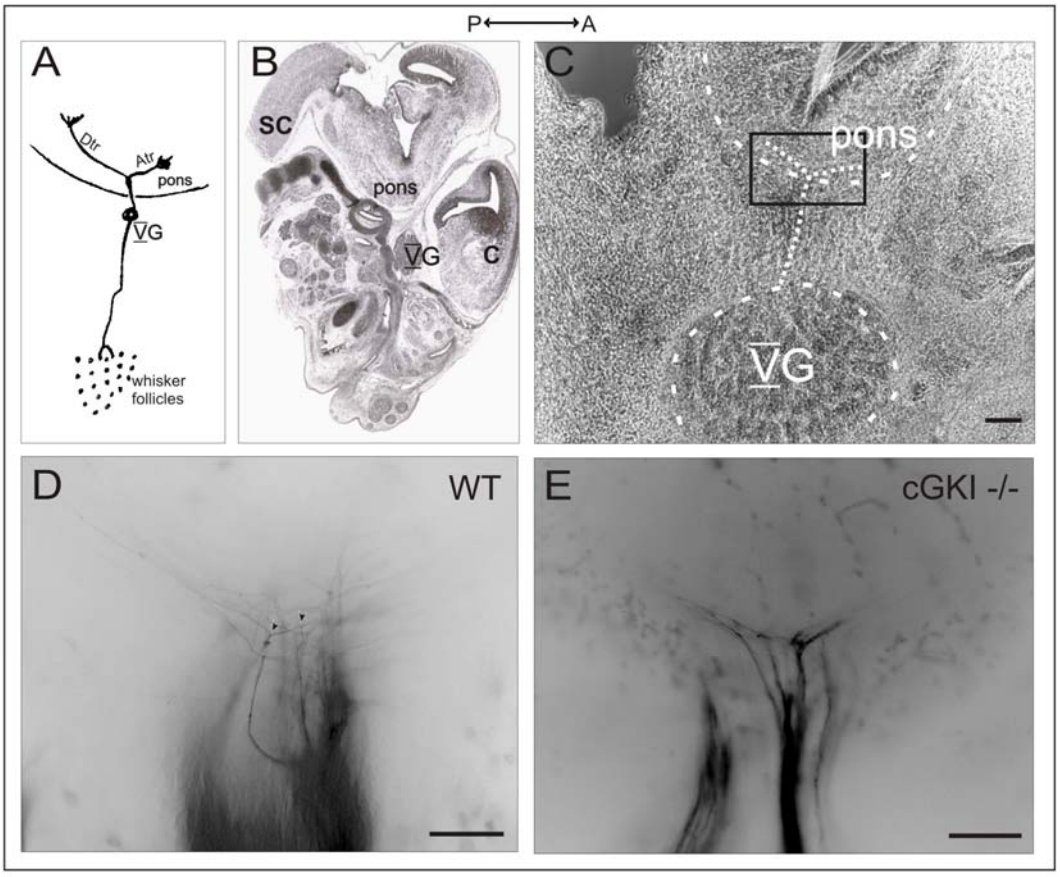

Fig. 3.21: DiI labelled trigeminal sensory axons bifurcate upon reaching the brainstem in wild-type mice but fail to bifurcate in cGKI knock-out mice. Trigeminal ganglia in sagital vibrosections of E13 cGKI knock-out and wild-type mice were labelled with DiI and projections of sensory axons were analysed. (A) Schematic illustration of trigeminal neuron. Trigeminal cell bodies are in trigeminal ganglion, from here trigeminal axons grow in the direction of pons and after reaching it bifurcate producing ascending and descending axonal tracts. (adjusted from (Ulupinar et al., 2000)) (B) Sagital section of mouse brain (Schambra et al., 1991). The illustration is in the same direction as previous schematic drawing. Locations of trigeminal ganglion and pons are indicated. (C) Trigeminal ganglion is easily detectable under the light microscope. DiI labelling of trigeminal ganglion was carried out touching the ganglion with capillary pipette coated with tiny DiI crystals under the light microscope. White dashed lines mark the borders of pons and trigeminal ganglion. White dotted line represents trigeminal axon pathway. Boxed area marks the area of the photos of DiI labelled axons that are presented below (D-E). (D) DiI labelled trigeminal sensory neurons bifurcate (arrowheads) in the pons and form ascending and descending tracts. (E) DiI labelled trigeminal sensory neurons turn either towards ascending or descending tract. Bars: (B) 100µm; (C-D) 50µm. SC – spinal cord; VG – trigeminal ganglion; C – cortex; Dtr – descending tract; Atr – ascending tract. Direction in all pictures is anterior (A) to the left side and posterior (P) to the right side.

Table 3.6: Quantification of bifurcating and turning trigeminal axons in wild type and cGKI knock-out embryos

	Number of embryos	Caudal turns (in posterior direction)	Rostral turns (in anterior direction)	Bifurcations
Wild type	5	-	-	12
cGKI knock-out	4	13	9	-

3.3 Analysis of the role of known or putative phosphorylation targets of cGKI in the bifurcation of sensory axons

Analysis of mutant mice described in previous chapters demonstrated that sensory axon bifurcation is regulated by cGMP signalling. CNP was found to be an upstream activator of Npr2, which generates cGMP, and cGMP activates cGKI. All three cGMP signalling components - CNP, Npr2 and cGKI - are crucial for the sensory axon bifurcation. Downstream target(s) of cGKI that would play a role in sensory axon bifurcation are not known yet. I addressed this question using two different approaches: I searched for new phosphorylation targets of cGKI (described in chapter 3.4) and I analysed known phosphorylation targets of cGKI in regard to their role in sensory axon bifurcation.

cGKI is a well studied kinase having many known, described phosphorylation targets (for a review see (Hofmann et al., 2009;Schlossmann and Desch, 2009)). Moreover it is known that some phosphorylation targets of cGKI are important in different cell types, e.g. BK_{Ca} in kidney is implicated in contractility of mesangial cells, in reproductive system it plays a major role in penile erection, and in Purkinje cells BK_{Ca} is critical factor for cell activity (Schlossmann and Desch, 2009). Hence, I decided to analyse some known phosphorylation targets of cGKI that could play a role in sensory axon bifurcation. First of all I chose to analyse those phosphorylation targets that were known to regulate cytoskeleton because branching of axons involves cytoskeleton rearrangement.

3.3.1 Analysis of the role of Mena and VASP proteins in sensory axon bifurcation

Vasodilator stimulated phosphoprotein (VASP) and mammalian enabled (Mena) together with Ena-VASP like protein (EVL) belong to the Ena/VASP protein family. Members of this family are involved in actin dynamics and cell motility. They can bind directly to both monomeric and filamentous actin and promote in vitro actin filament nucleation, bundling and elongation in the presence of capping proteins. Phosphorylation of Ena/VASP proteins makes them sensitive to capping proteins. All Ena/VASP proteins can be phosphorylated by cAMP dependent kinase. (Breitsprecher et al., 2008;Krause et al., 2002;Krause et al., 2003;Kwiatkowski et al., 2003)

3.3.1.1 Absence of VASP does not have an effect on sensory axon bifurcation at the dorsal root entry zone

VASP is the only Ena/VASP family member shown to be phosphorylated not only by PKA but by cGKI as well. Most of studies on VASP and its phosphorylation were carried out in human platelets (Halbrugge and Walter, 1989). Our group looked whether VASP is phosphorylated by cGKI in DRG as well. The findings showed that indeed, VASP became phosphorylated upon stimulation of cGK in embryonic DRG of wild-type mice but not in embryonic DRG of cGKI knock-out mice, indicating that VASP was phosphorylated by cGKI (Schäffer, 2005).

Since VASP is a downstream target of cGKI and is known to play a role in actin dynamic processes it was a promising candidate to be involved in sensory axon bifurcation at the dorsal root entry zone. In order to test this, I analysed DiI labelled sensory axons in VASP knock-out mouse embryos. However, DiI labelling revealed that absence of VASP does not have any effect on sensory axon bifurcations. As figure 3.22 shows, sensory axons in VASP knock-out mouse embryos do not have any abnormal growth pattern at the dorsal root entry zone. Quantification of bifurcating and turning sensory axons also indicates that there is no bifurcation error in VASP knock-out mouse embryos: 98.8% of all observed axons bifurcate and only 1.2% turn either rostrally or caudally (Fig. 3.23). This allows to conclude that either VASP does not play any role in sensory axon bifurcation despite the fact, that it is phosphorylated by cGKI, or that other members of Ena/VASP family can replace VASP and carry out its functions.

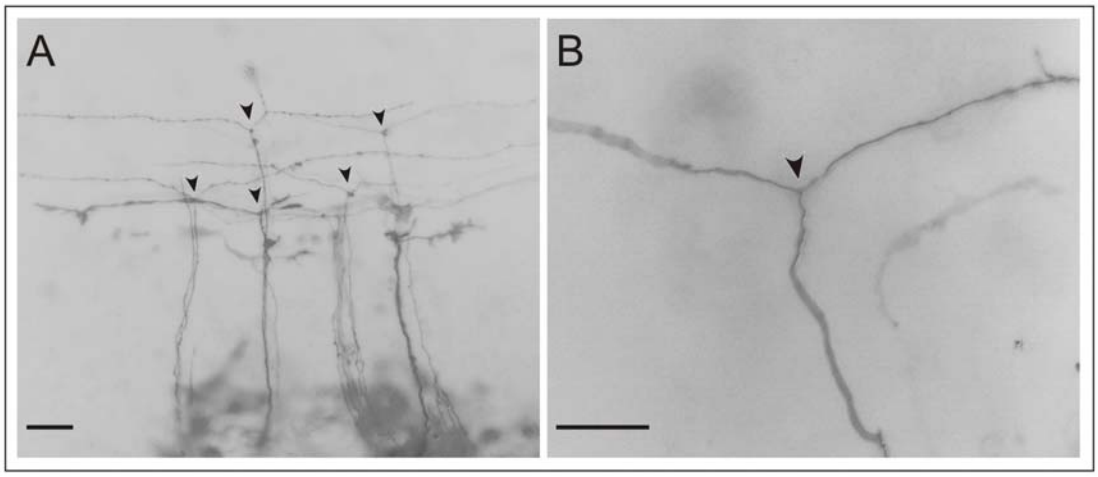

Fig. 3.22: Sensory axons in VASP knock-out mice bifurcate. (A) Overview picture of bifurcating sensory axons labelled with DiI in E12 VASP knock-out mouse embryo. (B) Higher magnification of single DiI labelled

sensory axon bifurcation in VASP knock-out mouse embryo. Scale bar: (A-B) 50 µm. Bifurcation points are indicated by arrowheads.

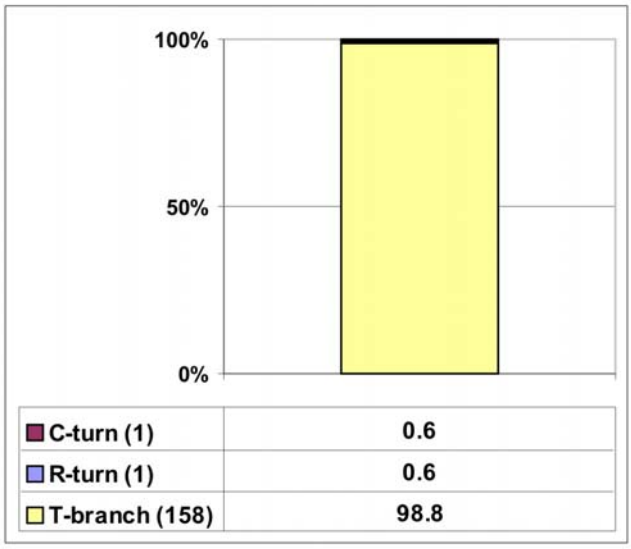

Fig. 3.23: Quantification of DiI-labelled bifurcations and turns in VASP knock-out mice . Percentage values are indicated in the table below the percentage graph. Number of observed sensory axons is given in the brackets. VASP knock-out mice are bred as homozygous mutants, therefore, all analysed littermates are knock-out and comparison with wild-type littermates is absent. 11 knock-out mouse embryos E13 were analysed.

3.3.1.2 Phosphorylation of Mena by cGKI in dorsal root ganglia

The three members of Ena/VASP family are highly related, have overlapping activities and might substitute each other, therefore, I analysed another member of the Ena/VASP family – Mena and its role in sensory axon bifurcation. Mena has three isoforms, the 140 kDa form produced by the alternate inclusion of an axon (the [+] axon) and two other forms migrating at 80 and 88 kDa. In vitro translation of the Mena cDNA results in 80 kDa form, the most broadly expressed form of Mena. Translation of Mena cDNA from neural cells results in the 140 kDa Mena form. This Mena isoform, also called Mena (+), is enriched in the developing nervous system. No cDNA of Mena that would account for the 88 kDa isoform was found which suggests that it might be a posttranslationally modified form of Mena (Gertler et al., 1996;Lanier et al., 1999).

All Ena/VASP family members are phosphorylated by cAMP dependent kinase but only VASP was shown to be phosphorylated by cGKI as well (Halbrugge and Walter, 1989). I

analysed whether Mena can be phosphorylated by cGKI in DRG. Phosphorylation shifts mobility of the 80kDa isoform of Mena to the slower migrating form (Gertler et al., 1996).
I stimulated E13 C57/Bl6 mouse DRG with the cGMP analogue 8-pCPTcGMP for 5 minutes and analysed the phosphorylation of Mena. Anti-Mena Western blot with both stimulated and not stimulated DRG lysates shows (Fig. 3.25 A,C), that mobility of Mena shifts after the stimulation with 8-pCPTcGMP which implies presence of phosphorylation.

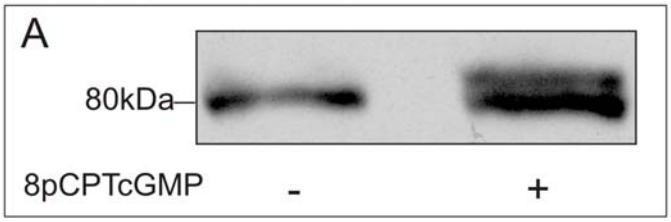

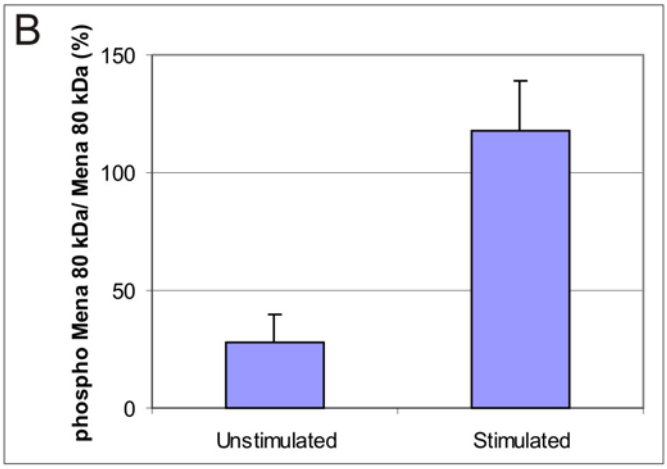

	Unstimulated	Stimulated
Average	0.3	1.2
Number of analysed WB	3	3
Standard deviation	0.2	0.4
Standard error	0.1	0.2
Minimum	0.22	0.75
Maximum	0.45	1.44
p-value	0.052	

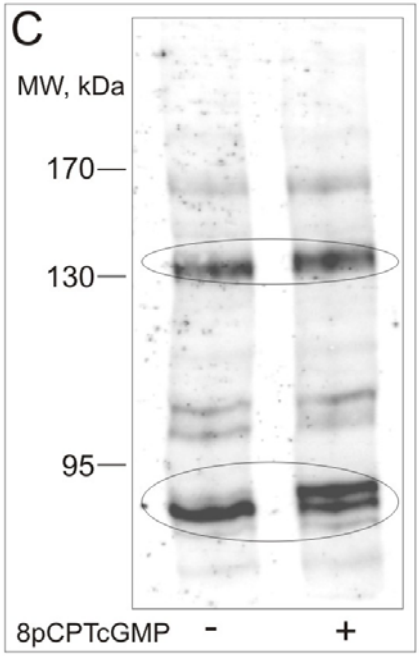

Fig. 3.24: Phosphorylation of Mena by cGKI in DRG. (A) A part of anti-Mena Western blot analysis of lysates prepared from E13 C57/Bl6 mouse DRG with or without stimulation with 8-pCPTcGMP for 5 min at 37°C. Shift in mobility of 80 kDa Mena is observed after stimulation with 8-pCPTcGMP indicating phosphorylation of Mena. (B) Quantification of band intensities from anti-Mena Western blot analyses of 3 independent preparations and statistical analysis. Amount of phosphorylated Mena rises more than twice after stimulation of cGKI with 8-pCPTcGMP. The table shows statistical indicators of Western blot evaluations. The difference in Mena phosphorylation between stimulated and not stimulated samples is significant at p=0.05 (Student's t-test, two-tailed, heteroscedastic). (C) Anti-Mena Western blot analysis of E13 C57/Bl6 DRG lysates. In the whole blot not only 80 kDa band which changes its mobility after cGKI stimulation with 8-pCTPcGMP is observed but also the 140 kDa Mena isoform (both are encircled).

Quantification of ratios between intensities of phospho-Mena and Mena bands between unstimulated and stimulated samples shows that this ratio significantly increases ($p=0.05$, Student's t-test) after stimulation of cGKI with 8-pCPTcGMP (Fig. 3.24 B) which suggests that Mena is phosphorylated by cGKI.

3.3.1.3 Absence of both Mena and VASP does not have an effect on sensory axon bifurcation at the dorsal root entry zone

Both Mena and VASP can be phosphorylated by cGKI. Moreover, they are closely related proteins and might substitute each other. Such similarity of both proteins supports the assumption that even if VASP plays a role in sensory axon bifurcation, VASP knock-out mouse could have a normal phenotype regarding sensory axon bifurcation because absent VASP is substituted by Mena in knock-out mouse. In order to explore this hypothesis I analysed double Mena/VASP knock-out mice. These mice die perinatally and display defects in neurulation, craniofacial structures and the formation of several fiber tracts in the CNS and peripheral nervous system (Menzies et al., 2004). First, I analysed whole mount stainings with anti-neurofilament of E10 embryos in order to confirm the described abnormalities. Although DRG of double knock-out mice develop normally, the axons extending from DRG which comprise the sensory and spinal branches of spinal nerves do not converge at the forelimb level to form the branchial plexus as it can be observed in Figure 3.25.

I labelled sensory axons in embryos of Mena/VASP double knock-out mouse (E12) and analysed their growth pattern at the dorsal root entry zone. There is no sensory axon bifurcation error in mice lacking both Mena and VASP (Fig. 3.26). Almost 97% of all observed sensory axons bifurcate and only the rest 3% were observed turning either caudally or rostrally (Fig. 3.27). These results imply that Mena and VASP are not crucial for sensory axon bifurcation, although they are phosphorylated by cGKI in DRG.

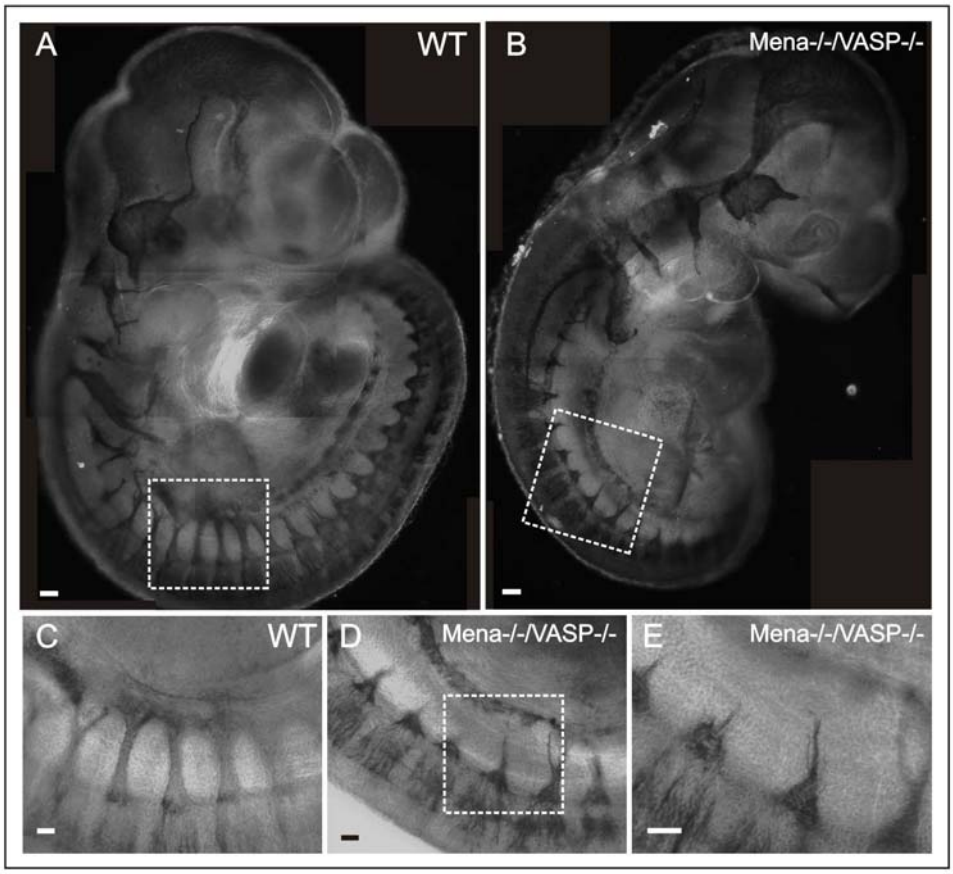

Fig. 3.25: Spinal nerves in Mena/VASP knock-out mouse embryos fail to extend. (A) Overview picture of whole-mount wild-type mouse embryos (E10.5) anti-neurofilament staining. (B) Overview picture of whole-mount Mena/VASP mouse embryos (E10.5) anti-neurofilament staining. (C) Magnified view of box area in (A) where converged spinal nerves in wild-type mouse are observed. (D) Magnified view of boxed area in (B). Spinal nerves in Mena/VASP knock-out mouse have failed to extend. (E) Magnified view of boxed area in (D). Scale bar: (A-B) 100µm; (C-E) 50µm

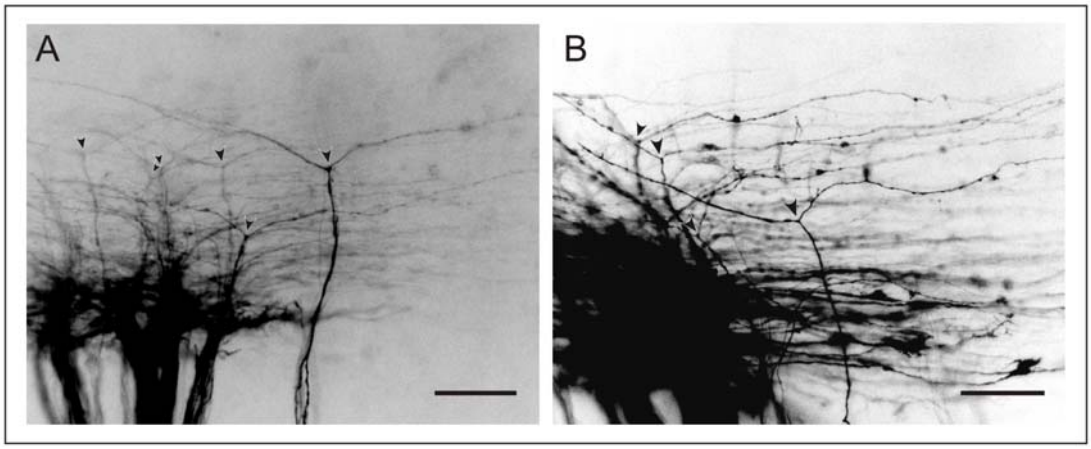

Fig. 3.26: Sensory axons in Mena/VASP knock-out mice bifurcate. (A-B) Both pictures represent DiI labelled sensory axons of double Mena/VASP knock-out mouse embryos (E12). Sensory axons bifurcate (pointed with arrowheads) even in the absence of both Mena and VASP. Scale bar: 50 µm.

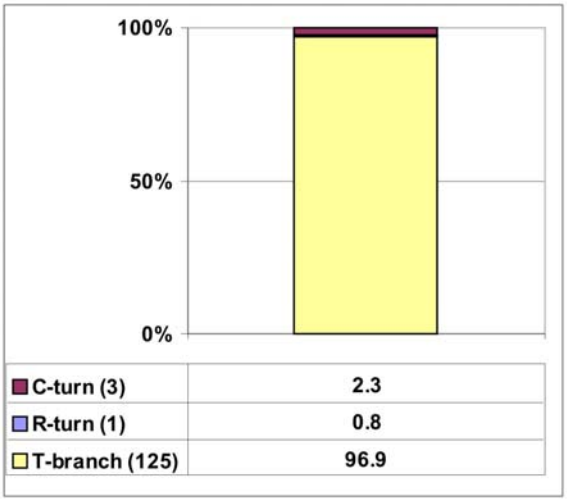

Fig. 3.27: Quantification of DiI-labelled bifurcations and turns in Mena/VASP double knock-out mice. Percentage values are indicated in the table next to the percentage graph. 5 knock-out embryos E13 were analysed.

3.3.2 Analysis of the role of glycogen synthase kinase 3-β (GSK3-β) in sensory axon bifurcation

3.3.2.1 GSK3-β becomes phosphorylated in DRG and sensory axons of DRG but not in the DRG derived cell line F11 upon stimulation of cGKI

GSK-3 is a serine/threonine kinase originally identified as a kinase phosphorylating glycogen synthase, downstream of insulin signalling. Later it was shown that GSK-3 is a key downstream regulator in signalling pathways triggered by many extracellular cues including Wnts, NGF, EGF and hedgehog. GSK3 is involved in axon growth, branching since it regulates microtubule growth and stability phoshorylating many microtubule associated proteins such as tau, MAP1b, CRP-2 or APC. GSK3 has a high basal kinase activity. Inactivation is achieved by phosphorylation of Ser 9 (in GSK-3β isoform) or on Ser 21 (in GSK3-α isoform) (Cohen and Frame, 2001;Doble and Woodgett, 2003;Garrido et al., 2007;Kim et al., 2006;Zhou et al., 2004). Recently it has been shown that cGKI phosphorylates GSK3 in cultured rat DRG neurons (Zhao et al., 2009) and cGKII phosphorylates GSK3-β in murine chondrocytes (Kawasaki et al., 2008). The role of GSK3 in axonal growth and microtubule dynamics together with the fact that it is a downstream target of cGKI suggested that GSK3 might be a crucial downstream component of the cGMP signalling cascade regulating axon bifurcation.

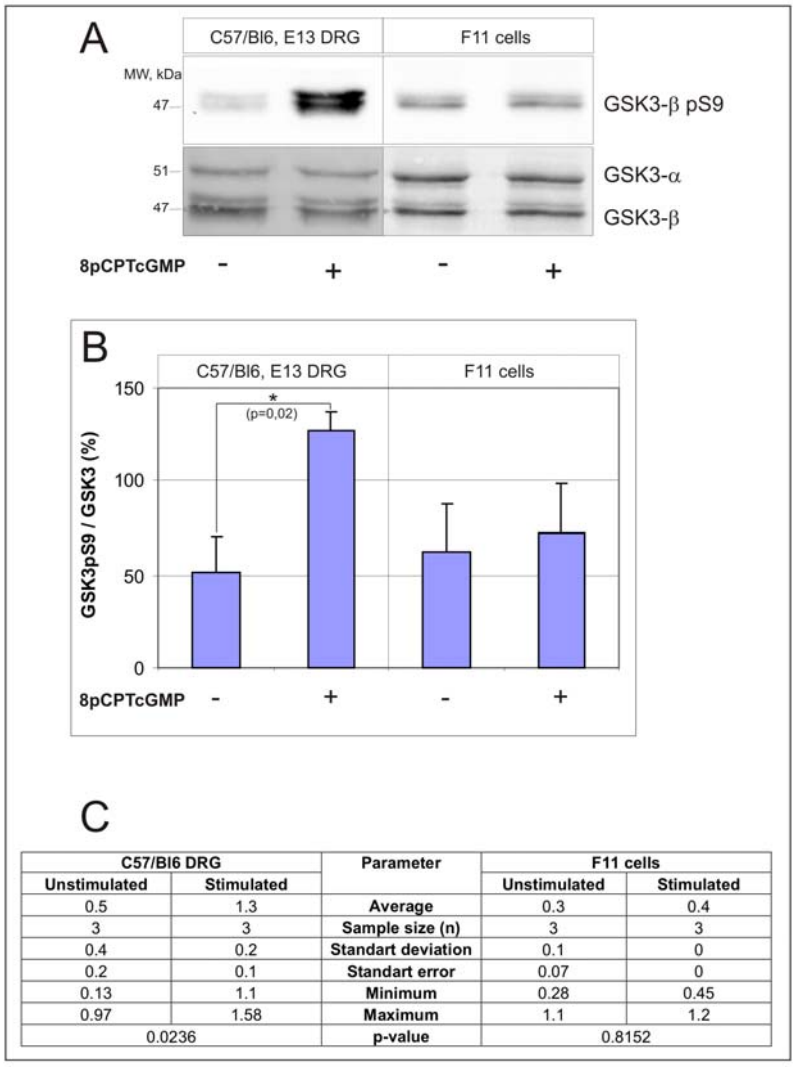

C

C57/Bl6 DRG		Parameter	F11 cells	
Unstimulated	Stimulated		Unstimulated	Stimulated
0.5	1.3	Average	0.3	0.4
3	3	Sample size (n)	3	3
0.4	0.2	Standart deviation	0.1	0
0.2	0.1	Standart error	0.07	0
0.13	1.1	Minimum	0.28	0.45
0.97	1.58	Maximum	1.1	1.2
0.0236		p-value	0.8152	

Fig. 3.28: Phosphorylation of GSK3 upon cGKI stimulation in DRG and in F11 cells. (A) Anti-GSK3 and anti-phospho-GSK3β Western blot analysis of lysates made from E13 C57/Bl6 embryonic mouse DRG with or without stimulation with 8-pCPTcGMP for 5 min. Both Western blot analyses were performed on the same nitrocellulose membrane using different secondary antibodies (goat anti rabbit HRP for anti-phospho- GSK3β and goat anti mouse AP for anti GSK3). Remarkable increase in intensity of phospho-GSK3β band is observed in DRG lysate after cGKI stimulation whereas no phosphorylation takes place in F11 cells. (B) Quantification of band intensities from 3 anti-GSK3 and anti-phospho-GSK3β Western blots and statistical analysis. There is a more than double increase in GSK3β phosphorylation in DRG after stimulation of cGK with 8-pCPTcGMP whereas there is no difference in GSK3β phosphorylation in stimulated and not stimulated F11 cells. (C) The table shows statistical indicators of Western blots evaluation. The difference in GSK3β phosphorylation between stimulated and not stimulated DRG samples is significant at $p<0.02$ (Student's t-test, two-tailed, heteroscedastic) whereas there is no significant difference in GSK3β phosphorylation in F11 cells.

I analysed whether GSK-3 becomes phosphorylated in E13 mouse DRG upon stimulation of cGKI. Freshly isolated DRG from E13 embryos were stimulated for 5 min with the cGMP

analogue 8-pCPTcGMP. Lysates from control DRG and stimulated DRG were analysed by anti-p-GSK3-β(Ser9) and anti-GSK3 Western blots. Indeed, intensity of phospho-GSK3-β band significantly increases ($p<0.05$) after stimulation of cGKI in DRG (Fig.3.28) which implies that cGKI phosphorylates GSK3-β.

I also tested whether GSK3-β is phosphorylated in the DRG derived cell line F11. The F11 cell line is a fusion product of mouse neuroblastoma cell line N18TG-2 with embryonic rat DRG neurons. F11 cells express cGKIα and cGKII as well as GSK3. However, although both cGKI and its alleged target are present, GSK3 is not phosphorylated in F11 after stimulation of cGKI. Fig. 3.28 A-B depicts similar phospho-GSK3-β band intensities in stimulated as well as unstimulated samples. This unexpected result could be explained in several ways: either GSK3-β is not a direct target of cGKI and some link protein which is missing in F11 cells is required or cGKI and GSK3-β are not able to get into a close contact because they are in different cell compartments in contrast to DRG.

Stimulation of cGKI in embryonic DRG results in GSK3-β phosphorylation. GSK3-β acts on microtubules and thereby regulates axonal growth and branching. If inactivation of GSK3-β upon cGKI stimulation would be related to cytoskeleton rearrangements and thereby to axonal bifurcation, it is most likely that GSK3-β would be phosphorylated in the sensory axons and their growth cones. However, when DRG are isolated sensory axons are cut and only part of them are included into DRG lysate. Majority of the material in the DRG lysate is constituted by cell bodies of DRG neurons but not by axons themselves. To determine whether GSK3-β phosphorylation takes place in the sensory axons I analysed anti-phospho-GSK3-β immunostainings of transverse sections of spinal cord that was stimulated with 8pCPTcGMP (fig. 3.29).

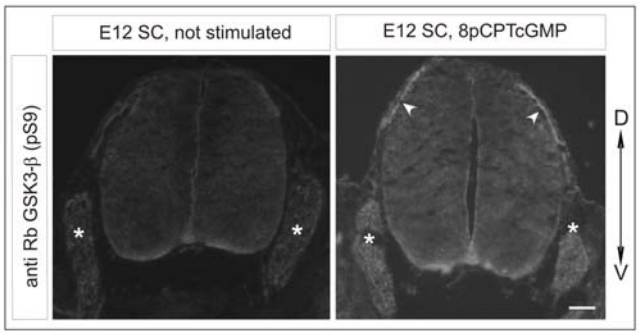

Fig. 3.29: Phosphorylation of GSK3-β by cGKI in the spinal cord. Immunostaining of transversal spinal cord sections with anti-phospho-GSK3β shows that after stimulation of cGKI with 8-pCPTcGMP not only GSK3β in DRG but especially in sensory axons of DRG that have reached dorsal root entry zone (indicated by

arrowheads) becomes phosphorylated. Ventral part of the spinal cord is recognized by anti-phospho-GSK3-β both in not stimulated and 8-pCPTcGMP stimulated spinal cord suggesting that phosphorylation and inactivation of GSK3-β in ventral part of spinal cord is independent and takes place before cGKI stimulation. DRG are indicated by asterisks. Scale bar: 100μm.

Immunostainings of transverse spinal cord sections with anti-phospho-GSK3-β disclosed that GSK3-β becomes phosphorylated and inactivated in sensory axons upon stimulation of cGKI. This finding confirms results obtained by anti-phospho-GSK3-β Western blotting analysis of DRG lysates and suggests that phosphorylation and inactivation of GSK3-β upon cGKI activation in sensory axons might play a role in sensory axon bifurcation.

3.3.2.2 Mutation preventing phosphorylation of GSK3 does not have an effect on sensory axon bifurcation at the dorsal root entry zone

GSK3 regulates microtubule growth and stability, since many of its substrates are microtubule associated proteins (Garrido et al., 2007;Kim et al., 2006). Phosphorylation and inactivation of GSK3 is necessary for growth cone dynamics (Eickholt et al., 2002). Zhao et al. suggested that it enables branching capacity of DRG axons after cGKI stimulation (Zhao et al., 2009). Finding that GSK3 is a downstream target of cGKI, moreover becomes phosphorylated and inactivated in sensory axons, together with its described role in axon branching suggests that GSK3-β knock-out mouse might have errors in sensory axon bifurcation. However, analysis of GSK3-β knock-out mouse is aggravated by the fact that hepatocytes of GSK3-β embryos start to undergo apoptosis at E13.5, as a result embryos are pale and non-viable. Finally, they die due to severe liver degeneration (Hoeflich et al., 2000).
Study of GSK3-β phosphorylation in embryonic mouse DRG suggests that GSK3-β is phosphorylated and thereby inactivated when cGMP signalling is active, i.e. during the time when sensory axons are bifurcating. Mouse having mutated GSK3-β which can not be phosphorylated and, therefore, should be constantly active, would allow to explore whether phosphorylation and inactivation of GSK3-β is crucial for sensory axon bifurcation With this intent I analyzed sensory axons in GSK3 double knockin mouse. This mouse has constitutively active mutated GSK3-α and -β isoforms (Ser21 in GSK3-α and Ser9 in GSK3-β were changed to alanine) (McManus et al., 2005). If phosphorylation of GSK3-β by cGKI would be important for sensory axon bifurcation, these mice would have mutant phenotype with rostral and caudal turns instead of bifurcations, since GSK3-β as well as GSK3-α cannot

be phosphorylated. However, DiI tracing of sensory axons in GSK3 double knock-in mouse embryos revealed normal phenotype: sensory axons bifurcate, there are almost no rostral or caudal turns (Fig. 3.30). Quantification of observed DiI labelled bifurcations and caudal or rostral turns proves that bifurcation of sensory axons in GSK3 double knockin mouse is not affected – almost 99% of all observed sensory axons bifurcate (Fig. 3.31). This result suggests that phosphorylation of GSK3 and its inactivation does not play a crucial role in sensory axon bifurcation.

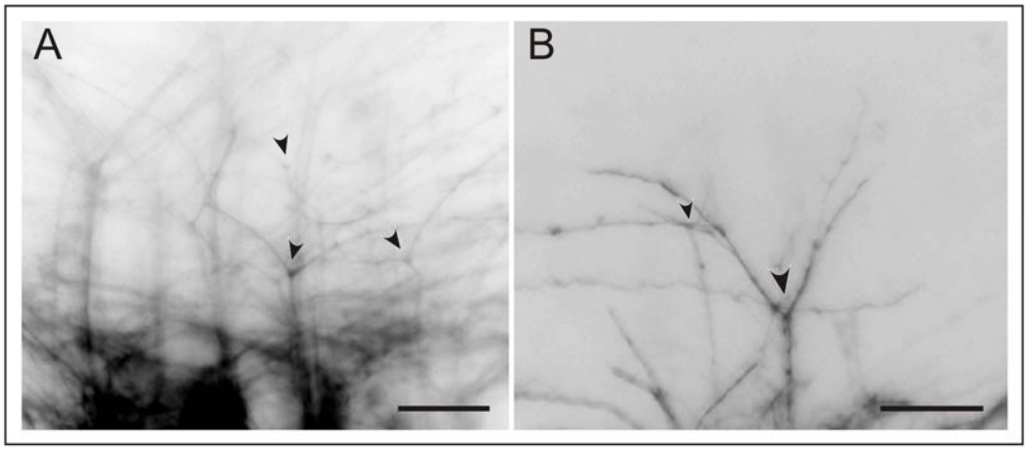

Fig. 3.30: Sensory axons in GSK3 double knock-in mouse embryos bifurcate. (A-B) DiI labelled sensory axons in E13 mouse embryos with constitutively active GSK-3. Sensory axons bifurcate even when GSK3 is active and cannot be inactivated by phosphorylation. Scale bar: (A-B) 50 μm.

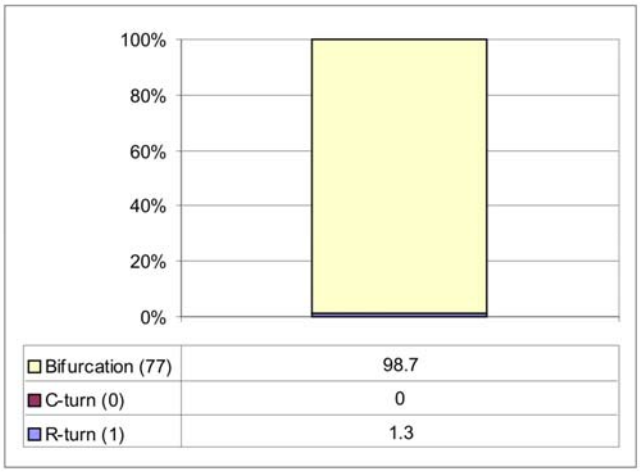

Fig. 3.31: Quantification of DiI-labelled bifurcations and turns in GSK3 double knock-in mice. Percentage values are indicated in the table next to the percentage graph. Number of observed bifurcated or turning sensory axons is given in brackets. Three E13 GSK3 double knock-in mouse embryos were analysed.

Immunostainings with anti-L1 and anti-trkA on transverse sections of E13 GSK3 double knockin mouse showed that spinal cord anatomy is normal in mice with constitutively active GSK3 (Fig. 3.32).

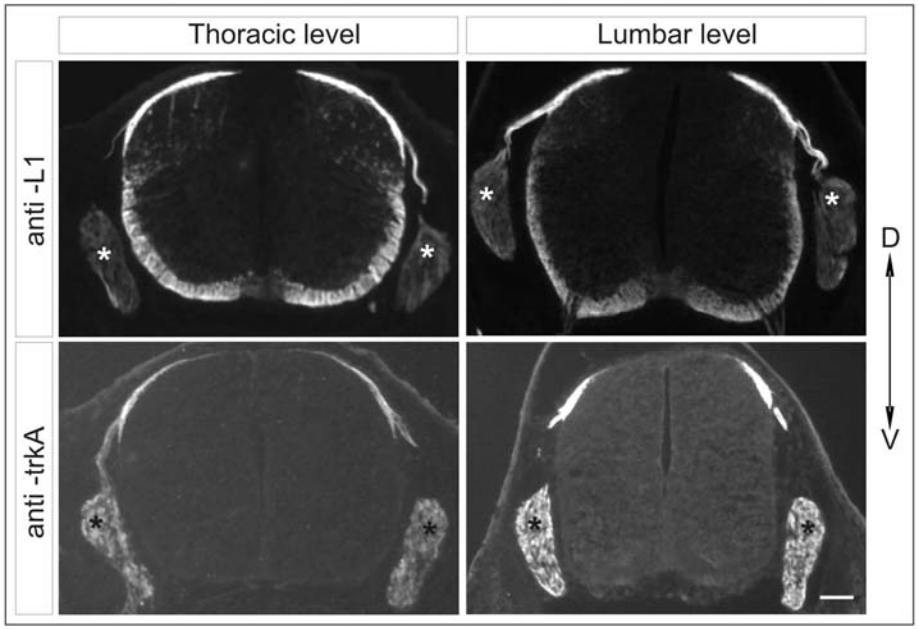

Fig. 3.32: Immunostaining of transverse spinal cord section from E13 GSK-3 double knock-in mice. General axonal marker anti-L1 as well as anti-trkA which stains a subset of DRG neurons, namely, nociceptors, do not reveal any abnormalities. DRG are marked with asterisks. Scale bar: 100µm.

3.3.3 RhoA is not a downstream target of cGKI in DRG

Rho GTPases transduce extracellular signals to the actin cytoskeleton and therefore are involved in the neuronal growth cone motility, axon growth and cell migration (Heasman and Ridley, 2008;Linseman and Loucks, 2008). Typically, activity of Rho GTPases is controlled by guanine nucleotide exchange factors (GEFs) and GTPase activating proteins (GAPs). However it can be regulated also through direct phosphorylation or ubiquitination (Heasman and Ridley, 2008;Jaffe and Hall, 2005). One of the best studied Rho GTPases is RhoA. Several reports demonstrated that cGK phosphorylates RhoA *in vitro* (Sauzeau et al., 2000;Sawada et al., 2001). Moreover, cGK phosphorylates and inhibits RhoA in vascular myocytes (Sawada et al., 2009).

I analysed whether stimulated cGK phosphorylates RhoA in DRG. RhoA is detected in DRG as expected, but there is no phosphorylation of RhoA observed after stimulation of cGKI with 8-pCPTcGMP for 5 min at 37^{o}C (Fig.3.33).

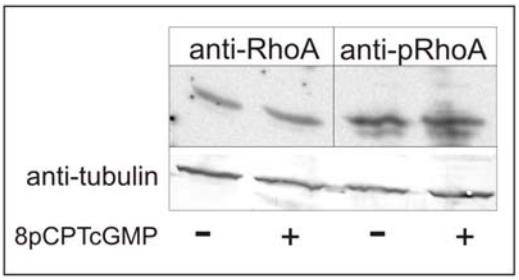

Fig. 3.33: RhoA and pRhoA in C57/Bl6 mouse DRG. DRG were stimulated with 10mM 8-pCPTcGMP for 5 min. Intensity of phosphorylated RhoA band does not change after stimulation of cGKI.

Investigators who studied RhoA phosphorylation by PKA claim that cellular RhoA is present in the cytosol and membrane. Cytosolic RhoA is bound to GDP dissociation inhibitor (GDI) which masks the phosphorylation site. Only membrane-bound RhoA, which is in a GTP state and free from GDI can be phosphorylated. Phosphorylation of RhoA increases its association with GDI which leads to extraction of RhoA from the membrane (Forget et al., 2002;Lang et al., 1996). I analysed subcellular localization of RhoA in DRG with or without addition of 8-pCPTcGMP in order to see whether RhoA becomes depleted from the membrane fraction and enriched in cytoplasmatic fraction after cGKI stimulation. I did not observe any differences in cytoplasmatic or membrane RhoA before and after cGKI stimulation (Fig. 3.34), which suggests that in DRG RhoA does not become phosphorylated upon stimulation of cGKI.

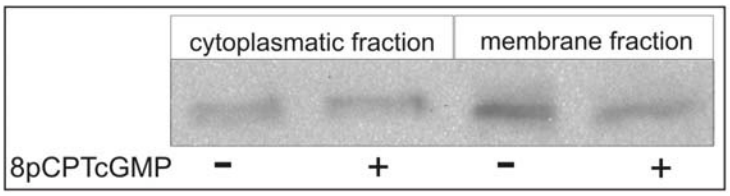

Fig. 3.34: Subcellular RhoA distribution in DRG before and after cGK stimulation. No translocation of RhoA is observed after stimulation of cGK with 8-pCPTcGMP for 30 min.

Both anti-phospho RhoA (S188) Western blot and analysis of subcellular localization before and after cGKI stimulation did not demonstrate RhoA phosphorylation by cGKI in DRG.

3.3.4 Myosin IIB is not required for sensory axon bifurcation

Myosins are involved in the retrograde F-actin flow, a process fundamental to growth cone guidance and other forms of directed cell motility (Lin, 1996). Myosin II is the main myosin subtype responsible for the retrograde actin flow (Medeiros, 2006). There are three isoforms of nonmuscle myosin II expressed by mammalian neurons: myosin IIA, IIB and IIC (Brown, 2004). Myosin IIB is the most abundant myosin II form in growth cones, therefore, it dominates in influencing retrograde flow. Neurons grown in cell culture from a myosin IIB knock-out mouse exhibited slowed outgrowth rates but significantly increased retrograde actin flow, their growth cones showed altered actin organization, size and motility. Increased retrograde actin flow affects microtubules as well – they penetrate less into actin-rich filopodia. In the absence of myosin IIB, myosin IIA takes over all the functions and the increased rate of retrograde flow mainly reflects the properties of this myosin (Brown, 2003). Myosin is regulated mainly through the phosphorylation of the regulatory myosin light chain (MLC). It can be phosphorylated by Ca^{2+}/calmodulin dependent myosin light chain kinase (MLCK) (Brown, 2004). Or it can be dephosphorylated by myosin phosphatase (Lontay, 2005). Both processes are regulated by cGKI. cGKI can change calcium concentration by regulating its release from the intracellular calcium stores via phosphorylation of IP_3R and by regulating influx of calcium via phosphorylation of the L-type Ca^{2+} channel (Hofmann, 2009). cGKI can also regulate activity of the myosin phosphatase by phosphorylating its myosin phosphatase target subunit (MYPT1). Phosphorylation of MYPT1 by cGKI blocks inhibition of the myosin phosphatase (Lontay, 2005;Surks, 1999).

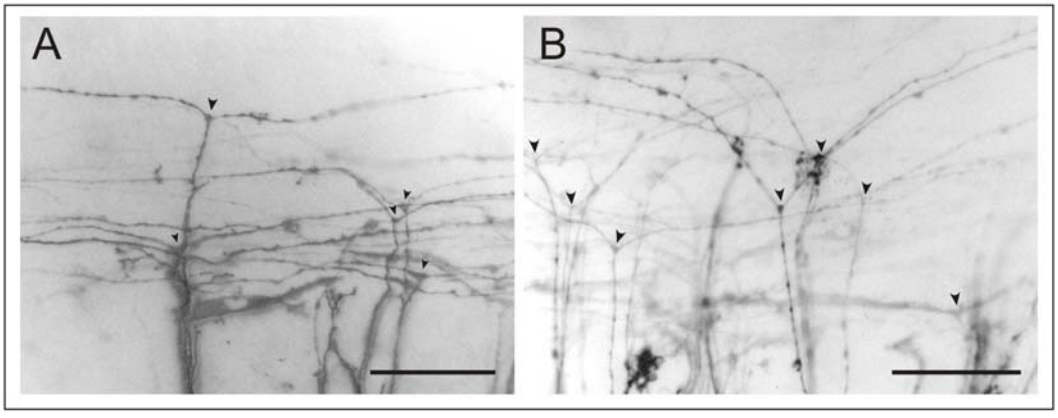

Fig. 3.35: Sensory axons bifurcate in Myo IIB knock-out mouse. (A-B) Sensory axons of E13 Myo IIB knock-out embryos labelled with DiI. Scale bar: (A-B) 50 µm.

Although myosin IIB is not a direct target of cGKI, it is indirectly regulated by cGKI activity. Myosin IIB plays an important role in retrograde flow of actin cytoskeleton which also affects microtubules. This suggests that myosin IIB might be required for the sensory axon bifurcation. To test this assumption, I analysed a myosin IIB knock-out mouse. This mouse was already investigated by the group of F.Rathjen using whole-mount neurofilament staining. There were no defects in sensory axon bifurcation detected (Schäffer, 2006). I used DiI tracing to analyse single sensory axons (Fig. 3.35). Although quantitative analysis was not carried out, observed DiI labelled bifurcating axons confirmed the results of the previous study, suggesting that Myo IIB is not required for the sensory axon bifurcation. This result leads to an assumption that the regulation of the myosin system by cGKI is not crucial for the sensory axon bifurcation.

3.4 Search for new cGK targets in DRG

Investigation of known and putative phosphorylation targets of cGKI revealed that VASP, Mena, GSK3-β, are indeed phosphorylated in embryonic DRG upon cGKI stimulation, however, none of them was detected to be implicated in sensory axon bifurcation. Therefore, I searched for new cGKI phosphorylation targets in DRG which is described in this chapter. It would be most reliable to search for cGK phosphorylation targets directly in the DRG cells of mice embryos however biochemical studies are frustrated in this case by difficulties in obtaining adequate numbers of DRG cells. Therefore the DRG derived F11 cell line was also used as an alternative. The F11 cell line is a fusion product of cells of mouse neuroblastoma cell line N18TG-2 with embryonic rat DRG neurons. F11 cells express cGKIα and cGKII and also established targets of cGKI: VASP, Mena, GSK3. VASP becomes phosphorylated in these cells upon stimulation of cGKI with 8-pCPTcGMP as it does in DRG, but GSK3 does not (see section 3.2.2.1). Another feature distinct from DRG is that cGKI does not become activated by addition of CNP in F11, suggesting that functional Npr2 is absent in these cells.

Several strategies were employed in search for new phosphorylation substrates of cGKI. Reduction of sample complexity is critical for the analysis of low-abundance kinase phosphorylation substrates. It can be achieved by enrichment of phosphoproteins using immobilised metal/metal oxide affinity chromatography. In this work metal oxide ($Al(OH)_3$) affinity chromatography was used. Specific feature of cGK, i.e. its preference to phosphorylate proteins with the amino acid sequence RRXS/T or RKXS/T (X stands for any amino acid) (Dostmann et al., 1999;Glass and Krebs, 1979;Tegge et al., 1995) was employed as well. Enrichment of phospho-proteins by immunoprecipitation with the antibody against phosphorylated RRXpS/pT motif was carried out. Antibodies recognizing another consensus phosphorylation site of cGK (RKXS/T) or phosphorylated serine/threonine amino acid were exploited as well. Two dimensional gels combined with immunobloting were used for analysis of phopshoproteins.

3.4.1 Enrichment of phosphoproteins with Al(OH)3 and phosphostaining

Affinity chromatography is often used for phosphoprotein or phosphopeptide enrichment. This method is based upon the affinity of negatively charged phopshate groups for positively charged metal ions (e.g. Fe^{3+}, Ga^{3+}) immobilized on a chromatographic support (IMAC – immobilized metal affinity chromatography). IMAC is based largely on ionic interactions, so peptides rich in glutamic and aspartic acid residues are often co-purified. Other amino acid

residues such as cystein and histidine may also interact with the IMAC material making selectivity for the phosphate group difficult (Metodiev et al., 2004). An alternative for IMAC is metal hydro-oxide affinity chromatography (MOAC). It has the same drawbacks as IMAC, but is easier accessible (Wolschin et al., 2005;Wolschin and Weckwerth, 2005). TiO_2 or $Al(OH)_3$ are used in this approach. $Al(OH)_3$ can be used both for phosphopeptide and phosphoprotein enrichment. I carried out phosphoprotein enrichment. Phosphopeptide enrichment could be the next step after excision of enriched phosphoprotein band.

Pro-Q Diamond phosphoprotein dye technology suitable for the fluorescent detection of phosphoserine, phosphothreonine, and phosphotyrosine containing proteins directly on SDS-PAGE gels (Steinberg et al., 2003) was also used to study the differences in phosphorylation between 8-pCPTcGMP treated and untreated samples as well as to assess the phosphoprotein enrichment efficiency.

For enrichment of phosphoproteins from 8-pCPTcGMP treated or untreated F11 cell lysates $Al(OH)_3$ was used. Samples were resolved by SDS-PAGE on a 10% acrylamide gel. Gels were stained first with phosphostain Pro-Q Diamond and, after documentation of phosphostaining, Coomassie staining was performed on the same gel. No increase in phosphoprotein staining intensity compared to the total protein staining is observed after $Al(OH)_3$ phosphoprotein enrichment which implies that phosphoprotein enrichment was not succesful (Fig. 3.36).

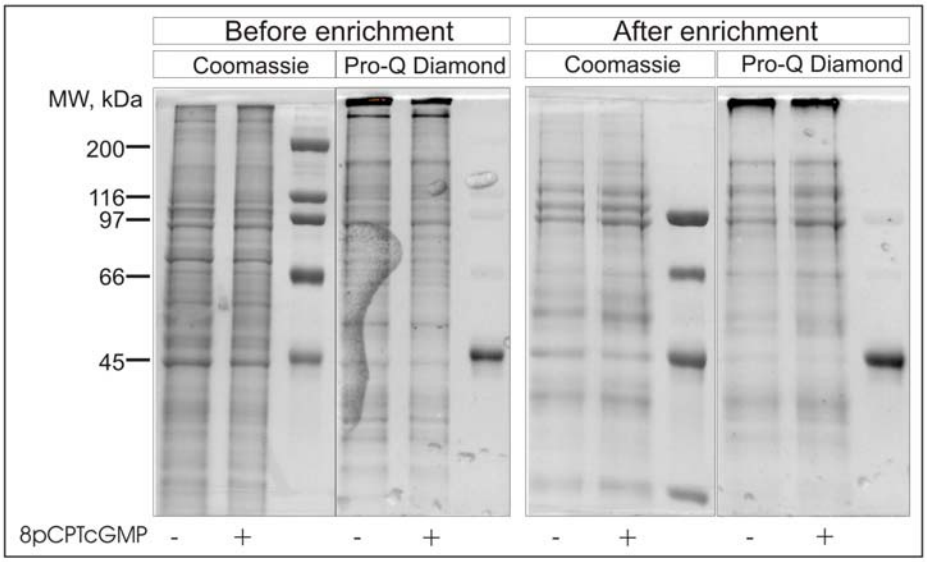

Fig. 3.36: Phosphoprotein enrichment with metal oxide ($Al(OH)_3$) affinity chromatography in F11 cell lysate. (A)Total protein staining with Coomassie and phospho-protein staining with Pro-Q Diamond are shown before and after phosphoprotein enrichment. Coomassie staining was carried out after Pro-Q Diamond staining on the same acrylamide gel, therefore, intensity of phosphoprotein staining can be directly compared to the

intensity of total protein staining. Intensity of Pro-Q Diamond stain in stimulated sample compared to total protein staining did not increase after phosphoprotein enrichment suggesting that phosphoprotein enrichment was not sufficient. Phosphoprotein ovalbumin used as a 45 kDa molecular mass marker is stained by Pro-Q Diamond whereas other unphopshorylated proteins in the molecular mass marker mixture remained unstained in phosphoprotein staining. 10% separating acrylamide gel was used for SDS-PAGE.

No difference in phosphostaining intensity between unstimulated and 8-pCPTcGMP stimulated samples is observed both before and after phosphoprotein enrichment which suggests that either phosphostain is not specific enough or that the amount of proteins phosphorylated after cGKI stimulation is too low to be detected by Pro-Q staining. Pro-Q Diamond stains ovalbumin, which has two phosphate groups (Nisbet et al., 1981), in contrast to unphosphorylated proteins in molecular mass marker mixture (Fig.3.36) which confirms phospho-specificity of the dye. Therefore, little amount of proteins phosphorylated upon cGKI stimulation compared to the total amount of phosphoproteins in the cell could explain the fact, that no difference in phosphorylation is observed between stimulated and not stimulated F11 cell lysates.

3.4.2 Screen for targets of cGKI in DRG using anti-phospho antibodies

Since enrichment of phosphoproteins with MOAC was not successful and did not help to find phosphorylation targets of cGKI, I used anti-phospho antibodies in order to reveal proteins phosphorylated upon cGKI stimulation. cGKI is a serine/threonine kinase, therefore, I used anti-phospho-serine and anti-phospho-threonine antibodies to look for differently phosphorylated proteins upon cGKI stimulation. Moreover, cGKI has a preference for RRXS/T and RKXS/T amino acid sequences and I used antibodies for these phosphorylated sequences in the search for new phosphorylation targets of cGKI.

3.4.2.1 Screen with anti-pS and anti-pT antibodies did not reveal any differentially phosphorylated bands

cGKI is a serine/threonine kinase. Therefore, antibodies against phospho-serine and phospho-threonine were also used to screen for proteins differentially phosphorylated upon stimulation of cGKI. Anti-phospho-tyrosine antibodies have been widely used in phosphoprotein studies. They are of good specificity, show little cross-reactivity to unphosphorylated tyrosine or serine-/threonine phosphorylated residues, are efficient in immunoprecipitation. However,

anti-phospho-serine and –threonine antibodies are mostly dependent on consensus sequences in addition to the phosphorylated residue and are thus more likely to be unable to access a phopshorylation site due to steric hindrance resulting in poor immunoprecipitation power. (Morandell et al., 2006;Reinders and Sickmann, 2005)

In the screen for cGKI phosphorylation targets antibodies against phospho-serine (BD biosciences) or phospho-threonine (Cell signalling) did not reveal any changes in phopshorylation neither in embryonic DRG samples nor in F11 cell culture samples (Fig. 3.37).

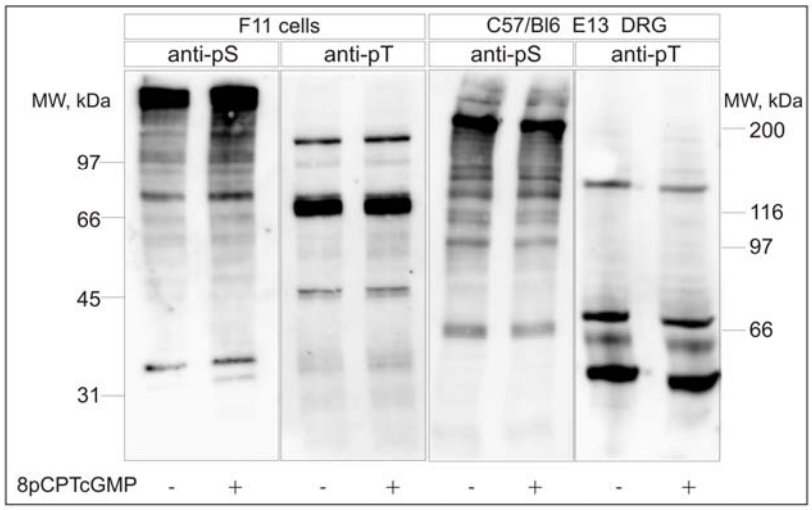

Fig. 3.37: Anti-pS and anti-pT Western blot analysis of DRG and F11 lysates. Embryonic mouse DRG and F11 cells were stimulated with 8-pCPTcGMP for 5 min and afterwards analysed by Western blotting with antibody against phosphorylated serine (BD biosciences) or threonine (Cell signalling). No differences in phosphorylation are observed between the unstimulated and 8-pCPTcGMP stimulated samples. F11 cell lysate was resolved by SDS-PAGE on 10% acrylamide gel and embryonic DRG lysate – on 7.5% acrylamide gel.

3.4.2.2 Screen with anti-RRXpS/pT reveals both phosphorylated and dephosphorylated bands upon stimulation of cGK

An antibody recognizing the phosphorylated sequence RRXpS/pT, a preferred phosphorylation motif of cGKI, was used to screen for proteins that become phosphorylated in DRG upon stimulation of cGKI with the cGMP analogue 8-pCPTcGMP. Both DRG from E13 mouse embryos as well as F11 cells, derived from DRG neurons, were screened. This approach identified several bands phosphorylated upon cGKI stimulation of about 95 kDa, 100 kDa, 140 kDa and a band of approximately 200 kDa in DRG samples (Fig.3.38 A). The

latter band was most prominent and observed in all repetitive Western blots. Intensity of other differentially phosphorylated bands tended to vary by repetitive experiments. Successive search for a new DRG target was mainly concentrated on 200 kDa protein band phosphorylated upon stimulation of cGKI. Surprisingly, the stimulation of F11 cells resulted in dephosphorylation of about 51 kDa size protein (Fig. 3.38). This result might be caused by one of the following mechanisms:

- cGKI inhibits an unknown kinase either by phosphorylating it or by binding to the 51 kDa protein and thereby preventing access to it for another kinase. Phosphorylation of 51 kDa protein by an unknown kinase would be prevented in this way and phosphorylation status of the protein would gradually decrease due to phosphatase activity.
- It is also possible that the 51 kDa protein becomes dephosphorylated by a phosphatase activated by cGKI.

To confirm that the anti-RRXpS/pT specifically recognizes only phosphoproteins I dephosphorylated crude lysates of both 8-pCPTcGMP stimulated and not stimulated DRG and F11 cells with lambda-phosphatase prior to Western blotting. Whereas anti-RRXpS/pT recognizes copious bands in the lanes, where DRG lysates without lambda-phosphatase treatment were loaded, there are no bands at all recognized in the lanes where DRG lysates after lambda-phosphatase treatment were loaded (Fig.3.38 A). This confirms anti-RRXpS/pT specificity against phosphorylated proteins.

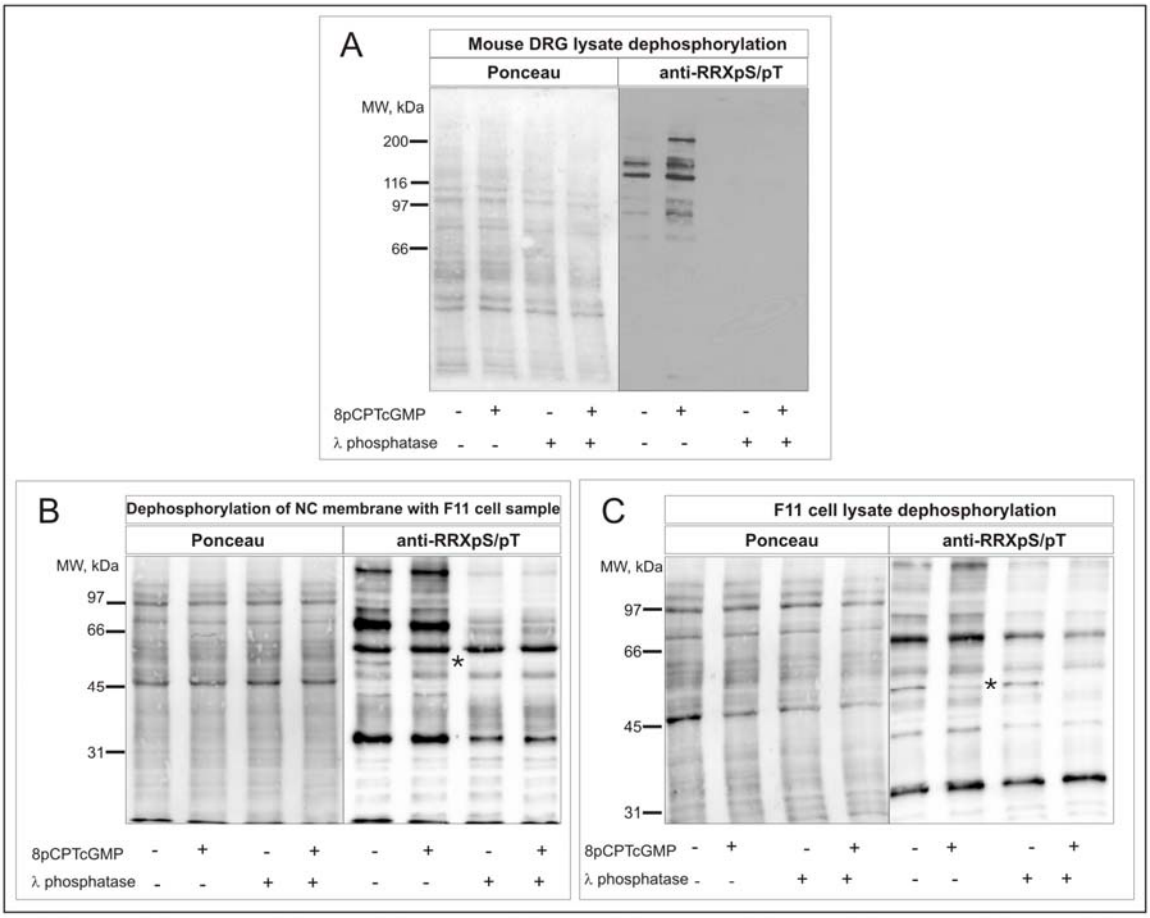

Fig. 3.38: Western blot analysis of DRG and F11 lysates with the antibody recognizing consensus phosphorylation motif of cGK (RRXpS/pT). (A) Anti-RRXpS/pT Western blotting analysis of unstimulated and stimulated mouse DRG lysates. There are several phospho-bands appearing after cGKI stimulation. Lambda- phosphatase dephosphorylated them and they are no longer observed in anti-RRXpS/pT Western blot confirming, that the antibody indeed recognizes phosphoproteins. (B) Anti-RRXpS/pT Western blotting analysis of unstimulated and stimulated F11 lysates. There is a 51 kDa phospho-band which becomes less intensive after cGKI stimulation. Treatment with lambda-phosphatase carried out on nitrocellulose membrane dephosphorylated the 51kDa band and the antibody against RRXpS/pT does not recognize it anymore confirming its specificity. (C) Anti-RRXpS/pT Western blotting analysis of unstimulated and stimulated F11 lysates as well as of lysates dephosphorylated with lambda-phosphatase. 51 kDa band is recognized by the anti-RRXpS/pT after lambda-phosphatase treatment showing that the 51 kDa protein did not become dephosphorylated. Asterisks indicate the 51 kDa band. NC, nitrocellulose. DRG lysates were resolved on 7.5% acrylamide gel and F11 cell lysates – on 10% acrylamide gel.

The intensity of bands recognized by the anti-RRXpS/pT declines significantly after the lambda-phosphatase dephosphorylation carried out both directly in the F11 cell lysate as well as on the nitrocellulose membrane to which F11 sample resolved on SDS-PAGE was transferred. However, the 51 kDa band becomes dephosphorylated only after the lambda-

phosphatase treatment carried out on the nitrocellulose membrane but not in the F11 cell lysate (Fig. 3.37 B-C). Dephosphorylation of the 51 kDa band only on the nitrocellulose membrane but not in the lysate can be explained by the unaccesibility of the phosphate group for lambda-phosphatase in the native protein in the F11 cell lysate. On nitrocellulose membrane proteins are denaturated, phosphate groups become exposed and, therefore, accesible for lambda-phosphatase.

cGKI is a well studied kinase with many downstream targets being published. To check whether the 200 kDa protein which becomes phosphorylated upon cGKI stimulation in DRG is identical to one of the established cGKI substrates I looked for the substrates with identical molecular mass. One of the targets phosphorylated by cGKI with close molecular mass is the inositol triphosphate receptor (IP3 receptor) (Schlossmann et al., 2000). I tested whether bands recognized by the antibody against phospho-motif and against IP3 receptor migrate similarly on the SDS-PAGE. The results showed that the bands migrate differently: IP3 receptor containing band migrates slower and has larger molecular weight as the 200 kDa band phosphorylated upon cGKI stimulation (Fig. 3.39)

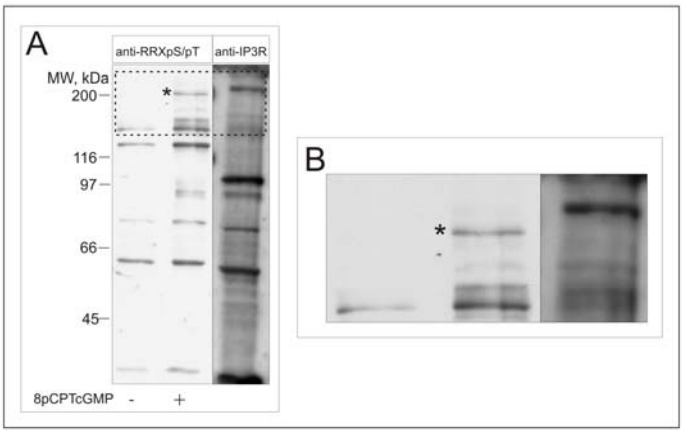

Fig. 3.39: 200 kDa band which becomes phosphorylated upon cGKI stimulation is not the inositol triphosphate receptor (IP3R). (A) E13 embryonic DRG lysates were analysed by Western blot with antibodies against RRXpS/pT motif and against IP3 receptor. The size of IP3 receptor is about 240 kDa and it migrates visibly slower as the 200 kDa band recognized by the antibody against RRXpS/pT motif. (B) magnified view of boxed area around 200 kDa in (A). DRG lysate was resolved by SDS-PAGE on 7.5% acrylamide gel.

3.4.2.3 A screen with antiserum against CGGLRKVpSK reveals VASP and Mena phosphorylation upon cGKI stimulation

Antiserum that was raised against CGGLRKVpSK motif and recognizes RKXpS motif phosphorylated by cGKI was used for screening of proteins that become phosphorylated

upon cGKI stimulation. This antiserum was raised against a very specific recognition sequence which is contained in Mena/VASP family members and is phosphorylated by cGKI (Butt et al., 1994). Anti-CGGLRKVpSK Western blot studies with stimulated and not stimulated DRG and F11 cell samples show that several bands become phosphorylated upon stimulation of cGKI with 8-pCPTcGMP (Fig. 3.40). The size of one of the bands corresponds to the size of phosphorylated VASP protein, the size of another band corresponds to 80kDa isoform of Mena protein. Since the antibody recognizes phosphorylated sequence which is present in both proteins and can be phosphorylated by cGKI (LRKVpSK in murine VASP and LRKVpSR in murine Mena), it is likely that VASP and Mena are the bands that are observed to be differently phosphorylated after stimulation of cGKI. However, the antibody did not recognize other candidate proteins in DRG or F11 cells that would become phosphorylated after stimulation of cGKI.

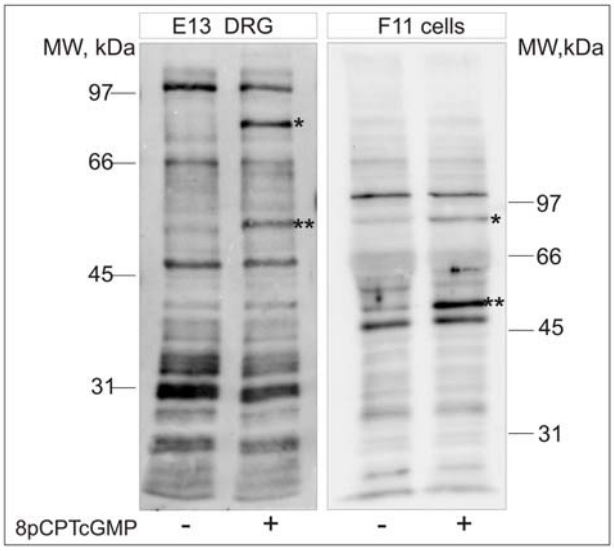

Fig. 3.40: Anti-CGGLRKVpSK Western blot analysis of DRG and F11 cell lysates. Embryonic (E13) DRG and F11 cells were stimulated with 8-pCPTcGMP for 5 min. Afterwards stimulated DRG and F11 cell lysates as well as unstimulated control DRG and F11 cell lysates were analysed by Western blotting with antiserum recognizing the sequence LRKVpS which is present in Mena/VASP family proteins. Asterisks show bands which become phosphorylated upon stimulation of cGKI. One of the bands (two asterisks) corresponds to the size of phosphorylated VASP (50kDa) and another one (one asterisk) corresponds to 80 kDa isoform of Mena protein. Embryonic mouse DRG and F11 cells lysates were resolved on 10 % acrylamide gel.

3.4.3 Approaches used to identify differentially phosphorylated proteins observed in anti-RRXpS/pT Western blots

Many of the signalling molecules, which are major targets of phosphorylation events are present at low abundance within cells and, in these cases, enrichment is a prerequisite to clarify their identity by mass spectrometry. Western blot analysis allows detection of very low abundance proteins but their identification by MS requires enrichment of a protein to a level visible on a silver stained gel. While phosphorylation targets of cGKI are observed on anti-RRXpS/pT Western blots they are not visible on a Pro-Q Diamond stained gel whose sensitivity is comparable to a silver stain. I used several enrichment strategies which are described in this section. First of all I tried immunoprecipitation of cGKI phosphorylation targets using antibody against RRXpS/pT. Next I analysed whether phosphorylation substrates of cGKI recognized by anti-RRXpS/pT antibody are enriched in some subcellular fractions and analysed postnuclear and cytoplasmatic fractions on one-dimensional and two-dimensional SDS-PAGE gels and Western blots. These experiments were carried out using mainly F11 cells and trying to enrich the 51 kDa protein because F11 cell material was easier available compared to embryonic mouse DRG.

3.4.3.1 Immunoprecipitation with antibody against phospho-motif RRXpS/pT

The straightforward approach to enrich and identify the differently phosphorylated proteins observed in anti-RRXpS/pT Western blots after stimulation of cGKI would be immunoprecipitation with anti-RRXpS/pT antibody. Immunoprecipitation from protein lysates of embryonic DRG was carried out in order to determine whether the 200 kDa protein phosphorylated upon cGKI stimulation could be enriched by anti-RRXpS/pT antibody. As shown in figure 3.41 the protein of 200 kDa is bound by the antibody against the RRXpS/pT motif, but not so strongly that it would become significantly enriched. Apart from the 200 kDa band two other protein bands show somewhat higher level of enrichment. Immunoprecipitates from unstimulated and stimulated embryonic DRG resolved on SDS-PAGE gel were silver-stained in order to test whether the amount of phospho-proteins enriched by anti-RRXpS/pT antibody and observed in the Western blot is sufficient and visible in silver-stained gel. The lack of prominent bands in both lanes loaded with control or

8-pCPTcGMP treated protein lysates indicates the insufficiency of the antibody against RRXpS/pT motif to enrich phosphorylated proteins, in particular the 200 kDa component.

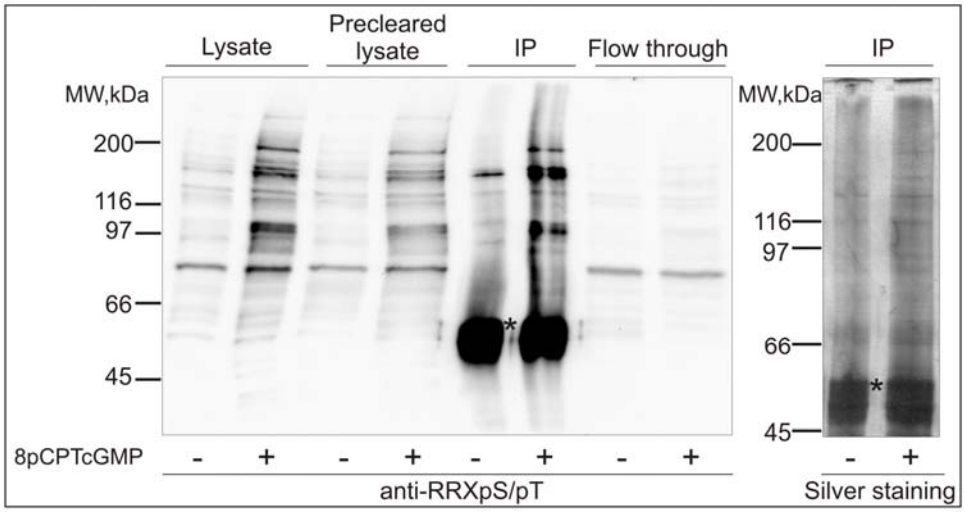

Fig. 3.41: Immunoprecipitation with anti-RRXpS/pT antibody from embryonic (E13) DRG lysates. Embryonic DRG lysates were precleared by incubation with protein A-sepharose beads and incubated overnight with anti-RRXpS/pT antibody. Several bands could be observed in the anti-RRXpS/pT Western blot lanes loaded with the immunoprecipitate, however, they are not significantly enriched. Proteins that were not bound by anti-RRXpS/pT but are recognized by this antibody are visible in the last "Flow through" lanes. Absence of significant enrichment by immunoprecipitation with anti-RRXpS/pT antibody is confirmed by the silver stained SDS-PAGE gel of immunoprecipitates – there are no prominent bands observed. Lysates for Western blot analysis and silver gel staining were resolved on 7.5 % acrylamide gel. Asterisks denote the heavy chain of the anti-RRXpS/pT antibody

3.4.3.2 Subcellular fractionation of crude lysates in order to enrich phosphorylated bands and subsequent mass spectrometry analysis of a band cut from a one dimensional SDS-PAGE

Subcellular fractionation of embryonic (E13) mouse DRG as well as F11 cells was carried out in an attempt to enrich the 200 kDa and 51 kDa components. Western blot analysis showed that many proteins are removed with the nuclear pellet, but the 200 kDa and 51 kDa protein remain in the postnuclear supernatant (Fig 3.42). 200 kDa band does not become significantly enriched. Due to the limited availability of embryonic mouse DRG tissue further experiments concentrated on F11 cells and the 51 kDa band. The 51 kDa band becomes considerably enriched in the cytoplasmic fraction of F11 cells. Interestingly, this band becomes visible in the postnuclear and cytoplasmic fractions of DRG as well, which suggests

that the 51 kDa band becomes dephosphorylated upon cGKI stimulation in DRG too and is not a specific feature characteristic only to F11 cells. Lesser amount of embryonic DRG lysate loaded due to its limited availability or lesser relative amount of 51 kDa protein in the DRG phospho-proteome compared to F11 cells would explain the difficulty to visualize the 51 kDa protein in crude DRG lysates analyzed by anti-RRXpS/pT Western blotting. Dephosphorylation of the 51 kDa protein is observed in anti-RRXpS/pT Western blot, however in Coomassie stained gel the band is still under detection limit (Fig. 3.42). Despite this fact the band from Coomassie stained gel in the region of 51 kDa was cut out and given for mass spectrometry analysis assuming that putative cGKI phosphorylation targets could be identified by the presence of the RRXS/T motif in their sequence. Six of all identified proteins had the RRXS/T motif and molecular mass close to 51 kDa (table 3.7).

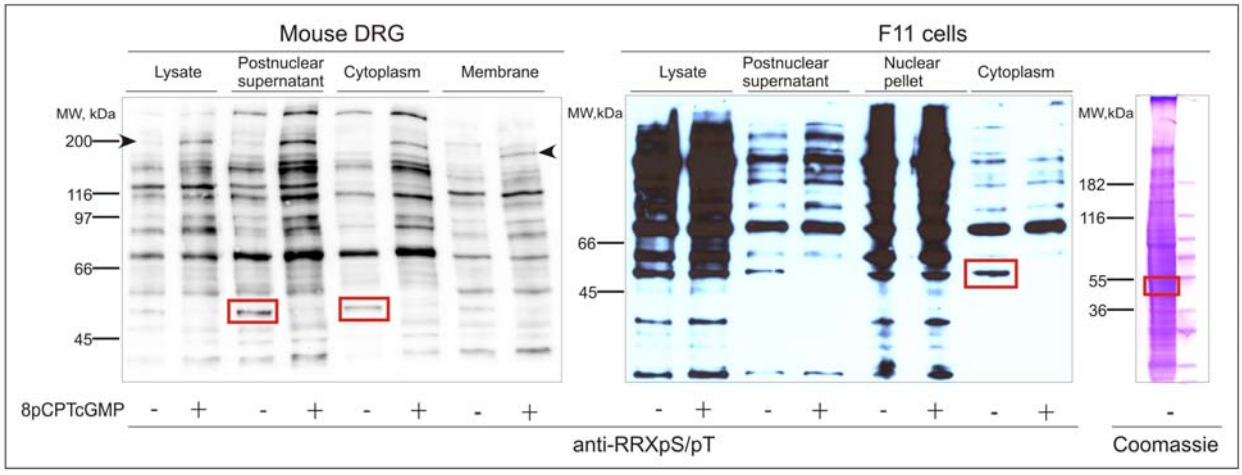

Fig.3.42: Enrichment of 200 kDa and 51 kDa proteins by subcellular fractionation for subsequent mass spectrometry analysis. Both 200 kDa and 51 kDa bands remain in the cytoplasmic fraction. The 51 kDa protein becomes considerably enriched by subcellular fractionation. After enrichment it is observed not only in the F11 postnuclear supernatant and cytoplasmatic fraction but also in the DRG postnuclear supernatant and cytoplasmic fraction. The cytoplasmic F11 cell fraction was resolved by SDS-PAGE, stained by Coomassie and the region of the 51 kDa band was cut out and analysed by mass spectrometry. The 51 kDa protein enriched in postnuclear supernatatant and cytoplasmic fraction as well as the band with the 51 kDa protein cut out from the Coomassie stained gel are shown in boxes. The 200 kDa band is indicated by arrowheads. Embryonic (E13) DRG fractions were resolved on 7.5 % acrylamide gel and F11 cell fractions – on 10 % acrylamide gel.

Table 3.7: Proteins, detected by mass spectrometry analysis of the F11 cytoplasmic fraction of approximately 51 kDa and having the RRXS/T sequence. (The whole list of proteins detected by MS is given in table 1 of the Appendix.)

Accession No.	Protein	Theoretical MW, kDa	Putative phosphorylation sequence motif
P61203	COP9 signalosome complex subunit 2	52	RRTT
Q4QRB8	Dead end homolog 1	57	RRRT, RRRS
Q3B8Q2	Similar to DEAD Asp Glu Ala Asp box polypeptide 48	47	RRRS
P50503	Hsc70 interacting protein	41	RRQS, RKVS
Q4KM87	Actin like 6A	47	RRFS
Q9QXU8	Cytoplasmic dynein 1 light intermediate chain 1	57	RRAT

The list of candidate proteins to become dephosphorylated upon stimulation of cGKI is too long to come to a decision about the identity of the 51 kDa component. Either all the candidate proteins revealed by the MS analysis should be separately investigated whether they become dephosphorylated upon stimulion of cGKI or the list of candidate proteins should be narrowed down.

3.4.3.3 Two dimensional separation of F11 and embryonic DRG samples for subsequent mass spectrometry analysis of differentially phosphorylated spots

3.4.3.3.1 Two dimensional anti-RRXpS/pT Western blots with F11 and embryonic DRG samples

In order to narrow down the candidate list that was obtained after the mass spectrometry analysis of the 51 kDa band cut out from the one dimensional Coomassie stained SDS-PAGE gel the mass spectrometry analysis was repeated but this time from the 51 kDa spot cut out from a two-dimensional Coomassie stained gel.

Western blot analysis with anti-RRXpS/pT was carried out in order to find the dephosphorylated 51 kDa spot in two dimensional gel (Fig. 3.43). The difference in phosphorylation pattern between unstimulated and 8-pCPTcGMP stimulated samples could be reproducibly visualized in Western blots of two-dimensional SDS-PAGE preparations.

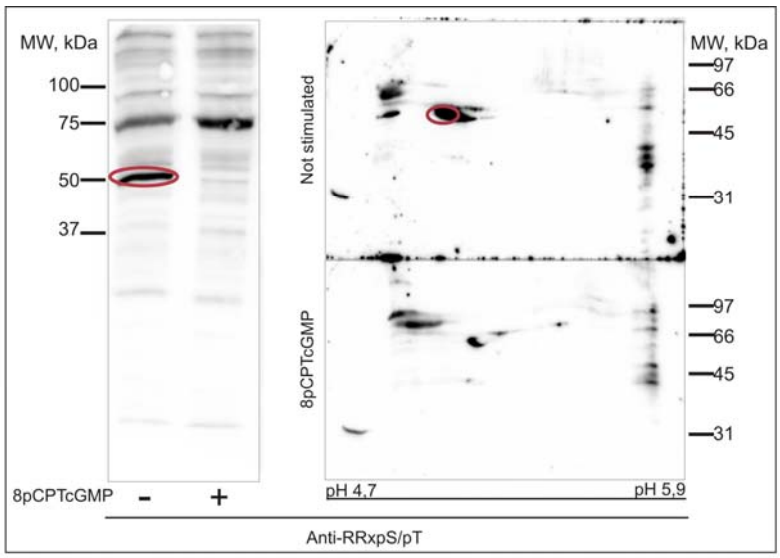

Fig.3.43: Postnuclear fraction of F11 cells separated on one-dimensional and two-dimensional gels subsequently analysed by anti-RRXpS/pT Western blotting. The 51 kDa protein which becomes dephosphorylated upon stimulationof cGKI with 8-pCPTcGMP is shown in a red circle both in 1D and 2D gels. IPG stripe with pH interval from 4.7 to 5.9 was used for the first dimensional separation by IEF and 10% acrylamide gel – for second dimensional separation on SDS-PAGE.

In parallel studies a two dimensional anti-RRXpS/pT Western blot analysis of 8-pCPTcGMP stimulated and unstimulated embryonic DRG lysates was carried out as well. In one-dimensional Western blot with embryonic mouse DRG samples only proteins additionally phosphorylated upon cGKI stimulation were observed, but no dephosphorylation of the 51 kDa component or any other bands (Fig. 3.38). Interestingly, in the two-dimensional anti-RRXpS/pT Western blot dephosphorylation of a spot of about 50-55 kDa was visible (Fig. 3.44). Molecular mass and pI characteristics of this spot observed in the two dimensional gel resemble those of the 51 kDa component observed in F11 samples resolved on a two dimensional gel (Fig. 3.43) implying that the same 51 kDa component becomes dephosphorylated upon cGKI stimulation both in F11 and DRG cells. Subcellular fractionation also revealed that the 51 kDa protein dephosphorylated upon cGKI stimulation is present in DRG (Fig. 3.42). The 51 kDa protein dephosphorylation is probably not readily observed in 8-pCPTcGMP stimulated DRG lysates due to its low concentration. Enrichment of the 51 kDa component in the cytoplasmic fraction as well as a higher amount of total protein resolved on two dimensional gel allow to visualize the 51 kDa component. Two-dimensional anti- RRXpS/pT Western blot analysis together with the results of subcellular fractionation of DRG lysates suggests that dephosphorylation of the 51 kDa component upon stimulation of cGKI is not specific to F11 cells but is also found in DRG.

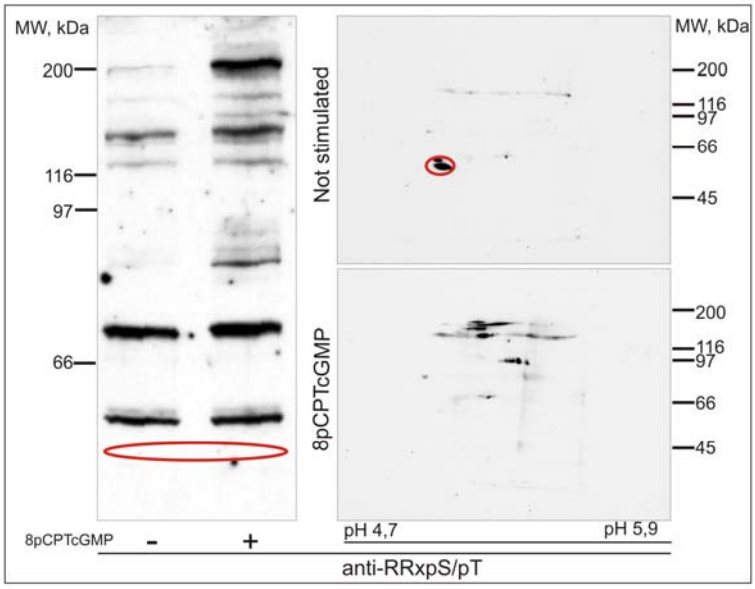

Fig.3.44: Embryonic (E13) mouse DRG lysates resolved on one-dimensional and two-dimensional SDS-PAGE gels were subsequently analysed by anti-RRXpS/pT Western blotting. Many phospho-spots in 2D Western blot appear after stimulation of cGKI. Some of them reveal a mass of 200 kDa and correspond to the 200 kDa phospho band appearing in 1D gel after lysate incubation with 8-pCPTcGMP. The 51 kDa protein which becomes dephosphorylated upon stimulation of cGKI with 8-pCPTcGMP is shown in a red circle both in 1D (implied location based on the results of enrichment by subcellular fractionation) and 2D gels. SDS-PAGE was carried out on 7.5 % acrylamide gel, IEF – on IPG stripe with pH range 4.7-5.9.

3.4.3.3.2 Mass spectrometry analysis of the 51 kDa protein spot cut from two-dimensional Coomassie stained SDS-PAGE

To assign spots on two-dimensional anti-RRXpS/pT Western blots to their corresponding proteins, it is necessary to visualize the entire proteome directly on the membrane. For this purpose the membrane was stained with Ponceau and spots visible on the Ponceau labelled membrane were marked with a pencil. Afterwards Western blot analysis with the antibody against RRXpS/pT was carried out. The scan of the anti-RRXpS/pT Western blot was overlayed with the pencil marks. As demostrated in figure 3.45, the position of the 51 kDa component in relation to protein spots stained by Ponceau could be detected on the composite image of the Western blot and Ponceau stains marked by pencil.

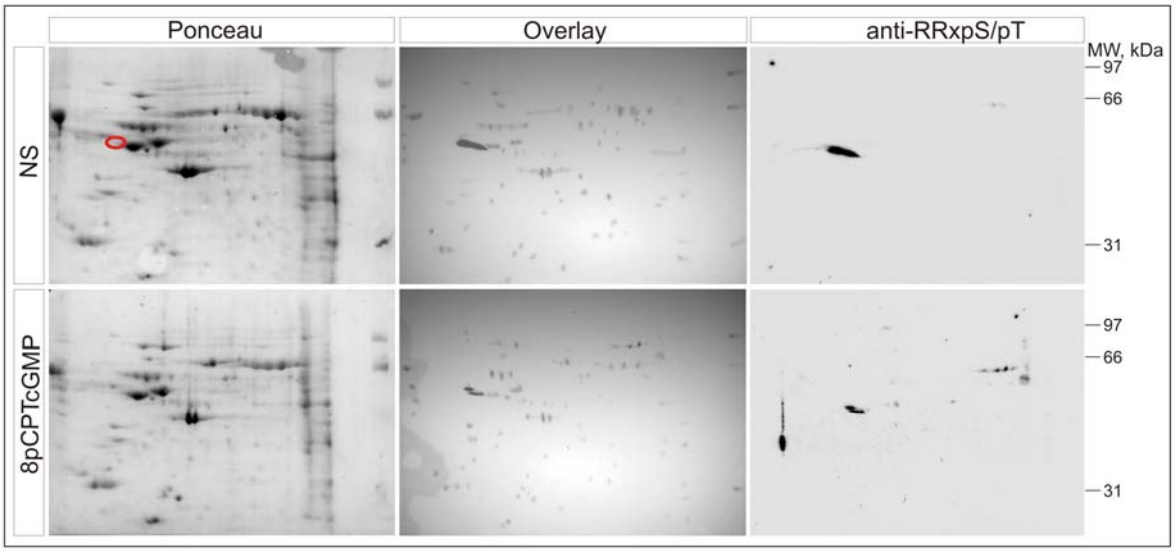

Fig.3.45: Location of the 51 kDa phospho-spot in relation to protein spots stained by Ponceau. The 51kDa spot which becomes dephosphorylated upon stimulation of cGKI with 8-pCPTcGMP can be observed only in anti-RRXpS/pT Western blot. Ponceau stained proteins were marked with a pencil on the nitrocellulose mambrane. The photo of anti-RRXpS/pT Western blot was taken, immediately followed by a photo of pencil marks. Then both photos were overlayed enabling visualization of the 51 kDa spot in relation to Ponceau stained protein spots. The circle indicates location of the 51 kDa phospho-spot in relation to total protein spots on Ponceau stained membrane. IPG stripe with pH interval from 4.7 to 5.9 was used for the first dimensional separation by IEF and 10% acrylamide gel – for second dimensional separation by SDS-PAGE.

Having defined the position of the 51 kDa spot, sample of the unstimulated postnuclear fraction of F11 cells was resolved on a large two dimensional SDS-PAGE gel (first dimension was carried out on an IPG stripe of 17 cm) and the area around the 51 kDa spot location was cut out for a mass spectrometry analysis (Fig. 3.46). However, the results obtained by the mass spectrometry analysis did not narrow down the list of candidate-proteins to be phosphorylated by cGKI, obtained after mass spectrometry analysis of a band cut out from the one-dimensional gel. Moreover, it added new candidate-proteins to the list (table 3.8).

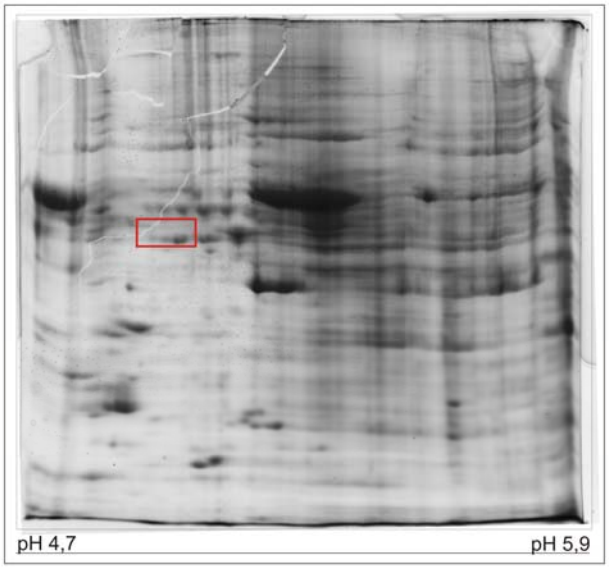

Fig.3.46: Coomassie staining of proteins of the postnuclear fraction of unstimulated F11 cells separated on a two-dimensional SDS-PAGE. The region that was cut out for the mass spectrometry analysis of the putative 51 kDa spot is shown in a box. IEF was carried out on 17 cm long IPG stripe with pH range 4.7-5.9 and SDS-PAGE - on 10 % acrylamide gel.

Table 3.8: Proteins, detected by the mass spectrometry analysis of the 51 kDa spot cut from a two-dimensional SDS-PAGE with resolved unstimulated F11 postnuclear sample. Only proteins of approximately 51 kDa having consensus phosphorylation sequence of cGKI are shown. (The whole list of proteins detected by MS is given in table 2 of the Appendix.)

Accession No.	Protein	MW, kDa	Putative phosphorylation sequence motif
Q61553	Fascin	55	RRIT
P63101	KCIP-1 Protein kinase C inhibitor – 1 (alternative name for 14-3-3)	30	RRSS
A8IP69	14-3-3 protein gamma subtype	30	RRSS
P12369	cAMP dependent protein kinase type II beta regulatory subunit	46	RRAS
Q8K1M3	cAMP dependent protein kinase type II alpha regulatory subunit	46	RRVS
A2AQ07	Tubulin beta 1	55	RRES
B1WBN9	Pyruvate kinase, liver and red blood cell	59	RRAS
A1L113	Keratin 1	65	RRST
B2RQH6	Keratin 75	59	RRVS
Q9Z2L7	Cytokine receptor like factor 3	50	RRDS
B2RRT9	Zinc finger, RAN binding domain containing 2	37	RRTS
Q5XI13	Glutamate rich WD repeat containing protein 1	49	RRHT

There might be several reasons, why the mass spectrometry analysis gave different results for the 51 kDa band regions cut out from the one-dimensional and from the two-dimensional gels. Firstly, dephosphorylation is visible only on anti-RRXpSpT Western blots but not on Coomassie stained gels, therefore, cutting of the 51 kDa protein region from a Coomassie stained gel guided by the molecular mass marker or other cues is inaccurate. Secondly, in a band for MS analysis cut out from one-dimensional SDS-PAGE proteins with minor differences in their molecular mass are enriched whereas in a spot from two-dimensional SDS-PAGE proteins not only with minor differences in their molecular mass but also in their isoelectric point are enriched. Protein population in two-dimensional SDS-PAGE spot is reduced, therefore, level of some low abundance proteins which are not detected by MS in the band from one-dimensional SDS-PAGE rises compared to other proteins and becomes high enough to be detected by MS.

3.4.3.3.3 Mass spectrometry analysis of the 51 kDa protein spot cut from two-dimensional Western blot

In order to visualize and cut out the 51 kDa phosphoprotein spot precisely, it was cut out from an anti-RRXpSpT Western blot on a nitrocellulose membrane. Although usually SDS-PAGE gels are used to identify proteins by mass spectrometry analysis but it is also possible to identify proteins on nitrocellulose membranes (Dufresne-Martin et al., 2005;Luque-Garcia et al., 2006;Luque-Garcia et al., 2008) An AP conjugated secondary antibody was used for the Western blot in order to visualize the spot directly on the membrane. Protein free blocking solution was used to avoid sticking of extraneous proteins to the membrane.

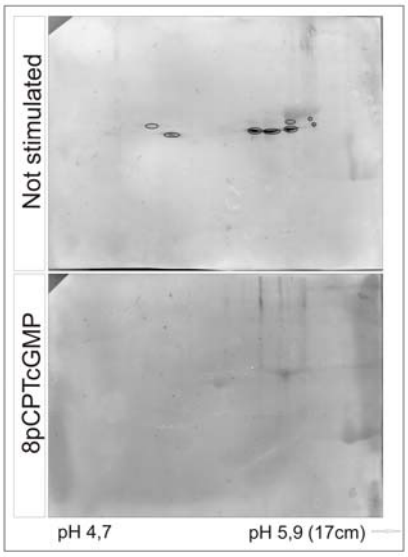

Fig.3.47: Comparison of two dimensional anti-RRXpS/pT Western blot with unstimulated and stimulated F11 postnuclear samples from which spots for mass spectrometry were cut out. Grey stains in the background are Ponceau stained proteins and they show that similar amounts of proteins were loaded in both Western blots. Two-dimensional SDS-PAGE gel was carried out on a big gel (IPG stripe 17 cm). Big rectangular area (7x9 cm) around the 51 kDa spot was cut from the SDS-PAGE and transferred onto nitrocellulose membrane followed by anti-RRXpS/pT Western blotting. Western blot membrane covers the area between 30 and 65 kDa. There are several spots recognized by the anti-RRXpS/pT in the area of dephosphorylated 51 kDa spot because the F11 sample was resolved on a bigger SDS-PAGE as usual and separation is higher compared to the initial Western blots in figures 3.43 and 3.44. Spots marked with circles were cut out and sent for mass spectrometry analysis.

Identification of the spots cut out from the Western blot on nitrocellulose membrane by mass spectrometry analysis (Fig. 3.47) gave in general less proteins, compared to the spots cut from the SDS-PAGE gels. There was only one protein containing RRXS sequence (table 3.9). However, this protein was not present in the previous lists of candidate proteins to be dephosphorylated upon cGKI stimulation compiled according to the results of mass spectrometry analysis. Moreovew, it has a theoretical molecular mass of 101 kDa, although majority of other identified proteins have a molecular mass around 50 kDa showing that spots were cut correctly.

Table 3.9: Proteins, detected by mass spectrometry analysis of the 51 kDa spots cut from a two-dimensional Western blot. Only protein having consensus sequence of cGKI is presented. (The whole list of proteins detected by MS is given in table 3 of the Appendix.)

Accession No.	Protein	MW, kDa	Putative phosphorylation sequence motif
A2AAY5	SH3 and PX domain containing protein 2B	101	RRYS

Although MS analysis of proteins on a nitrocellulose membrane is possible it is a complicated experiment. The main drawbacks are loss of proteins due to blotting and presence of high concentration of immunoglobulins on the nitrocellulose membrane compared to the sample proteins trapped on it. This explains the low number of proteins detected by MS.

Anti-RRXpS/pT is a useful tool to detect proteins phosphorylated upon stimulation of cGKI in DRG neurons as well as in F11 cells. Detected phosphorylation targets of cGKI are most likely novel phosphorylation targets because their properties do not fit with the known downstream targets. Moreover, an unexpected dephosphorylation event dependent on cGKI was observed which is an unusual function for a kinase. The main challenge for identification of phosphorylated proteins was their enrichment to enable MS analysis. However, different strategies used for enrichment of these detected targets were not successful.

4 DISCUSSION

In this work a crucial role of cGMP signalling in the bifurcation of sensory DRG axons and central branches of trigeminal sensory axons is shown and the cGMP signalling pathway including CNP, Npr2 and cGKI is elucidated using mutant mouse analysis with the DiI labelling technique. Absence of one of these components affects bifurcation of sensory axons but not their interstitial branching which shows that these two types of branching are mechanistically different. These results suggest that CNP, Npr2 and cGKI most likely act in a signalling cascade where CNP activates Npr2. This results in the generation of cGMP from GTP by the guanylyl cyclase activity of Npr2. cGMP activates cGKI leading to phosphorylation of its downstream targets. Several proteins that are phosphorylated by cGKI in DRG were identified, however, a downstream phosphorylation target of cGKI that is also involved in sensory axon bifurcation was not found.

4.1 Is cGMP signalling sufficient to induce bifurcation of sensory axons, or why sensory neurons bifurcate *in vivo* but not *in vitro*?

What environmental factors force an axon to bifurcate? The simplest explanation would be as given by Zhou et al. – an inhibitory cue acts at the center of the growth cone, the cytoskeleton retracts in the center and proceeds to grow on both sides resulting in the bifurcation of the growth cone (Zhou et al., 2002). Such bifurcation is an exclusive case of turning, when an inhibitory cue acts on the center of the growth cone instead of acting from the side. Sensory axons stop upon reaching the dorsal root entry zone, suggesting that dorsal spinal cord acts inhibitory/repellent on these axons (Masuda et al., 2008;Ozaki and Snider, 1997;Watanabe et al., 2006). Since sensory axons extend towards the spinal cord at a straight angle, the center of the growth cone would be exposed to the inhibitory effect from the spinal cord and the growth cone would split. However, the fact, that sensory axons in mice deficient in cGMP signalling do not bifurcate and, instead, turn caudally or rostrally disagrees with this explanation (Fig. 4.1).

If only inhibitory/repellent cues from the spinal cord acting on the center of the growth cone would induce axon bifurcation, then this does not explain, why cGMP signalling mutants do not bifurcate, but turn either rostrally or caudally. These mutants lack either cGKI, functional Npr2 or CNP. Both cGKI and Npr2 are expressed in the DRG neurons (Schmidt et al., 2002;Schmidt et al., 2007) and CNP is secreted by dorsal horn neurons (Schmidt et al.,

2009). Absence of cGKI or functional Npr2 affects cGMP signalling in sensory neurons rather than inhibitory/repellent cues from the spinal cord. Therefore, an inhibitory/repellent signal alone is not sufficient to induce bifurcation of sensory axons, instead CNP-Npr2-cGKI signalling is essential for this.

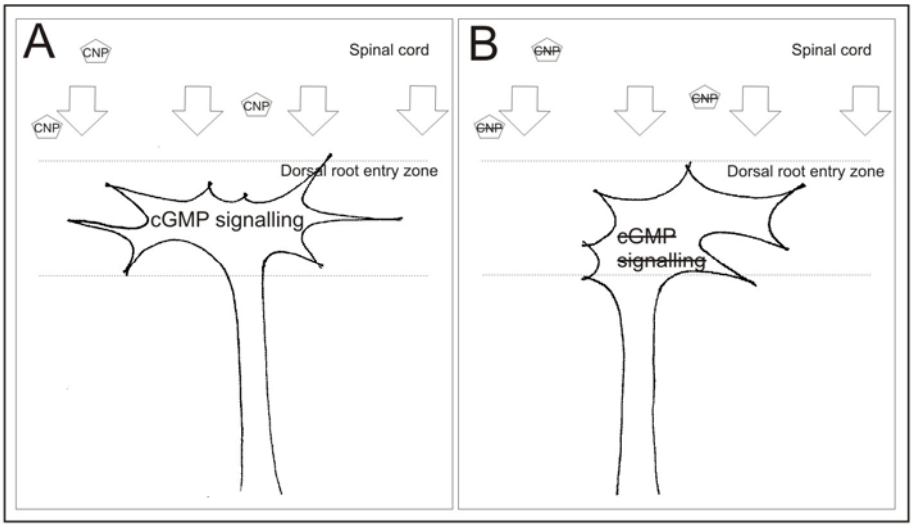

Fig.4.1: Schematic representation of sensory axon growth cone behaviour at the dorsal root entry zone. (A) The growth cone of a sensory axon in a wild type mice detects inhibitory/repellent cues from the spinal cord upon arrival at the DREZ as well as the CNP signal which induces a cGMP signalling cascade in the sensory axon leading to bifurcation. (B) The growth cone of a sensory axon in mice mutant for components of cGMP signalling detects inhibitory/repellent cues from the spinal cord as well. However, due to the disrupted cGMP signalling the growth cone does not bifurcate, it just turns away from inhibitory signals of the spinal cord and grows in the rostral or caudal direction.

Experiments with sensory axons grown in culture analysing different factors which could effect their bifurcation did not give unequivocal results. On the one hand, only 5-13 % of sensory axons in culture are bifurcating which suggests that in the vast majority of sensory neurons *in vitro* some of the signals important for axonal bifurcation are missing (Müller, 2002). This could be explained by the fact that CNP is not produced by sensory neurons themselves and there is no alternative source of CNP in the cell culture (in FCS free medium), therefore, the cGMP signalling cascade leading to bifurcation is not activated. On the other hand, addition of CNP to the cell culture of sensory neurons does not induce their bifurcation (Schmidt et al., 2007;Zhao and Ma, 2009). Moreover, application of membrane permeable cGMP derivative did not increase sensory axon bifurcation *in vitro* (Müller, 2002). Probably, the CNP signal and even activation of cGKI is not sufficient to force sensory neurons in a cell culture to bifurcate and other concomitant signals are required for this special branching mode. Slit proteins are proposed as an additional bifurcation factor of

sensory axons in several publications of Le Ma who started to analyse the influence of Slit proteins on sensory axon branching in the group of Tessier-Lavigne (Ma and Tessier-Lavigne, 2007;Wang et al., 1999;Zhao and Ma, 2009). Slit proteins are ligands for Robo receptors. Slit1 and Slit2 are expressed in the dorsal spinal cord at the time, when sensory axons reach the dorsal root entry zone, whereas sensory axons express Robo1 and Robo2 receptors (Ma and Tessier-Lavigne, 2007). Slit2 was found to be a repulsive cue for neurons expressing Robo receptors, however, it acts positively on sensory axon growth *in vitro* (Brose et al., 1999;Brose and Tessier-Lavigne, 2000;Kidd et al., 1998). Moreover, Slit2 was found to regulate branching of sensory axons *in vitro* (Wang et al., 1999). Analysis of double knock-out mouse lacking Slit1 and Slit2 revealed that DRG axons bifurcate and form collateral branches, suggesting that Slit proteins do not affect bifurcation and collateral branching of sensory axons *in vivo*. However, some bifurcated axons of Slit1 and Slit2 double knock-out mice as well as of Robo1 and Robo2 double knock-out mice grow prematurely into the spinal cord instead of growing in longitudinal direction which confirms a repellent axonal guidance role of Slit proteins.

Signals acting in concert with CNP at the dorsal root entry zone on bifurcation of sensory axons most probably do not act as branching factors. If there would be other branching signals besides the cGMP signalling, the phenotype of the cGMP signalling mutants would be at least partly compensated by them. However, almost all sensory axons observed in cGMP signalling mutant mice do not bifurcate. Axonal guidance cues could help cGMP signalling to induce axonal bifurcation at the dorsal root entry zone. If repulsive signal(s) acting on axonal growth cones and forcing them to change their growth direction are a necessary complement for cGMP signalling to induce bifurcation, then absence of such signal(s) in cell culture would explain why sensory axons do not start to bifurcate after addition of CNP. From this point of view Slit could be a complementary signal regulating sensory axon bifurcation. Slit is not the only inhibitory cue acting at the dorsal spinal cord at the time when sensory axons reach the dorsal root entry zone. This could explain that only minor defects of bifurcations are observed in Slit knock-out mice. Netrin-1 and Semaphorin 3A also act as inhibitory cues for sensory axons (Fu et al., 2000;Masuda et al., 2008;Ozaki and Snider, 1997;Watanabe et al., 2006). Analysis of the Semaphorin 3A knock-out mouse, the receptor of semaphorin 3A – neuropilin - knock-out mouse or the netrin-1 knock-out mouse has not revealed sensory axon bifurcation defects (Kitsukawa et al., 1997;Serafini et al., 1996;Taniguchi et al., 1997). This result is not surprising having in mind that several

inhibitory/repellent signals act in the spinal cord and, therefore, a single knock-out mouse does not reveal any abnormalities in sensory axon bifurcation.

One more puzzle presented by *in vitro* experiments with sensory neurons is an ability of small fraction (5-13 %) of axons to bifurcate (Müller, 2002). As already mentioned, sensory neurons do not have any source of CNP in the cell culture with FCS free medium, therefore, the main factor inducing bifurcation - cGMP signalling - can not be stimulated by CNP in sensory neurons *in vitro*. Bifurcation of some sensory neurons in the absence of CNP could be explained by the ability of p21-activated kinase (PAK) to activate membrane bound guanylyl cyclases (Guo et al., 2007). PAK is activated by the small GTPase Rac which in turn can be activated by extracellular signals through various types of membrane receptors, including receptor tyrosine kinases (e.g. PDGF, EGF receptors)(Betson et al., 2002;Guo et al., 2007). If this pathway could be activated in a small fraction of sensory neurons *in vitro*, then, most probably, it could be activated in some sensory neurons *in vivo* as well. However, analysis of the CNP mutant mouse phenotype does not demonstrate any increase in bifurcations compared to cGKI knock-out or Npr2 mutant mice. Also analysis of the same strain of CNP mutant mouse by Zhao and Ma revealed only 2% of bifurcating axons in homozygous mutant mice (Zhao, 2009). Moreover, analysis of CNP knock-out mouse reported less than 1% of bifurcating axons in knock-out mice (Schmidt, 2009). All these results confirm my analysis of CNP mutant mouse and reject the theory that a small fraction of neurons activate cGMP signalling via an alternative pathway.

4.2 What prevents sensory axons from repeated bifurcation

First sensory axons reach the spinal cord at E 10.5, bifurcate and grow further in the rostrocaudal direction. After 48 h waiting period collateral branches sprout from both arms of the main axon and enter the spinal cord reaching dorsal or ventral horn. After the first bifurcation and change of the growth direction no further bifurcation of sensory axons takes place. Do some intrinsic properties of sensory axons change, or does the microenvironment of axons changes and prevents them from further bifurcation? Inhibitory signals are still in the spinal cord and sensory axons are sensitive to them over the period of their rostrocaudal extension (Fu et al., 2000;Masuda et al., 2008;Watanabe et al., 2006). This suggests that after the initial bifurcation cGMP signalling ceases in sensory axons. As reported here, CNP, Npr2 and cGKI are all indispensible for sensory axon bifurcation. Which of these cGMP

components can be quickly inactivated and thereby stop cGMP signalling and secondary bifurcation in sensory axons?

cGKI expression is observed in sensory axons at E11-E14 and is reduced at E15 (Schmidt et al., 2002;Schäffer, 2006). cGKI is expressed in sensory axons when they are growing rostrocaudally but do not bifurcate further. cGKI can be inhibited by small-molecule modulators (Valtcheva et al., 2009), but there are no natural direct inhibitors of cGKI. Its activity *in vivo* is regulated by cGMP dynamics, which, in turn, depends on activities of guanylyl cyclases and phosphodiesterases.

Npr2 guanylyl cyclase is activated by binding of its ligand, CNP. ATP is also required for this process, therefore it is hypothesized that CNP binding to the extracellular domain facilitates ATP binding to the kinase homology domain causing Npr2 to undergo conformational changes (Garbers and Lowe, 1994;Potter, 2005;Potter et al., 2006;Potter and Hunter, 2001). Npr2 is phosphorylated in unstimulated mode. After initial stimulation Npr2 becomes dephosphorylated and this coincides with decreased activity of guanylyl cyclase. It is suggested that dephosphorylation mediates desensitization of the receptor (Potter and Hunter, 1998;Potter and Hunter, 1999;Potter and Hunter, 2001). Npr2 can be dephosphorylated and desensitized not only by CNP, which is called homologous desensitization, but also by agents other than natriuretic peptides, which is called heterologous desensitization. In contrast to homologous desensitization, a single phospho-site (S523 in Npr2) is most important among other phospho-sites for heterologous desensitization (Potter, 2005;Potter and Hunter, 2001).

Apart from desensitization, another mechanism to terminate further Npr2 signalling would be ligand-mediated internalization. However, there are controversies in the literature whether internalization of Npr1 and Npr2 is occuring. Moreover, whereas there are several papers reporting internalization of Npr1 (Pandey et al., 2002;Pandey et al., 2005), there is no single paper describing internalization of Npr2 (Fan et al., 2005).

Blocked activity of Npr2 guanylyl cyclase terminates cGMP signalling. It should become terminated after the first bifurcation of a sensory axon and not become reactivated in order to prevent further bifurcations. Homologous desensitization lasts until a yet unknown kinase phosphorylates Npr2. In case of Npr1, activation of a desensitized receptor is possible after 60 min, which suggests that the receptor is re-phosphorylated in 60 min (Bryan et al., 2006). Assuming, that Npr2 has similar properties as Npr1, these data indicate, that Npr2 desensitization can not be responsible for a complete termination of cGMP signalling and further bifurcations, due to its short period of action. However, this could be a first step in

termination of cGMP signalling, during which further long lasting effects on cGMP signalling would take place.

Other proteins regulating concentration of cGMP in the cell are phosphodiesterases (PDEs). In contrast to Npr2, they reduce cGMP concentration by hydrolysis. PDE2A is expressed in cell bodies of DRG neurons and their axons. Its expression correlates with the expression of cGKI and Npr2 in spinal cord (Seiferth, 2008). PDE2A is activated by cGMP and hydrolyzes both cGMP and cAMP. It can be palmitoylated and anchored to the membrane, where it functions as a component of large signalling complexes assembled into lipid rafts, or it can be also found in a soluble intracellular compartment (Menniti et al., 2006;Omori and Kotera, 2007).

PDE2A can reduce the concentration of cGMP in the cell by hydrolyzing it. However, as soon, as Npr2 will be activated and will generate cGMP, the cGMP signalling will start again. PDE2A might, therefore, serve rather for a fine tuning of the cGMP signal, than for its termination. PDE2A can confine cGMP and cAMP to certain compartments creating gradients of these cyclic nucleotides (Conti and Beavo, 2007). In addition, it reduces levels of both cyclic nucleotides during the peak of cGMP elevation, creating dependence of the cAMP level on the level of cGMP (Zaccolo and Movsesian, 2007).

CNP is secreted at the dorsal spinal cord (Schmidt et al., 2009). It is synthesized as a 126 amino acid long prepropeptide. After removal of its signal peptide, furin mediated cleavage converts the propeptide to a biologically active 53- amino acid peptide which is secreted. The 53-amino acid CNP peptide can be further cleaved by an unknown exctracellular enzyme to a 22-amino acid form. Both 53- and 22-amino acid CNP forms seem to be functionally similar (Potter et al., 2006;Wu et al., 2003). The cGMP signalling cascade can be activated by 22-amino acid CNP form in embryonic mouse DRG resulting in the generation of cGMP by Npr2 (Schmidt et al., 2009). It is not shown which form of active CNP is implicated in sensory axon bifurcation at the spinal cord. Most probably, termination of cGMP signalling would require the abolishment of both active CNP forms, first of all furin, which is the precursor of the 22-amino acid CNP form.

Another mechanism of CNP signal depletion is binding of CNP to Npr3. Npr3 is also called natriuretic peptide clearance receptor. It lacks a guanylyl cyclase activity, therefore, binding of natriuretic peptides to Npr3 does not lead to cGMP generation (Potter et al., 2006). Npr3 is expressed in embryonic dorsal and ventral spinal cord, and along dorsal roots (DiCicco-Bloom, 2004).

Downregulated furin activity resulting in a reduction of active CNP or upregulation of Npr3 resulting in depletion of CNP would affect all sensory neurons by globally terminating cGMP signalling. Such scenario suggests that all sensory neurons would be deprived of a signal to bifurcate as soon, as conversion of propeptide to the active form of CNP ceases or as Npr3 is upregulated. It is reported that sensory axons reach the dorsal root entry zone and bifurcate beginning from embryonic day 10.5, followed by collateral branching after one-to two-day long delay (Ozaki and Snider, 1997). This development is not strictly timely followed by all sensory axons. Whereas first axons reach dorsal root entry zone at embryonic day 10.5 and bifurcate, there are axons which bifurcate a day or two later. Analysis of sensory axons by DiI labelling revealed such situations where fully formed axonal bifurcations are next to active growth cones which have recently bifurcated (see Fig. 3.2 H, Fig.). Such a prolonged time window for bifurcations objects to the hypothesis about a global inhibition of cGMP signalling in all sensory neurons simultaneously. Downregulation of active CNP or depletion of CNP would result in either of two outcomes: repeated bifurcation of early arrived sensory axons, if the CNP signal is downregulated at the end of the "waiting period", or a small but significant fraction of turning axons, if the CNP is downregulated immediately after arrival of first sensory axons to the dorsal root entry zone. Since neither of these phenomena has been observed, it is not likely that the CNP signal is downregulated in order to prevent secondary bifurcations.

To sum up, selective termination of bifurcation signalling in those sensory axons, which have bifurcated, requires an individual regulation of the cGMP signal in every single sensory neuron. The best candidates for such regulation would be Npr2 and PDE2A. After CNP binding and activation of cGMP signalling, Npr2 becomes desensitized and thereby stops further generation of in axons, which received the bifurcation signal. However, activation of some other mechanism, leading to cGMP signalling termination, should follow Npr2 desensitization, because the latter lasts only transiently. PDE2A is activated in those sensory axons, which received the CNP signal and have an increased level of cGMP. PDE2A hydrolyzes both cGMP and cAMP, which means that activation of PDE2A activates regulation of cAMP signalling which in turn might effect termination of cGMP signalling.

4.3 Collateral branching in cGMP mutant mice

4.3.1 Mechanisms of sensory axon bifurcation and collateral branching are different

Analysis of cGMP signalling mutant mice revealed that sensory axon bifurcation is impaired. In contrast, another type of axonal branching, collateral branching, is not affected. This suggests that axonal bifurcation is regulated by cGMP signalling, whereas collateral branching requires other signals.

There are many studies analysing the effect of a certain branching factor on neurons grown in culture, however, it is difficult to discriminate between different modes of branching without video recording analysis. In their work Gallo and Letourneau analysed video recordings of cytoskeletal reorganization followed by collateral branching of embryonic (E9-10) chick sensory axons in culture, and demonstrated that collateral sprouting of sensory axons can be activated and stabilized by NGF, which signals via TrkA receptor and PI-3 kinase (Gallo and Letourneau, 1998). Proprioceptive axons express TrkC, but not TrkA, therefore, they should not be affected by NGF. This study was carried out in cell culture where some subsets of sensory neurons, e.g. proprioceptive neurons requiring NT-3 for their survival might have died. However, *in vivo* all sensory axons form collaterals, suggesting that not only NGF is implicated in this process.

Although the main axon and collaterals sprouting from the main axonal shaft belong to the same neuronal cell, they have different characteristics. This study revealed that bifurcation of the main axon and collateral branching are regulated by different mechanisms. Another study by Gallo et al. (1999) has demonstrated that the main axon and axon collaterals of embryonic DRG neurons exhibit different sensitivities to treatments that inhibit the dynamic growth of microtubule plus ends. Inhibition of microtubule dynamics did not effect elongation of collaterals, suggesting that the transport of microtubules, and not their polymerization, may be the most important mechanism of collateral growth (Gallo and Letourneau, 1999). It is not likely that microtubule dynamics is inhibited in the absence of cGMP signalling. Although the main axon does not bifurcate, it is elongating after the turning to either rostral or caudal direction, which indicates that microtubules are polymerised. Overall, different characteristics of the main axon and collaterals suggest that cGMP signalling regulates certain cellular functions, that are indispensible for bifurcation of the main axon but are not required for the formation of collateral branches.

4.3.2 Collateral branching is affected indirectly by cGMP signalling

Sprouting of single collaterals is not impaired in the absence of cGMP signal. However, when cGMP signalling is defect, there is only one branch of sensory axon left instead of two branches formed via bifurcation. This affects the total number of sprouting collaterals by the reduction of the total length of axon shaft from which they arise. Reduced amount of sensory collaterals in the cGKI or functional Npr2 deficient mouse embryos compared to the wild type mice was shown by anti-trkA (trkA is expressed by nociceptive neurons) staining in transverse spinal cord sections (Schmidt et al., 2002;Schmidt et al., 2007).

The comparison of distances between two adjacent collaterals revealed smaller distances in cGMP signalling mutant mice compared to wild type mice, suggesting a compensation mechanism for reduced total number of collaterals. It is difficult to hypothesize, whether this slightly increased density of collaterals is a result of action of a certain branching factor(s), or whether it could be explained simply by an increased amount of structural precursors per axon arm, compared to bifurcated sensory axons of wild type mice. However, this compensatory mechanism does not restore the number of collateral branches in cGMP mutant mice to the level, detected in wild type mice.

Analysis of cGMP mutant mice using electrophysiological methods demonstrated that functional connectivity of collateral branches with second order neurons within the superficial dorsal horn is impaired (Schmidt et al., 2007;Schmidt et al., 2009). A reduced number of collateral branches synapsing on second order neurons explains this functional connectivity deficit. One could expect that impaired connectivity in spinal cord could lead to reduced perception of certain stimuli, e.g. pain stimuli (nociception). However, perception of acute pain in cGKI knock-out mice is not disturbed (based on hot-plate test), suggesting that impaired connectivity of collaterals with second order neurons due to absent sensory axon bifurcations does not affect acute pain signal transmission. On the other hand, cGKI knock-out mice have reduced formalin evoked nociception and inflammatory hyperalgesia induced by zymosan, suggesting that cGKI is involved in perception of inflammatory pain signals (Tegeder et al., 2004). Schmidtko et al. report that cGKI is involved in processing of nociceptive signals in spinal cord, however, the signalling is different from the signalling which regulates bifurcation. cGMP, playing a role of mediator in nociceptive processing, is produced by soluble guanylyl cyclase activated by NO. Moreover, the NO-GC signalling does not take place in DRG neurons, it is confined to the dorsal horn cells (Schmidtko et al., 2008a;Schmidtko et al., 2008b;Schmidtko et al., 2009). These data demonstrate that NO-GC-

cGMP-cGKI is involved in sensitization during inflammatory or neuropathic pain. But this pathway is not involved in basal pain perception (Schmidtko et al., 2009). Since pain perception should be processed during the relaying process from sensory neurons to second-order neurons, cGMP signalling, inducing bifurcation and thereby ensuring a proper length of axonal shafts generating collateral branches, could play a role in basal pain perception. Components of cGMP signalling play a role in other cellular functions, not only in axonal bifurcation. cGKI is required for relaxation of smooth muscle cells, CNP and Npr2 – for long bone formation. Therefore, cGMP signalling mutant mice have other phenotypes besides the absence of sensory axon bifurcation, which aggravates analysis of basal pain perception in these mice.

4.4 Do some of known phosphorylation targets of cGKI could play a role in axonal bifurcation?

cGKI plays a role in smooth muscle relaxation, and platelet aggregation and the downstream targets that lead to such effects are studied well. Branching of axons involves rearrangement of cytoskeletal elements, therefore it is likely that signalling pathways regulating branching will converge at the level of the cytoskeleton. Many of known cGKI targets, e.g. VASP which plays a role in platelet aggregation, myosin phosphatase target subunit 1 (MYPT1) and RhoA, which regulate relaxation of smooth muscle, act by regulating cytoskeletal dynamics. Hence, it is likely that already known phosphorylation targets of cGKI, which regulate the cytoskeleton, are implicated in sensory axon bifurcation. To test this hypothesis I analysed some known targets of cGKI regarding their role in sensory axon bifurcation. Moreover, I confirmed cGKI dependent phosphorylation of some putative targets of cGKI – Mena and GSK3β and analysed their effect on sensory axon bifurcation.

4.4.1 Ena/VASP family

Analysis of whole-mount stainings of VASP knock-out mice was carried out by S.Schäffer (Schäffer, 2006) and repeated on the single axon level using DiI staining in this study. It did not reveal any abnormalities in sensory axon bifurcation although it confirmed phosphorylation of VASP by cGKI. However, this finding is not sufficient to conclude that VASP is not involved in sensory axon bifurcation because VASP belongs to the Ena/VASP

protein family, where family members have closely related functions and can substitute each other (Krause et al., 2002;Krause et al., 2003;Kwiatkowski et al., 2003;Kwiatkowski et al., 2007). Double knock-out mice lacking both VASP and Mena also do not show sensory axon bifurcation defects, suggesting that either Ena/VASP family proteins are really dispensable for sensory axon bifurcation or the third family member, EVL (Ena/VASP like protein), substitutes VASP and Mena proteins in double knock-out mice. This uncertainity could be solved only by the analysis of triple double knock-out micse. Having in mind, that both VASP and Mena are phosphorylated by cGKI in DRG (this work; Schäffer, 2006), and this affects actin filaments by accelerating their elongation (Breitsprecher et al., 2008;Lebrand et al., 2004), it is very likely that this cytoskeleton rearrangement via actin elongation plays a role in bifurcation. On the other hand, this role might be not so crucial for axonal bifurcation to be reflected in a defect sensory axon bifurcation even in the triple knock-out mouse.

4.4.2 GSK3-β

GSK3-β becomes phosphorylated upon cGKI stimulation in DRG neurons (Zhao et al., 2009) and upon cGKII stimulation in chondrocytes (Kawasaki et al., 2008). Moreover, Zhao et al. demonstrated that inhibition of GSK3-β by phosphorylation is required for axonal branching *in vitro* induced by cGMP. Rat DRG neurons expressing dominant active GSK3-β show a much simpler morphology compared to wild type neurons, even in the presence of cGMP analogues (Zhao et al., 2009). These characteristics of GSK3-β make it a very likely candidate to be implicated in sensory axon bifurcation, however, analysis of GSK3 double knockin mice with constitutively active mutated GSK3 α and β forms did not reveal any defects in sensory axon bifurcation.

Active unphosphorylated GSK3-β inhibits most of its targets, like microtubule associated proteins: CRMP2, APC, MAP2 or kinesin light chain, but not MAP1B. MAP1B is activated upon phosphorylation of GSK3-β. Complete inhibition of GSK3-β prevents phosphorylation of MAP1B and, thereby, inhibits axonal growth. Moderate reduction of GSK3-β activity does not prevent phosphorylation of MAP1B and elongation of axon, but results in reduced phosphorylation of other microtubule associated proteins, leading to increased branching of axons (Fig. 4.2) (Kim et al., 2006).

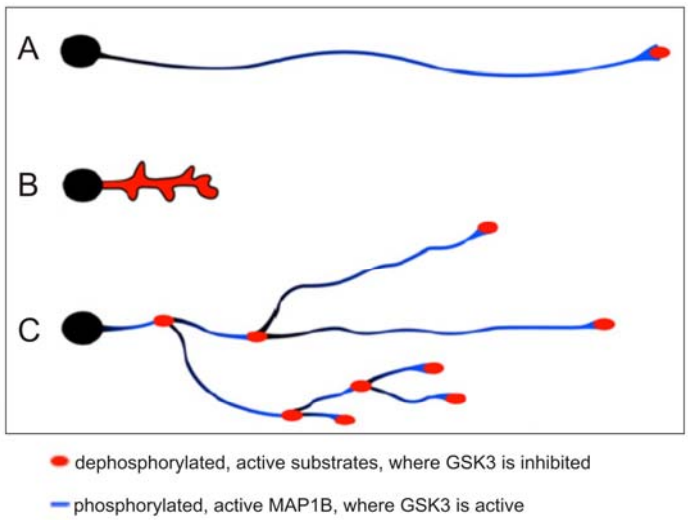

Fig.4.2: Regulation of axon morphology by GSK3 (Kim et al., 2006)**.** (A) GSK3 is phosphorylated and inactivated only at growth cone tips. Its substrates - APC, stabilizing microtubule plus ends, CRMP2, enhancing microtubule polymerization - remain unphosphorylated by GSK3 and are active at growth cone. MAP1B is phosphorylated and activated by active GSK3 in the rest of the axon, where it is required for the generation of dynamic microtubules. (B) When GSK3 is completely inactivated, none of its substrates is phosphorylated. Unphosphorylated active APC along the whole axon leads to excess microtubule stability. Unphosphorylated inactive MAP1B does not generate dynamic microtubules. Axon growth is inhibited. (C) Partial inhibition of GSK3 leads to unphophorylated and active APC and CRMP2 at multiple points along the axon. Microtubules reorganize at these points leading to axon bifurcation. Activity of GSK3 is sufficient to phosphorylate and activate MAP1B along the axon, thereby enabling growth of newly formed branches.

The model for regulation of axon morphology by GSK3 proposed by Kim et al. explains why the dominant active GSK3-β phosphomutant, used in experiments by Zhao et al., inhibited cGMP induced branching in DRG neurons (Zhao et al., 2009). Active GSK3-β inhibited APC and CRMP2, thereby reducing cytoskeletal rearrangement events and formation of branches, allowing only elongation of axon (Fig. 4.2 A). Based on the results of Kim et al. and the proposed model, one would expect that GSK3 double knockin mice has defect neurons, and bifurcation or collateral formation of sensory axons is impaired. However, this study did not reveal any defects (Fig. 3.21, Fig. 3.23). Another study of GSK3 double knockin mice carried out by Gärtner et al. also did not reveal any obvious neuronal defects (Gartner et al., 2006), suggesting that phosphorylation is not the major mechanism of GSK3 activity regulation. Modulation of subcellular distribution of GSK3, complex formation with GSK3 binding proteins and regulation of the phosphorylation state of substrates requiring priming, like CRMP2 and APC, is also of importance. Reduced activity of Cdk5, a priming kinase of

CRMP2 (Yoshimura et al., 2005), and of CK1, a priming kinase for APC (Ferrarese et al., 2007), would neutralise the effect of constantly active GSK3 phosphomutant.

In contrast to DRG, GSK3-β is not phosphorylated upon stimulation of cGKI in F11 cells. These cells express both cGKI and GSK3-β. cGKI in F11 cells can be activated by the cGMP analogue 8pCPTcGMP resulting in VASP phosphorylation. There is no proof that cGKI directly phoshorylates GSK3-β *in vivo*, but *in vitro* it can phosphorylate GSK3-β (Zhao et al., 2009). Moreover, phosphorylation takes place within 5 minutes of cGKI stimulation, as it is in the case of VASP, suggesting that the reaction is direct. Nevertheless it is possible that GSK3-β is phosphorylated upon stimulation of cGKI by another kinase which was activated by cGKI, and this kinase is not present in F11 cells, in contrast to DRG. However, a more likely scenario is that subcellular distribution of GSK3-β in F11 cells is different compared to DRG and not accessible for cGKI. There are reports, describing redistribution of GSK3-β in response to different factors, like lipid, glucose or glycogen uptake (Fernandez-Novell et al., 1992;Nielsen et al., 2001;Taylor et al., 2006).

Summing up, regulation of GSK3-β activity does not depend solely on phosphorylation. Many other factors can modulate the effect of GSK3 phosphorylation and inactivation by cGKI, therefore, it is difficult to dissect the role of GSK3 inactivation in sensory axons.

4.4.3 RhoA

RhoA belongs to the Rho GTPase protein family which transduces exctracellular signals to the actin cytoskeleton (Heasman and Ridley, 2008;Linseman and Loucks, 2008). Although nucleotide exchange factors (GEFs) and GTPase activating proteins (GAPs) constitute the major regulation mechanism of RhoA, direct phosphorylation or ubiquitination of RhoA also can regulate its activity (Heasman and Ridley, 2008;Jaffe and Hall, 2005). RhoA has been shown to be phosphorylated and inactivated by cGKI (Sauzeau et al., 2000;Sauzeau et al., 2003;Sawada et al., 2001;Sawada et al., 2009). Difficulties to detect phosphorylation of RhoA were described in earlier reports (Lang et al., 1996;Sauzeau et al., 2000). Cytosolic RhoA bound by GDP dissociation inhibitor (GDI) cannot be phosphorylated because the phosphorylation site is masced by GDP. Only GDP-free membrane-bound fraction of RhoA can be phosphorylated. Membrane-bound RhoA represents 2-3% of total RhoA in a cell, which explains why detection of phosphorylation in lysates is difficult (Lang et al., 1996). Analysis of phosphorylation of only those several percent of membrane-bound RhoA, by

immunoprecipitating them from membrane fraction, would facilitate detection of phosphorylation.

Preliminary results, which have to be confirmed by more thorough analysis, show that RhoA is not phosphorylated in DRG upon stimulation of cGKI. It has been reported in other studies on PKA that RhoA regulation can be achieved via indirect pathway as well as via direct phosphorylation. There are reports about phosphorylation of GDI by PKA, which leads to inhibition of RhoA (Qiao et al., 2008), or phosphorylation of GDI via thrombin-PKC leading to activation of RhoA (Qiao et al., 2003). Therefore, it is very likely, that RhoA is regulated by cGKI in DRG, but not via direct phosphorylation.

RhoA is expressed in DRG and is involved in cytoskeleton regulation, suggesting that it might be involved in sensory axon bifurcation. A RhoA knockout mouse has not been created, moreover, it would probably be embryonic lethal because of its role in implantation (Shiokawa et al., 2000).

4.4.4 Myosin IIB

Myosin IIB is one of three nonmuscle myosin II isoforms in mammalian neurons (Brown, 2004). It plays a role in retrograde actin flow in growth cones (Lin, 1996:Medeiros, 2006;Brown, 2003). The majour regulation mechanism of myosin is through phosphorylation of the regulatory myosin light chain (MLC) by the Ca^{2+}/calmodulin dependent myosin light chain kinase (MLCK) or dephosphorylation by the myosin phosphatase (Brown, 2004). cGKI can regulate calcium level and thereby activity of MLCK (Hofmann, 2009). cGKI can also phosphorylate myosin phosphatase target subunit (MYPT1) and thereby prevent inhibition of myosin phosphatase (Lontay, 2005;Surks, 1999).

RhoA can activate Rho kinase (ROCK) which inhibits myosin phosphatase. As a result, even under decreased concentration of Ca^{2+} MLC remains phosphorylated and activates myosin ATPase (Brown and Bridgman, 2004). In this work a direct regulation of RhoA by cGKI phosphorylation was not detected. However, RhoA could be indirectly activated by cGKI as discussed on previous page.

Since cGKI is involved in regulation of myosin activity and myosin IIB plays a role in retrograde actin flow in growth cones, myosin IIB is a likely candidate to be implicated in sensory axon bifurcation. However, analysis of myosin IIB knock-out mice did not reveal any defects of sensory axons. This suggests that myosin IIB is not essential in sensory axon

bifurcation and twofold increase in retrograde flow in growth cones of myosin IIB knock–out mice does not play a crucial role in this.
Moreover, if a regulatory function of RhoA in the myosin system would be important in sensory axon bifurcation, it would become apparent in the absence of myosin IIB, disrupting the balance of myosin system. However, this analysis shows that the myosin system itself and, therefore, the regulatory function of RhoA in the myosin system, is not essential in sensory axon bifurcation.

Overall, analysis of several of the known or putative phosphorylation targets of cGKI demonstrated that some of these targets are phosphorylated by cGKI in DRG, however, none of them was revealed to play a crucial role in sensory axon bifurcation. It is possible that a single target of cGKI, which is indispensable for axon bifurcation, exists. Although, it is most likely that a protein conducting axon bifurcation will regulate cytoskeleton dynamics, other proteins involved in transport, substrate adhesion or even local protein synthesis cannot be excluded. However, it is also possible that cGKI sets a network of proteins, which are equally important, into action, and absence of one single protein does not abolish the function of the whole network.

4.5 Phosphorylation targets detected by the phospho-motif antibody

4.5.1 Pros and cons of the antibody against RRXpS/pT motif

Phospho-motif antibodies can be used to identify specific kinase substrates. In theory, they should recognize substrates of a given kinase only when these substrates are phosphorylated. Anti-RRXpS/pT antibody was successfully used in studies of PKA substrates (Boo, 2006;Manning et al., 2002). cGKI is closely related with cAMP dependent kinase (PKA), and the RRXpS/pT motif as well as some downstream targets are even shared by both kinases. Therefore, the antibody against RRXpS/pT motif was used in the search for cGKI targets. Although the antibody recognizes several proteins differently phosphorylated upon stimulation of cGKI, it has some drawbacks.
Experiments with VASP demonstrate that the anti-RRXpS/pT does not recognize all substrates phosphorylated on RRXpS/pT motif. VASP contains RRVSN motif. Phosphorylation of this motif leads to a mobility shift of VASP from 46 to 50 kDa. (Krause et al., 2003). This shift can be observed in anti-VASP Western blots of DRG or F11 lysates stimulated with cGMP analogue, however, no band of 50 kDa recognized by the antibody

against RRXpS/pT was observed in Western blots of stimulated DRG lysates or stimulated F11 cell lysates. This shows that anti-RRXpS/pT does not recognize all phosphorylated RRXS/T motifs.

Lysates subjected to lambda-phosphatase treatment should not contain any phospho-proteins, therefore, anti-RRXpS/pT Western blotting analysis of such lysates should not reveal any bands. Indeed the antibody against RRXpS/pT does not recognize any proteins in mouse embryonic DRG lysate (3.38A). However, it recognizes several proteins on Western blot membranes that were dephosphorylated (3.38 B) or on Western blots of dephosphorylated F11 cell lysates (3.38 C), suggesting that the antibody can recognize non-phosphorylated proteins as well.

The phospho-motif specific antibody is a good tool to detect phosphorylation targets of cGKI, but the results should be carefully proved having in mind the drawbacks of the antibody.

4.5.2 Identity of the 51 kDa protein dephosphorylated in F11 cells and DRG upon stimulation of cGKI

Although anti-RRXpS/pT analysis revealed different phosphorylation pattern between lysates prepared from F11 cells and embryonic mouse DRG it detected dephosphorylation of a 51 kDa protein upon stimulation of cGKI in both Fll cells and DRG neurons. Dephosphorylation of this 51 kDa protein upon cGKI stimulation is an unusual outcome of the kinase activity. This result might be due to cGKI dependent inhibition of an unknown kinase by phosphorylation, or by cGKI binding to the 51 kDa protein, thereby preventing access to it for another kinase. This would lead to gradual dephosphorylation of the 51 kDa protein due to basal phosphatase activity. Another possibility is that the 51 kDa protein becomes dephosphorylated by a phosphatase activated by cGKI.

The only phosphatase known to interact with cGKI is myosine phosphatase. cGKI binds and phosphorylates myosin phosphatase target subunit 1 (MYPT1) (Lontay et al., 2005;Surks et al., 1999). Phosphorylation of Ser694 by cGKI prevents phosphorylation of Thr695 and, thereby, blocks inhibition of myosine phosphatase. Although phosphorylation by cGKI keeps myosin phosphatase active, there is no protein of 51 kDa known to be dephosphorylated by myosin phosphatase. The only known target is myosin light chain which has a molecular mass of approximately 20 kDa.

This study reported that GSK3-β is phosphorylated upon cGKI phosphorylation in embryonic mouse DRG. Upon phosphorylation GSK3-β becomes inactive and its phosphorylation targets would become dephosphorylated due to phosphatase activity. On the one hand, it could be an explanation for dephosphorylation of the 51 kDa protein in a cGKI dependent manner, and would lead to MAPs dephosphorylated upon phosphorylation of GSK3-β. On the other hand, there is no dephosphorylation of GSK3-β upon stimulation of cGKI in F11 cells, however, the 51 kDa targets becomes dephosphorylated, suggesting that this unknown 51 kDa protein is not a target of GSK3-β.

In conclusion, characteristics of the 51 kDa protein dephosphorylated in a cGKI dependent manner suggest that this protein is most likely a novel indirect downstream target of cGKI.

Attempts to identify the 51 kDa from the cytoplasmic fraction resolved by one-dimensional SDS-PAGE and postnuclear supernatant resolved by two-dimensional SDS-PAGE by MS analysis brought completely different results. Therefore, it is difficult to hypothesize, which protein might become dephosphorylated in a cGKI dependent manner, and whether this would play a role in sensory axon bifurcation. Cytoskeletal proteins like tubulin beta 1, or transport protein dynein, were found due to their high copy-number, and it is rather coincidence, that they have a cGKI phosphorylation motif. Fascin is expressed in the nervous system, moreover its actin bundling activity is inhibited by phosphorylation, implying a role in axonal bifurcation, if it is really an indirect target of cGKI. However, no study reports phosphorylation/dephosphorylation of Thr346 in amino acid sequence RRIT, only phosphorylation of Ser39 in amino acid sequence SASS (Ono et al., 1997), which would not be detected by anti-RRXpS/pT antibody.

4.6 Conclusions

This study investigated cGMP signalling and its role in sensory axon bifurcation by analysing sensory axons of mutant mice lacking known or putative components of the cGMP signalling cascade (CNP, Npr2, cGKI) and by searching downstream phosphorylation targets of cGKI with the help of biochemical methods. Analysis of DiI labelled sensory axons in cGKI knock-out, Npr2 and CNP mutant mice showed that all these proteins are components of the cGMP signalling involved in sensory axon bifurcation (Fig. 4.3). If any of these components is absent or is functionally defect, the cGMP signalling is impaired resulting in the absence of

sensory axon bifurcations at the DREZ. Collateral branching remains even if the cGMP signalling is disrupted suggesting that this signalling is not required for collaterl branching.

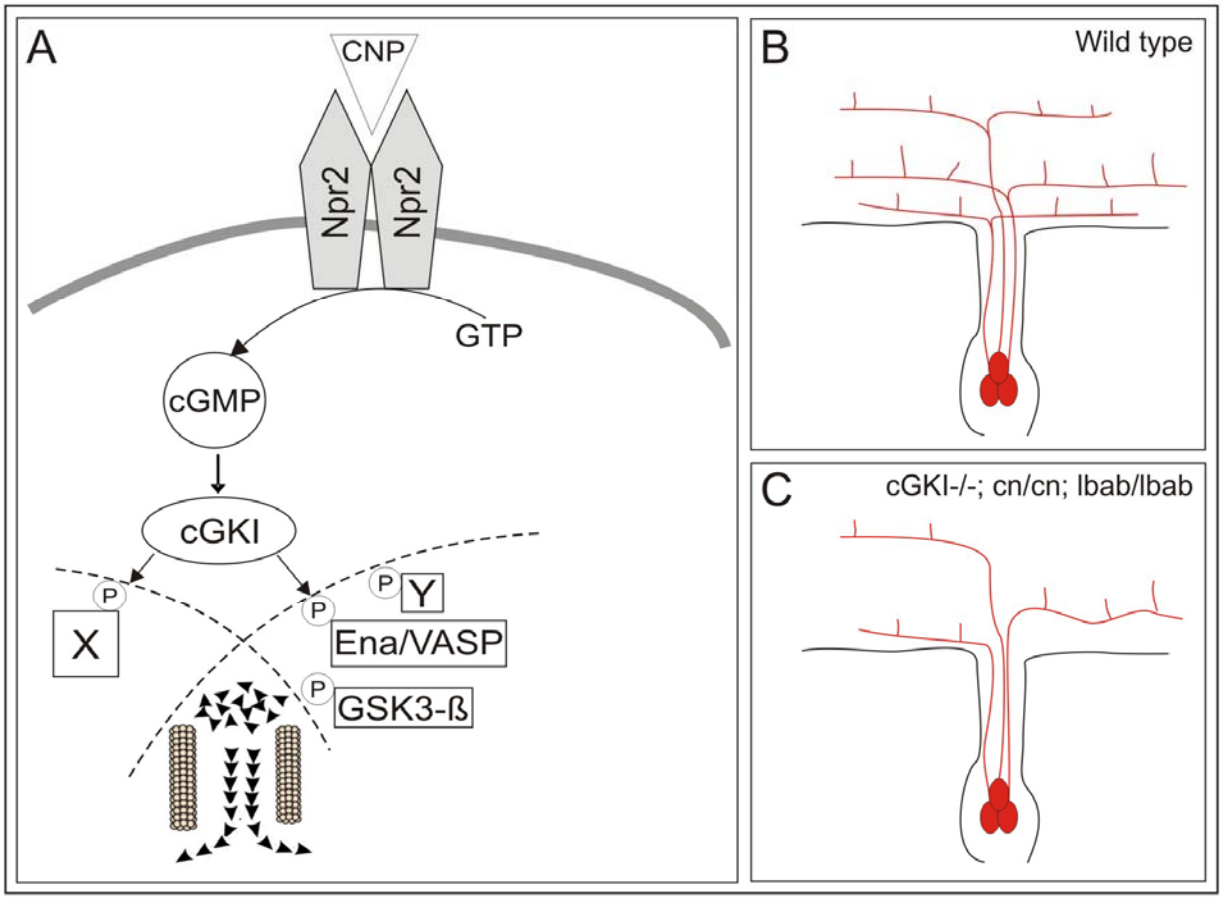

Fig.4.3: cGMP signalling in sensory axon bifurcation. (A) cGMP signalling cascade in DRG. CNP binds Npr2 and thereby activates it. Activated Npr2 generates cGMP from GTP. cGMP binds and activates cGKI. The signalling downstream of cGKI is not clear yet, therefore, two possible outcomes are represented.

- On the left side cGKI phosphorylates target X, which alone is required for the bifurcation of sensory axons.
- On the right side cGKI phosphorylates multiple proteins simultaneously. Some of these proteins are known targets like VASP, Mena or GSK3-β, whereas Y represents not yet identified downstream target of cGKI. These proteins form a network, where all members are involved in sensory axon bifurcation. A loss of one member, does not lead the collapse of the whole network, only a loss of several members will lead to this.

(B) cGMP signalling induces bifurcation of sensory axons at the dorsal root entry zone. (C) In mice mutant for cGMP signalling components sensory axons turn either to caudal or rostral direction without bifurcation. Interstitial branching is not affected by deficient cGMP signalling.

This study also demonstrated that Mena and GSK3-β are phosphorylated in DRG upon stimulation of cGKI. However, neither the Mena/VASP double knock-out mouse, nor the GSK3-β knock-in mouse showed any sensory axon defects. This suggests two explanations:

- Mena, VASP, and GSK3-β do not play any role in sensory axon bifurcation, although they are phosphorylated upon stimulation of cGKI in DRG. cGKI has some other phosphorylation target in DRG, which is not detected yet, and which alone leads to cytoskeleton rearrangements resulting in sensory axon bifurcation.
- cGKI has multiple phosphorylation targets in DRG, which all play a role in sensory axon bifurcation and build a system functioning even if some of its components is/are missing. Only the lack of several components brings the system to collapse reflected in a loss of sensory axon bifurcations.

Finding of phosphorylation targets of cGKI involved in sensory axon bifurcation is necessary to understand how cGMP signalling induces axonal bifurcation. If the first scenario is the correct one, then detection of new cGKI phosphorylation targets in DRG is crucial. Analysis of a knock-out mouse lacking this phospho-target of cGKI would show, whether it is indispensable for sensory axon bifurcation. If multiple cGKI targets induce sensory axon bifurcation, then it will be difficult to dissect which of them are indispensible for this process and which are rather auxiliary ones. Even in this scenario detection of new cGKI targets and their analysis is important. It would help to understand the network of multiple proteins involved in sensory axon bifurcation. Therefore, the search for new cGKI targets in DRG should proceed. There are other methods, which could be also used in this search. Metabolic labelling of cell culture or even the whole mouse with stable isotopes for quantitative proteomic analysis is a promising technique which could provide data for changes in phosphorylation of certain proteins (Ishihama et al., 2005;Krijgsveld et al., 2003;Wu et al., 2004;Wu and Maccoss, 2007).

5 SUMMARY

Axon guidance to its targets is accomplished not only via navigation of the primary growth cone but also by initiation and elaboration of branches. Axonal branching enables innervation of multiple targets by the same neuron, leading to the formation of a complex neural network. Whereas guidance of a growth cone is a quite well studied phenomenon, axonal branching is less understood.

In this work I studied branching of DRG axons, which display two modes of branching – bifurcation and interstitial branching. Based on results of previous works, suggesting that cGKI is required for sensory axon bifurcation, I analysed cGKI knock-out mice using DiI tracing to confirm initial observations. cGKI is a part of cGMP signalling, therefore, I analysed mice mutant for other components of cGMP signalling pathway, namely for the guanylyl cyclase Npr2 and its ligand CNP, by DiI labelling. The results of this analysis demonstrated that CNP, Npr2 and cGKI act in a cGMP signalling cascade, which is crucial for sensory axon bifurcation. Sensory axons in all mice mutant for CNP-Npr2-cGKI signalling do not bifurcate at the dorsal root entry zone, instead they turn either to rostral or caudal direction. Interestingly, interstitial branching of sensory axons is not impaired by deficient cGMP signalling.

I analysed branching of pyramidal neuron dendrites in cortex and hippocampus as well as central projection of trigeminal sensory axon in order to determine, whether bifurcations observed there are regulated by cGMP signalling. The results demonstrated that bifurcation of central projection of trigeminal sensory axon is indeed regulated by cGMP signalling. In the cGKI knock-out mouse trigeminal sensory axons do not bifurcate upon reaching the brainstem but turn to join either the ascending or descending tract.

Further, I searched for downstream phosphorylation target(s) of cGKI that would play a role in sensory axon bifurcation. First of all, I analysed known/putative targets of cGKI. VASP was already shown to be phosphorylated by cGKI in DRG. I could demonstrate that Mena and GSK3-β are also phosphorylated in DRG upon stimulation of cGKI. Analysis of Mena/VASP double knock-out mouse as well as analysis of GSK3-β double knock-in mouse (Ser21 in GSK3-α and Ser9 in GSK3-β were changed to alanine preventing phosphorylation of GSK3-β) using DiI tracing demonstrated, that sensory axon bifurcation is not impaired, suggesting that VASP, Mena and GSK3-β are not crucial for sensory axon bifurcation.

Search for new phosphorylation targets of cGKI using the antibody recognizing a motif, preferably phosphorylated by cGK - RRXpS/pT - resulted in detection of several proteins phosphorylated, and, interestingly, one protein dephosphorylated upon stimulation of cGKI.
This work elucitated CNP-Npr2-cGKI signalling which is crucial for sensory axon bifurcation. It remains unclear, whether a single phosphorylation target of cGKI, which alone would induce bifurcation, exists, or it is rather a network of multiple cGKI targets, which can be unfolded only by knock-out of multiple components of such network.

5 ZUSAMMENFASSUNG

Die Lenkung der Axone zu ihren Zielen wird nicht nur über die Navigation des primären Wachstumskegels sondern auch durch die Initiation und Weiterentwicklung von Verzweigungen hergestellt. Die axonale Verzweigung ermöglicht Innervation von vielfachen Zielen durch dasselbe Neuron, so dass ein kompliziertes Nervennetz entsteht. Obwohl die Lenkung eines Wachstumskegels ein ganz gut studiertes Phänomen ist, weiß man wenig über den Mechanismus der axonalen Verzweigung.
In dieser Arbeit untersuchte ich die Verzweigungen von Spinalganglienaxonen, welche zwei Arten der Verzweigung – die Bifurkation und die interstitielle Verzweigung - zeigen. Ausgehend von Ergebnissen von vorherigen Arbeiten, dass die cGKI für die axonale Vergabelung erforderlich ist, analysierte ich cGKI-defiziente Mäuse mittels DiI Färbung, um diese anfängliche Beobachtungen zu bestätigen. cGKI ist eine Komponente der cGMP-Signalkaskade. Deshalb analysierte ich Maus-Mutanten für andere Bestandteile des cGMP Signalpfades, nämlich die Guanylylzyclase Npr2, und sein Ligand CNP, mittels DiI Färbung. Die Ergebnisse dieser Analyse demonstrierten, dass CNP, Npr2 und cGKI Komponenten der cGMP Kaskade sind, die für die axonale Verzweigung entscheidend ist. Sensorische Axone in Maus-Mutanten für die CNP-Npr2-cGKI-Signalkaskade vergabeln sich nicht an der Dorsalwurzeleingangszone, stattdessen wachsen sie entweder zur rostralen oder caudalen Richtung. Interessanterweise, wird die interstitielle Verzweigung von sensorischen Axonen durch die abwesende cGMP-Signalkaskade nicht verschlechtert. Ich analysierte auch die Verzweigung von Dendriten der pyramidalen Neurone im Kortex und Hippocampus sowie zentrale Projektionen von trigeminalen sensorischen Axonen, um zu bestimmen, ob die dort beobachtete Vergabelungen durch die cGMP-vermittelte Signaltransduktion geregelt werden. Die Ergebnisse demonstrierten, dass die Vergabelung der zentralen Projektion vom trigeminalen sensorischen Axonen tatsächlich durch die cGMP-Signalkaskade geregelt wird.

Trigeminale sensorische Axone in der cGKI- defizienten Maus verzweigen sich nicht beim Erreichen des Hinterhirns, aber wachsen entweder entlang des steigenden oder des absteigenden Axonentraktes. Weiter suchte ich nach Phosphorylierungssbstraten der cGKI, die eine Rolle in der Vergabelung von Axonen spielen könnte. Zuallererst analysierte ich bekannte Substrate der cGKI. Wie bereits gezeigt wurde, wird VASP durch die cGKI in Spinalganglien phosphoryliert. Ich konnte demonstrieren, dass Mena und GSK3-β in Spinalganglien durch die Stimulation der cGKI ebenfalls phosphoryliert werden. Die Analyse von der Mena/VASP doppelt Knock-out-Maus sowie der GSK3-β doppelt Knock-in-Maus (Ser21 der GSK3-α und Ser9 der GSK3-β wurden ersetzt durch Alanin) mittels DiI Färbung zeigte, dass die Vergabelung der Axone nicht verschlechtert wird. Daher scheinen VASP, Mena und GSK3-β für die Vergabelung der Axone nicht wichtig zu sein.

Bei der Suche nach neuen Phosphorylierungs-Substraten der cGKI wurde ein Antikörper, der ein Phosphorylierungsmotiv der cGKI - RRXpS/pT - erkennt, verwendet. Dies führte zur Entdeckung von mehreren Proteinen, die nach Stimulation der cGKI phosphoryliert werden und interessanterweise, von einem Protein, das durch die Stimulation der cGKI dephosphoryliert wird.

Diese Arbeit zeigte, dass die CNP-Npr2-cGKI Signalkaskade für die Vergabelung der Axone entscheidend ist. Es bleibt unklar, ob ein einzelnes Phosphorylierungssubstrat der cGKI, das allein die Vergabelung veranlässt, besteht, oder ob eher ein Netz von mehreren cGKI-Substraten existiert, um eine Bifurkation auszulösen.

6 REFERENCE LIST

Acebes,A., and Ferrus,A. (2000). Cellular and molecular features of axon collaterals and dendrites. Trends Neurosci. *23*, 557-565.

Akiyama,H., Matsu-ura,T., Mikoshiba,K., and Kamiguchi,H. (2009). Control of neuronal growth cone navigation by asymmetric inositol 1,4,5-trisphosphate signals. Sci. Signal. *2*, ra34.

Aszodi,A., Pfeifer,A., Ahmad,M., Glauner,M., Zhou,X.H., Ny,L., Andersson,K.E., Kehrel,B., Offermanns,S., and Fassler,R. (1999). The vasodilator-stimulated phosphoprotein (VASP) is involved in cGMP- and cAMP-mediated inhibition of agonist-induced platelet aggregation, but is dispensable for smooth muscle function. EMBO J. *18*, 37-48.

Bannister,N.J., and Larkman,A.U. (1995). Dendritic morphology of CA1 pyramidal neurones from the rat hippocampus: I. Branching patterns. J. Comp Neurol. *360*, 150-160.

Betson,M., Lozano,E., Zhang,J., and Braga,V.M. (2002). Rac activation upon cell-cell contact formation is dependent on signalling from the epidermal growth factor receptor. J. Biol. Chem. *277*, 36962-36969.

Boo,Y.C. (2006). Shear stress stimulates phosphorylation of protein kinase A substrate proteins including endothelial nitric oxide synthase in endothelial cells. Exp. Mol. Med. *38*, 63-71.

Breitsprecher,D., Kiesewetter,A.K., Linkner,J., Urbanke,C., Resch,G.P., Small,J.V., and Faix,J. (2008). Clustering of VASP actively drives processive, WH2 domain-mediated actin filament elongation. EMBO J. *27*, 2943-2954.

Brose,K., Bland,K.S., Wang,K.H., Arnott,D., Henzel,W., Goodman,C.S., Tessier-Lavigne,M., and Kidd,T. (1999). Slit proteins bind Robo receptors and have an evolutionarily conserved role in repulsive axon guidance. Cell *96*, 795-806.

Brose,K., and Tessier-Lavigne,M. (2000). Slit proteins: key regulators of axon guidance, axonal branching, and cell migration. Curr. Opin. Neurobiol. *10*, 95-102.

Brown,J., Bidgman,P.C. (2003). Role of Myosin II in axon outgrowth. Histochem Cytochem *51*:421-428.

Brown,M.E., and Bridgman,P.C. (2004). Myosin function in nervous and sensory systems. J. Neurobiol. *58*, 118-130.

Bryan,P.M., Smirnov,D., Smolenski,A., Feil,S., Feil,R., Hofmann,F., Lohmann,S., and Potter,L.R. (2006). A sensitive method for determining the phosphorylation status of natriuretic peptide receptors: cGK-Ialpha does not regulate NPR-A. Biochemistry *45*, 1295-1303.

Butt,E., Abel,K., Krieger,M., Palm,D., Hoppe,V., Hoppe,J., and Walter,U. (1994). cAMP- and cGMP-dependent protein kinase phosphorylation sites of the focal adhesion vasodilator-stimulated phosphoprotein (VASP) in vitro and in intact human platelets. J. Biol. Chem. *269*, 14509-14517.

Cameron,V.A., Aitken,G.D., Ellmers,L.J., Kennedy,M.A., and Espiner,E.A. (1996). The sites of gene expression of atrial, brain, and C-type natriuretic peptides in mouse fetal development: temporal changes in embryos and placenta. Endocrinology *137*, 817-824.

Castellani,V., Chedotal,A., Schachner,M., Faivre-Sarrailh,C., and Rougon,G. (2000). Analysis of the L1-deficient mouse phenotype reveals cross-talk between Sema3A and L1 signalling pathways in axonal guidance. Neuron *27*, 237-249.

Chilton,J.K. (2006). Molecular mechanisms of axon guidance. Dev. Biol. *292*, 13-24.

Chisholm,A., and Tessier-Lavigne,M. (1999). Conservation and divergence of axon guidance mechanisms. Curr. Opin. Neurobiol. *9*, 603-615.

Cohen,P., and Frame,S. (2001). The renaissance of GSK3. Nat. Rev. Mol. Cell Biol. *2*, 769-776.

Conti,M., and Beavo,J. (2007). Biochemistry and physiology of cyclic nucleotide phosphodiesterases: essential components in cyclic nucleotide signalling. Annu. Rev. Biochem. *76*, 481-511.

Dent,E.W., Barnes,A.M., Tang,F., and Kalil,K. (2004). Netrin-1 and semaphorin 3A promote or inhibit cortical axon branching, respectively, by reorganization of the cytoskeleton. J. Neurosci. *24*, 3002-3012.

Dent,E.W., Callaway,J.L., Szebenyi,G., Baas,P.W., and Kalil,K. (1999). Reorganization and movement of microtubules in axonal growth cones and developing interstitial branches. J. Neurosci. *19*, 8894-8908.

Dent,E.W., and Kalil,K. (2001). Axon branching requires interactions between dynamic microtubules and actin filaments. J. Neurosci. *21*, 9757-9769.

Dent,E.W., Tang,F., and Kalil,K. (2003). Axon guidance by growth cones and branches: common cytoskeletal and signalling mechanisms. Neuroscientist. *9*, 343-353.

DiCicco-Bloom,E., Lelievre,V., Zhou,X.,Rodriguez,W.,Tam,J.,Waschek,J.A. (2004). Embryonic expression and multifunctional actions of the natriuretic peptides and receptors in the developing nervous system. Dev Biol. *271(1)*:161-75.

Doble,B.W., and Woodgett,J.R. (2003). GSK-3: tricks of the trade for a multi-tasking kinase. J. Cell Sci. *116*, 1175-1186.

Domek-Lopacinska,K., and Strosznajder,J.B. (2005). Cyclic GMP metabolism and its role in brain physiology. J. Physiol Pharmacol. *56 Suppl 2*, 15-34.

Dostmann,W.R., Nickl,C., Thiel,S., Tsigelny,I., Frank,R., and Tegge,W.J. (1999). Delineation of selective cyclic GMP-dependent protein kinase Ialpha substrate and inhibitor peptides based on combinatorial peptide libraries on paper. Pharmacol. Ther. *82*, 373-387.

Dufresne-Martin,G., Lemay,J.F., Lavigne,P., and Klarskov,K. (2005). Peptide mass fingerprinting by matrix-assisted laser desorption ionization mass spectrometry of proteins detected by immunostaining on nitrocellulose. Proteomics. *5*, 55-66.

Eickholt,B.J., Walsh,F.S., and Doherty,P. (2002). An inactive pool of GSK-3 at the leading edge of growth cones is implicated in Semaphorin 3A signalling. J. Cell Biol. *157*, 211-217.

Erzurumlu,R.S., and Jhaveri,S. (1995). Target influences on the morphology of trigeminal axons. Exp. Neurol. *135*, 1-16.

Fan,D., Bryan,P.M., Antos,L.K., Potthast,R.J., and Potter,L.R. (2005). Down-regulation does not mediate natriuretic peptide-dependent desensitization of natriuretic peptide receptor (NPR)-A or NPR-B: guanylyl cyclase-linked natriuretic peptide receptors do not internalize. Mol. Pharmacol. *67*, 174-183.

Farrar,N.R., Dmetrichuk,J.M., Carlone,R.L., and Spencer,G.E. (2009). A novel, nongenomic mechanism underlies retinoic acid-induced growth cone turning. J. Neurosci. *29*, 14136-14142.

Fedorowicz,G.M., Fry,J.D., Anholt,R.R., and Mackay,T.F. (1998). Epistatic interactions between smell-impaired loci in Drosophila melanogaster. Genetics *148*, 1885-1891.

Feil,R., Hofmann,F., and Kleppisch,T. (2005a). Function of cGMP-dependent protein kinases in the nervous system. Rev. Neurosci. *16*, 23-41.

Feil,R., and Kemp-Harper,B. (2006). cGMP signalling: from bench to bedside. Conference on cGMP generators, effectors and therapeutic implications. EMBO Rep. *7*, 149-153.

Feil,S., Zimmermann,P., Knorn,A., Brummer,S., Schlossmann,J., Hofmann,F., and Feil,R. (2005b). Distribution of cGMP-dependent protein kinase type I and its isoforms in the mouse brain and retina. Neuroscience *135*, 863-868.

Feng,G., Mellor,R.H., Bernstein,M., Keller-Peck,C., Nguyen,Q.T., Wallace,M., Nerbonne,J.M., Lichtman,J.W., and Sanes,J.R. (2000). Imaging neuronal subsets in transgenic mice expressing multiple spectral variants of GFP. Neuron *28*, 41-51.

Fernandez-Novell,J.M., Arino,J., Vilaro,S., and Guinovart,J.J. (1992). Glucose induces the translocation and the aggregation of glycogen synthase in rat hepatocytes. Biochem. J. *281 (Pt 2)*, 443-448.

Ferrarese,A., Marin,O., Bustos,V.H., Venerando,A., Antonelli,M., Allende,J.E., and Pinna,L.A. (2007). Chemical dissection of the APC Repeat 3 multistep phosphorylation by the concerted action of protein kinases CK1 and GSK3. Biochemistry *46*, 11902-11910.

Forget,M.A., Desrosiers,R.R., Gingras,D., and Beliveau,R. (2002). Phosphorylation states of Cdc42 and RhoA regulate their interactions with Rho GDP dissociation inhibitor and their extraction from biological membranes. Biochem. J. *361*, 243-254.

Fu,S.Y., Sharma,K., Luo,Y., Raper,J.A., and Frank,E. (2000). SEMA3A regulates developing sensory projections in the chicken spinal cord. J. Neurobiol. *45*, 227-236.

Gallo,G., Lefcort,F.B., and Letourneau,P.C. (1997). The trkA receptor mediates growth cone turning toward a localized source of nerve growth factor. J. Neurosci. *17*, 5445-5454.

Gallo,G., and Letourneau,P.C. (1998). Localized sources of neurotrophins initiate axon collateral sprouting. J. Neurosci. *18*, 5403-5414.

Gallo,G., and Letourneau,P.C. (1999). Different contributions of microtubule dynamics and transport to the growth of axons and collateral sprouts. J. Neurosci. *19*, 3860-3873.

Garbers,D.L., and Lowe,D.G. (1994). Guanylyl cyclase receptors. J. Biol. Chem. *269*, 30741-30744.

Garrido,J.J., Simon,D., Varea,O., and Wandosell,F. (2007). GSK3 alpha and GSK3 beta are necessary for axon formation. FEBS Lett. *581*, 1579-1586.

Gartner,A., Huang,X., and Hall,A. (2006). Neuronal polarity is regulated by glycogen synthase kinase-3 (GSK-3beta) independently of Akt/PKB serine phosphorylation. J. Cell Sci. *119*, 3927-3934.

Geraldo,S., and Gordon-Weeks,P.R. (2009). Cytoskeletal dynamics in growth-cone steering. J. Cell Sci. *122*, 3595-3604.

Gertler,F.B., Niebuhr,K., Reinhard,M., Wehland,J., and Soriano,P. (1996). Mena, a relative of VASP and Drosophila Enabled, is implicated in the control of microfilament dynamics. Cell *87*, 227-239.

Glass,D.B., and Krebs,E.G. (1979). Comparison of the substrate specificity of adenosine 3':5'-monophosphate- and guanosine 3':5'-monophosphate-dependent protein kinases. Kinetic studies using synthetic peptides corresponding to phosphorylation sites in histone H2B. J. Biol. Chem. *254*, 9728-9738.

Godement,P., Vanselow,J., Thanos,S., and Bonhoeffer,F. (1987). A study in developing visual systems with a new method of staining neurones and their processes in fixed tissue. Development *101*, 697-713.

Goldstein,L.S.B., Fryberg,E.A. (1995). Methods in Cell Biology: Drosophila Melanogaster: Practical Uses in Cell and Molecular Biology:44. Academic Press Inc.

Guo,D., Tan,Y.C., Wang,D., Madhusoodanan,K.S., Zheng,Y., Maack,T., Zhang,J.J., and Huang,X.Y. (2007). A Rac-cGMP Signalling Pathway. Cell *128*, 341-355.

Halbrugge,M., and Walter,U. (1989). Purification of a vasodilator-regulated phosphoprotein from human platelets. Eur. J. Biochem. *185*, 41-50.

Hasegawa,H., Abbott,S., Han,B.X., Qi,Y., and Wang,F. (2007). Analyzing somatosensory axon projections with the sensory neuron-specific Advillin gene. J. Neurosci. *27*, 14404-14414.

Heasman,S.J., and Ridley,A.J. (2008). Mammalian Rho GTPases: new insights into their functions from in vivo studies. Nat. Rev. Mol. Cell Biol. *9*, 690-701.

Herman,J.P., Dolgas,C.M., Rucker,D., and Langub,M.C., Jr. (1996). Localization of natriuretic peptide-activated guanylate cyclase mRNAs in the rat brain. J. Comp Neurol. *369*, 165-187.

Hoeflich,K.P., Luo,J., Rubie,E.A., Tsao,M.S., Jin,O., and Woodgett,J.R. (2000). Requirement for glycogen synthase kinase-3beta in cell survival and NF-kappaB activation. Nature *406*, 86-90.

Hofmann,F. (2005). The biology of cyclic GMP-dependent protein kinases. J. Biol. Chem. *280*, 1-4.

Hofmann,F., Ammendola,A., and Schlossmann,J. (2000). Rising behind NO: cGMP-dependent protein kinases. J. Cell Sci. *113 (Pt 10)*, 1671-1676.

Hofmann,F., Bernhard,D., Lukowski,R., and Weinmeister,P. (2009). cGMP regulated protein kinases (cGK). Handb. Exp. Pharmacol. 137-162.

Hofmann,F., Feil,R., Kleppisch,T., and Schlossmann,J. (2006). Function of cGMP-dependent protein kinases as revealed by gene deletion. Physiol Rev. *86*, 1-23.

Huber,A.B., Kolodkin,A.L., Ginty,D.D., and Cloutier,J.F. (2003). Signalling at the growth cone: ligand-receptor complexes and the control of axon growth and guidance. Annu. Rev. Neurosci. *26*, 509-563.

Imondi,R., and Kaprielian,Z. (2001). Commissural axon pathfinding on the contralateral side of the floor plate: a role for B-class ephrins in specifying the dorsoventral position of longitudinally projecting commissural axons. Development *128*, 4859-4871.

Ishihama,Y., Sato,T., Tabata,T., Miyamoto,N., Sagane,K., Nagasu,T., and Oda,Y. (2005). Quantitative mouse brain proteomics using culture-derived isotope tags as internal standards. Nat. Biotechnol. *23*, 617-621.

Jaffe,A.B., and Hall,A. (2005). Rho GTPases: biochemistry and biology. Annu. Rev. Cell Dev. Biol. *21*, 247-269.

Kalil,K., Szebenyi,G., and Dent,E.W. (2000). Common mechanisms underlying growth cone guidance and axon branching. J. Neurobiol. *44*, 145-158.

Kamiguchi,H., and Lemmon,V. (2000). Recycling of the cell adhesion molecule L1 in axonal growth cones. J. Neurosci. *20*, 3676-3686.

Kawasaki,Y., Kugimiya,F., Chikuda,H., Kamekura,S., Ikeda,T., Kawamura,N., Saito,T., Shinoda,Y., Higashikawa,A., Yano,F., Ogasawara,T., Ogata,N., Hoshi,K., Hofmann,F., Woodgett,J.R., Nakamura,K., Chung,U.I., and Kawaguchi,H. (2008). Phosphorylation of GSK-3beta by cGMP-dependent protein kinase II promotes hypertrophic differentiation of murine chondrocytes. J. Clin. Invest *118*, 2506-2515.

Kidd,T., Brose,K., Mitchell,K.J., Fetter,R.D., Tessier-Lavigne,M., Goodman,C.S., and Tear,G. (1998). Roundabout controls axon crossing of the CNS midline and defines a novel subfamily of evolutionarily conserved guidance receptors. Cell *92*, 205-215.

Kim,W.Y., Zhou,F.Q., Zhou,J., Yokota,Y., Wang,Y.M., Yoshimura,T., Kaibuchi,K., Woodgett,J.R., Anton,E.S., and Snider,W.D. (2006). Essential roles for GSK-3s and GSK-3-primed substrates in neurotrophin-induced and hippocampal axon growth. Neuron *52*, 981-996.

Kitsukawa,T., Shimizu,M., Sanbo,M., Hirata,T., Taniguchi,M., Bekku,Y., Yagi,T., and Fujisawa,H. (1997). Neuropilin-semaphorin III/D-mediated chemorepulsive signals play a crucial role in peripheral nerve projection in mice. Neuron *19*, 995-1005.

Kobialka,M., and Gorczyca,W.A. (2000). Particulate guanylyl cyclases: multiple mechanisms of activation. Acta Biochim. Pol. *47*, 517-528.

Koesling,D., and Friebe,A. (1999). Soluble guanylyl cyclase: structure and regulation. Rev. Physiol Biochem. Pharmacol. *135*, 41-65.

Koller,K.J., Lowe,D.G., Bennett,G.L., Minamino,N., Kangawa,K., Matsuo,H., and Goeddel,D.V. (1991). Selective activation of the B natriuretic peptide receptor by C-type natriuretic peptide (CNP). Science *252*, 120-123.

Kornack,D.R., and Giger,R.J. (2005). Probing microtubule +TIPs: regulation of axon branching. Curr. Opin. Neurobiol. *15*, 58-66.

Krause,M., Bear,J.E., Loureiro,J.J., and Gertler,F.B. (2002). The Ena/VASP enigma. J. Cell Sci. *115*, 4721-4726.

Krause,M., Dent,E.W., Bear,J.E., Loureiro,J.J., and Gertler,F.B. (2003). Ena/VASP proteins: regulators of the actin cytoskeleton and cell migration. Annu. Rev. Cell Dev. Biol. *19*, 541-564.

Krijgsveld,J., Ketting,R.F., Mahmoudi,T., Johansen,J., Artal-Sanz,M., Verrijzer,C.P., Plasterk,R.H., and Heck,A.J. (2003). Metabolic labeling of C. elegans and D. melanogaster for quantitative proteomics. Nat. Biotechnol. *21*, 927-931.

Kwiatkowski,A.V., Gertler,F.B., and Loureiro,J.J. (2003). Function and regulation of Ena/VASP proteins. Trends Cell Biol. *13*, 386-392.

Kwiatkowski,A.V., Rubinson,D.A., Dent,E.W., Edward,v., V, Leslie,J.D., Zhang,J., Mebane,L.M., Philippar,U., Pinheiro,E.M., Burds,A.A., Bronson,R.T., Mori,S., Fassler,R., and Gertler,F.B. (2007). Ena/VASP Is Required for neuritogenesis in the developing cortex. Neuron *56*, 441-455.

Laemmli,U.K. (1970). Cleavage of structural proteins during the assembly of the head of bacteriophage T4. Nature *227*, 680-685.

Lang,P., Gesbert,F., Delespine-Carmagnat,M., Stancou,R., Pouchelet,M., and Bertoglio,J. (1996). Protein kinase A phosphorylation of RhoA mediates the morphological and functional effects of cyclic AMP in cytotoxic lymphocytes. EMBO J. *15*, 510-519.

Lanier,L.M., Gates,M.A., Witke,W., Menzies,A.S., Wehman,A.M., Macklis,J.D., Kwiatkowski,D., Soriano,P., and Gertler,F.B. (1999). Mena is required for neurulation and commissure formation. Neuron *22*, 313-325.

Larkman,A.U. (1991). Dendritic morphology of pyramidal neurones of the visual cortex of the rat: I. Branching patterns. J. Comp Neurol. *306*, 307-319.

Lebrand,C., Dent,E.W., Strasser,G.A., Lanier,L.M., Krause,M., Svitkina,T.M., Borisy,G.G., and Gertler,F.B. (2004). Critical role of Ena/VASP proteins for filopodia formation in neurons and in function downstream of netrin-1. Neuron *42*, 37-49.

Lin,C.H., Espreafico,E.M., Mooseker,M.S., Forscher,P. (1996). Myosin drives retrograde F-actin flow in neuronal growth cones. Neuron *16*:769-782.

Lin,A.C., and Holt,C.E. (2007). Local translation and directional steering in axons. EMBO J. *26*, 3729-3736.

Linseman,D.A., and Loucks,F.A. (2008). Diverse roles of Rho family GTPases in neuronal development, survival, and death. Front Biosci. *13*, 657-676.

Lohmann,S.M., Vaandrager,A.B., Smolenski,A., Walter,U., and De Jonge,H.R. (1997). Distinct and specific functions of cGMP-dependent protein kinases. Trends Biochem. Sci. *22*, 307-312.

Lontay,B., Kiss,A., Gergely,P., Hartshorne,D.J., and Erdodi,F. (2005). Okadaic acid induces phosphorylation and translocation of myosin phosphatase target subunit 1 influencing myosin phosphorylation, stress fiber assembly and cell migration in HepG2 cells. Cell Signal. *17*, 1265-1275.

Lucas,K.A., Pitari,G.M., Kazerounian,S., Ruiz-Stewart,I., Park,J., Schulz,S., Chepenik,K.P., and Waldman,S.A. (2000). Guanylyl cyclases and signalling by cyclic GMP. Pharmacol. Rev. *52*, 375-414.

Luque-Garcia,J.L., Zhou,G., Spellman,D.S., Sun,T.T., and Neubert,T.A. (2008). Analysis of electroblotted proteins by mass spectrometry: protein identification after Western blotting. Mol. Cell Proteomics. *7*, 308-314.

Luque-Garcia,J.L., Zhou,G., Sun,T.T., and Neubert,T.A. (2006). Use of nitrocellulose membranes for protein characterization by matrix-assisted laser desorption/ionization mass spectrometry. Anal. Chem. *78*, 5102-5108.

Ma,L., and Tessier-Lavigne,M. (2007). Dual branch-promoting and branch-repelling actions of Slit/Robo signalling on peripheral and central branches of developing sensory axons. J. Neurosci. *27*, 6843-6851.

Maness,P.F., and Schachner,M. (2007). Neural recognition molecules of the immunoglobulin superfamily: signalling transducers of axon guidance and neuronal migration. Nat. Neurosci. *10*, 19-26.

Manning,B.D., Tee,A.R., Logsdon,M.N., Blenis,J., and Cantley,L.C. (2002). Identification of the tuberous sclerosis complex-2 tumor suppressor gene product tuberin as a target of the phosphoinositide 3-kinase/akt pathway. Mol. Cell *10*, 151-162.

Masuda,T., Sakuma,C., Taniguchi,M., Kobayashi,K., Kobayashi,K., Shiga,T., and Yaginuma,H. (2007). Guidance cues from the embryonic dorsal spinal cord chemoattract dorsal root ganglion axons. Neuroreport *18*, 1645-1649.

Masuda,T., Watanabe,K., Sakuma,C., Ikenaka,K., Ono,K., and Yaginuma,H. (2008). Netrin-1 acts as a repulsive guidance cue for sensory axonal projections toward the spinal cord. J. Neurosci. *28*, 10380-10385.

McManus,E.J., Sakamoto,K., Armit,L.J., Ronaldson,L., Shpiro,N., Marquez,R., and Alessi,D.R. (2005). Role that phosphorylation of GSK3 plays in insulin and Wnt signalling defined by knockin analysis. EMBO J. *24*, 1571-1583.

Medeiros,N.A., Burnette,D.T., Forscher,P. (2006). Myosin II functions in actin-bundle turnover in neuronal growth cones. Nat Cell Biol *8*:215-226.

Menniti,F.S., Faraci,W.S., and Schmidt,C.J. (2006). Phosphodiesterases in the CNS: targets for drug development. Nat. Rev. Drug Discov. *5*, 660-670.

Menzies,A.S., Aszodi,A., Williams,S.E., Pfeifer,A., Wehman,A.M., Goh,K.L., Mason,C.A., Fassler,R., and Gertler,F.B. (2004). Mena and vasodilator-stimulated phosphoprotein are required for multiple actin-dependent processes that shape the vertebrate nervous system. J. Neurosci. *24*, 8029-8038.

Metodiev,M.V., Timanova,A., and Stone,D.E. (2004). Differential phosphoproteome profiling by affinity capture and tandem matrix-assisted laser desorption/ionization mass spectrometry. Proteomics. *4*, 1433-1438.

Morandell,S., Stasyk,T., Grosstessner-Hain,K., Roitinger,E., Mechtler,K., Bonn,G.K., and Huber,L.A. (2006). Phosphoproteomics strategies for the functional analysis of signal transduction. Proteomics. *6*, 4047-4056.

Müller,C.C. Analyse der Bildung von T-förmigen Verzweigungen bei sensorischen axonen in einem in vitro Kultursystem. Diplomarbeit . 2002.

Nguyen Ba-Charvet,K.T., Brose,K., Ma,L., Wang,K.H., Marillat,V., Sotelo,C., Tessier-Lavigne,M., and Chedotal,A. (2001). Diversity and specificity of actions of Slit2 proteolytic fragments in axon guidance. J. Neurosci. *21*, 4281-4289.

Nguyen-Ba-Charvet,K.T., Brose,K., Marillat,V., Sotelo,C., Tessier-Lavigne,M., and Chedotal,A. (2001). Sensory axon response to substrate-bound Slit2 is modulated by laminin and cyclic GMP. Mol. Cell Neurosci. *17*, 1048-1058.

Nielsen,J.N., Derave,W., Kristiansen,S., Ralston,E., Ploug,T., and Richter,E.A. (2001). Glycogen synthase localization and activity in rat skeletal muscle is strongly dependent on glycogen content. J. Physiol *531*, 757-769.

Nisbet,A.D., Saundry,R.H., Moir,A.J., Fothergill,L.A., and Fothergill,J.E. (1981). The complete amino-acid sequence of hen ovalbumin. Eur. J. Biochem. *115*, 335-345.

O'Leary,D.D., and Terashima,T. (1988). Cortical axons branch to multiple subcortical targets by interstitial axon budding: implications for target recognition and "waiting periods". Neuron *1*, 901-910.

Omori,K., and Kotera,J. (2007). Overview of PDEs and their regulation. Circ. Res. *100*, 309-327.

Ono,S., Yamakita,Y., Yamashiro,S., Matsudaira,P.T., Gnarra,J.R., Obinata,T., and Matsumura,F. (1997). Identification of an actin binding region and a protein kinase C phosphorylation site on human fascin. J. Biol. Chem. *272*, 2527-2533.

Ozaki,S., and Snider,W.D. (1997). Initial trajectories of sensory axons toward laminar targets in the developing mouse spinal cord. J. Comp Neurol. *380*, 215-229.

Ozdinler,P.H., and Erzurumlu,R.S. (2001). Regulation of neurotrophin-induced axonal responses via Rho GTPases. J. Comp Neurol. *438*, 377-387.

Pandey,K.N., Nguyen,H.T., Garg,R., Khurana,M.L., and Fink,J. (2005). Internalization and trafficking of guanylyl (guanylate) cyclase/natriuretic peptide receptor A is regulated by an acidic tyrosine-based cytoplasmic motif GDAY. Biochem. J. *388*, 103-113.

Pandey,K.N., Nguyen,H.T., Sharma,G.D., Shi,S.J., and Kriegel,A.M. (2002). Ligand-regulated internalization, trafficking, and down-regulation of guanylyl cyclase/atrial natriuretic peptide receptor-A in human embryonic kidney 293 cells. J. Biol. Chem. *277*, 4618-4627.

Pfeifer,A., Klatt,P., Massberg,S., Ny,L., Sausbier,M., Hirneiss,C., Wang,G.X., Korth,M., Aszodi,A., Andersson,K.E., Krombach,F., Mayerhofer,A., Ruth,P., Fassler,R., and Hofmann,F. (1998). Defective smooth muscle regulation in cGMP kinase I-deficient mice. EMBO J. *17*, 3045-3051.

Portera-Cailliau,C., Weimer,R.M., De,P., V, Caroni,P., and Svoboda,K. (2005). Diverse modes of axon elaboration in the developing neocortex. PLoS. Biol. *3*, e272.

Potter,L.R. (2005). Domain analysis of human transmembrane guanylyl cyclase receptors: implications for regulation. Front Biosci. *10*, 1205-1220.

Potter,L.R., Abbey-Hosch,S., and Dickey,D.M. (2006). Natriuretic peptides, their receptors, and cyclic guanosine monophosphate-dependent signalling functions. Endocr. Rev. *27*, 47-72.

Potter,L.R., and Hunter,T. (1998). Identification and characterization of the major phosphorylation sites of the B-type natriuretic peptide receptor. J. Biol. Chem. *273*, 15533-15539.

Potter,L.R., and Hunter,T. (1999). Identification and characterization of the phosphorylation sites of the guanylyl cyclase-linked natriuretic peptide receptors A and B. Methods *19*, 506-520.

Potter,L.R., and Hunter,T. (2001). Guanylyl cyclase-linked natriuretic peptide receptors: structure and regulation. J. Biol. Chem. *276*, 6057-6060.

Puschel,A.W., Adams,R.H., and Betz,H. (1996). The sensory innervation of the mouse spinal cord may be patterned by differential expression of and differential responsiveness to semaphorins. Mol. Cell Neurosci. *7*, 419-431.

Qiao,J., Holian,O., Lee,B.S., Huang,F., Zhang,J., and Lum,H. (2008). Phosphorylation of GTP dissociation inhibitor by PKA negatively regulates RhoA. Am. J. Physiol Cell Physiol *295*, C1161-C1168.

Qiao,J., Huang,F., and Lum,H. (2003). PKA inhibits RhoA activation: a protection mechanism against endothelial barrier dysfunction. Am. J. Physiol Lung Cell Mol. Physiol *284*, L972-L980.

Reinders,J., and Sickmann,A. (2005). State-of-the-art in phosphoproteomics. Proteomics. *5*, 4052-4061.

Rodriguez,O.C., Schaefer,A.W., Mandato,C.A., Forscher,P., Bement,W.M., and Waterman-Storer,C.M. (2003). Conserved microtubule-actin interactions in cell movement and morphogenesis. Nat. Cell Biol. *5*, 599-609.

Salin,P., Tseng,G.F., Hoffman,S., Parada,I., and Prince,D.A. (1995). Axonal sprouting in layer V pyramidal neurons of chronically injured cerebral cortex. J. Neurosci. *15*, 8234-8245.

Sauzeau,V., Le Jeune,H., Cario-Toumaniantz,C., Smolenski,A., Lohmann,S.M., Bertoglio,J., Chardin,P., Pacaud,P., and Loirand,G. (2000). Cyclic GMP-dependent protein kinase signalling pathway inhibits RhoA-induced Ca2+ sensitization of contraction in vascular smooth muscle. J. Biol. Chem. *275*, 21722-21729.

Sauzeau,V., Rolli-Derkinderen,M., Marionneau,C., Loirand,G., and Pacaud,P. (2003). RhoA expression is controlled by nitric oxide through cGMP-dependent protein kinase activation. J. Biol. Chem. *278*, 9472-9480.

Sawada,N., Itoh,H., Miyashita,K., Tsujimoto,H., Sone,M., Yamahara,K., Arany,Z.P., Hofmann,F., and Nakao,K. (2009). Cyclic GMP kinase and RhoA Ser188 phosphorylation integrate pro- and antifibrotic signals in blood vessels. Mol. Cell Biol. *29*, 6018-6032.

Sawada,N., Itoh,H., Yamashita,J., Doi,K., Inoue,M., Masatsugu,K., Fukunaga,Y., Sakaguchi,S., Sone,M., Yamahara,K., Yurugi,T., and Nakao,K. (2001). cGMP-dependent protein kinase phosphorylates and inactivates RhoA. Biochem. Biophys. Res. Commun. *280*, 798-805.

Schäffer,S. (2006). Untersuchungen zur Funktion der cGMP-abhängigen Kinase I alpha während der Entwicklung des Nervensystems. Dissertation.

Schambra,U.B., Silver,J., and Lauder,J.M. (1991). An atlas of the prenatal mouse brain: gestational day 14. Exp. Neurol. *114*, 145-183.

Schlossmann,J., Ammendola,A., Ashman,K., Zong,X., Huber,A., Neubauer,G., Wang,G.X., Allescher,H.D., Korth,M., Wilm,M., Hofmann,F., and Ruth,P. (2000). Regulation of intracellular calcium by a signalling complex of IRAG, IP3 receptor and cGMP kinase Ibeta. Nature *404*, 197-201.

Schlossmann,J., and Desch,M. (2009). cGK substrates. Handb. Exp. Pharmacol. 163-193.

Schmidt,H., Stonkute,A., Juttner,R., Koesling,D., Friebe,A., and Rathjen,F.G. (2009). C-type natriuretic peptide (CNP) is a bifurcation factor for sensory neurons. Proc. Natl. Acad. Sci. U. S. A *106*, 16847-16852.

Schmidt,H., Stonkute,A., Juttner,R., Schaffer,S., Buttgereit,J., Feil,R., Hofmann,F., and Rathjen,F.G. (2007). The receptor guanylyl cyclase Npr2 is essential for sensory axon bifurcation within the spinal cord. J. Cell Biol. *179*, 331-340.

Schmidt,H., Werner,M., Heppenstall,P.A., Henning,M., More,M.I., Kuhbandner,S., Lewin,G.R., Hofmann,F., Feil,R., and Rathjen,F.G. (2002). cGMP-mediated signalling via cGKIalpha is required for the guidance and connectivity of sensory axons. J. Cell Biol. *159*, 489-498.

Schmidtko,A., Gao,W., Konig,P., Heine,S., Motterlini,R., Ruth,P., Schlossmann,J., Koesling,D., Niederberger,E., Tegeder,I., Friebe,A., and Geisslinger,G. (2008a). cGMP produced by NO-sensitive guanylyl cyclase essentially contributes to inflammatory and neuropathic pain by using targets different from cGMP-dependent protein kinase I. J. Neurosci. *28*, 8568-8576.

Schmidtko,A., Gao,W., Sausbier,M., Rauhmeier,I., Sausbier,U., Niederberger,E., Scholich,K., Huber,A., Neuhuber,W., Allescher,H.D., Hofmann,F., Tegeder,I., Ruth,P., and Geisslinger,G. (2008b). Cysteine-rich protein 2, a novel downstream effector of cGMP/cGMP-dependent protein kinase I-mediated persistent inflammatory pain. J. Neurosci. *28*, 1320-1330.

Schmidtko,A., Tegeder,I., and Geisslinger,G. (2009). No NO, no pain? The role of nitric oxide and cGMP in spinal pain processing. Trends Neurosci.

Seiferth,K. (2008). Analyse der Expression von cGMP-spezifischen Phosphodiesterasen in embryonalen Spinalganglien und Rückenmark. Diplomarbeit.

Serafini,T., Colamarino,S.A., Leonardo,E.D., Wang,H., Beddington,R., Skarnes,W.C., and Tessier-Lavigne,M. (1996). Netrin-1 is required for commissural axon guidance in the developing vertebrate nervous system. Cell *87*, 1001-1014.

Sharma,K., and Frank,E. (1998). Sensory axons are guided by local cues in the developing dorsal spinal cord. Development *125*, 635-643.

Shepherd,I.T., Luo,Y., Lefcort,F., Reichardt,L.F., and Raper,J.A. (1997) A sensory axon repellent secreted from ventral aspinal cord explants is neutralized by antibodies raised against collapsin-1. Development *124,* 1377-1385.

Shimada,T., Toriyama,M., Uemura,K., Kamiguchi,H., Sugiura,T., Watanabe,N., and Inagaki,N. (2008). Shootin1 interacts with actin retrograde flow and L1-CAM to promote axon outgrowth. J. Cell Biol. *181*, 817-829.

Shiokawa,S., Sakai,K., Akimoto,Y., Suzuki,N., Hanashi,H., Nagamatsu,S., Iwashita,M., Nakamura,Y., Hirano,H., and Yoshimura,Y. (2000). Function of the small guanosine triphosphate-binding protein RhoA in the process of implantation. J. Clin. Endocrinol. Metab *85*, 4742-4749.

Song,H., Ming,G., He,Z., Lehmann,M., McKerracher,L., Tessier-Lavigne,M., and Poo,M. (1998). Conversion of neuronal growth cone responses from repulsion to attraction by cyclic nucleotides. Science *281*, 1515-1518.

Song,H.J., and Poo,M.M. (1999). Signal transduction underlying growth cone guidance by diffusible factors. Curr. Opin. Neurobiol. *9*, 355-363.

Spruston,N. (2008). Pyramidal neurons: dendritic structure and synaptic integration. Nat. Rev. Neurosci. *9*, 206-221.

Steinberg,T.H., Agnew,B.J., Gee,K.R., Leung,W.Y., Goodman,T., Schulenberg,B., Hendrickson,J., Beechem,J.M., Haugland,R.P., and Patton,W.F. (2003). Global quantitative phosphoprotein analysis using Multiplexed Proteomics technology. Proteomics. *3*, 1128-1144.

Surks,H.K., Mochizuki,N., Kasai,Y., Georgescu,S.P., Tang,K.M., Ito,M., Lincoln,T.M., and Mendelsohn,M.E. (1999). Regulation of myosin phosphatase by a specific interaction with cGMP- dependent protein kinase Ialpha. Science *286*, 1583-1587.

Suter,D.M., and Forscher,P. (1998). An emerging link between cytoskeletal dynamics and cell adhesion molecules in growth cone guidance. Curr. Opin. Neurobiol. *8*, 106-116.

Szebenyi,G., Callaway,J.L., Dent,E.W., and Kalil,K. (1998). Interstitial branches develop from active regions of the axon demarcated by the primary growth cone during pausing behaviors. J. Neurosci. *18*, 7930-7940.

Taniguchi,M., Yuasa,S., Fujisawa,H., Naruse,I., Saga,S., Mishina,M., and Yagi,T. (1997). Disruption of semaphorin III/D gene causes severe abnormality in peripheral nerve projection. Neuron *19*, 519-530.

Taylor,A.J., Ye,J.M., and Schmitz-Peiffer,C. (2006). Inhibition of glycogen synthesis by increased lipid availability is associated with subcellular redistribution of glycogen synthase. J. Endocrinol. *188*, 11-23.

Tegeder,I., Del Turco,D., Schmidtko,A., Sausbier,M., Feil,R., Hofmann,F., Deller,T., Ruth,P., and Geisslinger,G. (2004). Reduced inflammatory hyperalgesia with preservation of acute thermal nociception in mice lacking cGMP-dependent protein kinase I. Proc. Natl. Acad. Sci. U. S. A *101*, 3253-3257.

Tegge,W., Frank,R., Hofmann,F., and Dostmann,W.R. (1995). Determination of cyclic nucleotide-dependent protein kinase substrate specificity by the use of peptide libraries on cellulose paper. Biochemistry *34*, 10569-10577.

Tessier-Lavigne,M., and Goodman,C.S. (1996). The molecular biology of axon guidance. Science *274*, 1123-1133.

Tojima,T., Akiyama,H., Itofusa,R., Li,Y., Katayama,H., Miyawaki,A., and Kamiguchi,H. (2007). Attractive axon guidance involves asymmetric membrane transport and exocytosis in the growth cone. Nat. Neurosci. *10*, 58-66.

Tsuji,T., Kondo,E., Yasoda,A., Inamoto,M., Kiyosu,C., Nakao,K., and Kunieda,T. (2008). Hypomorphic mutation in mouse Nppc gene causes retarded bone growth due to impaired endochondral ossification. Biochem. Biophys. Res. Commun. *376*, 186-190.

Tsuji,T., and Kunieda,T. (2005). A loss-of-function mutation in natriuretic peptide receptor 2 (Npr2) gene is responsible for disproportionate dwarfism in cn/cn mouse. J. Biol. Chem. *280*, 14288-14292.

Ulupinar,E., Datwani,A., Behar,O., Fujisawa,H., and Erzurumlu,R. (1999). Role of semaphorin III in the developing rodent trigeminal system. Mol. Cell Neurosci. *13*, 281-292.

Ulupinar,E., Jacquin,M.F., and Erzurumlu,R.S. (2000). Differential effects of NGF and NT-3 on embryonic trigeminal axon growth patterns. J. Comp Neurol. *425*, 202-218.

Vaandrager,A.B., Hogema,B.M., and De Jonge,H.R. (2005). Molecular properties and biological functions of cGMP-dependent protein kinase II. Front Biosci. *10*, 2150-2164.

Valtcheva,N., Nestorov,P., Beck,A., Russwurm,M., Hillenbrand,M., Weinmeister,P., and Feil,R. (2009). The commonly used cGMP-dependent protein kinase type I (cGKI) inhibitor Rp-8-Br-PET-cGMPS can activate cGKI in vitro and in intact cells. J. Biol. Chem. *284*, 556-562.

Van Horck,F.P., and Holt,C.E. (2008). A cytoskeletal platform for local translation in axons. Sci. Signal. *1*, e11.

Vercelli,A., Repici,M., Garbossa,D., and Grimaldi,A. (2000). Recent techniques for tracing pathways in the central nervous system of developing and adult mammals. Brain Res. Bull. *51*, 11-28.

Wang,K.H., Brose,K., Arnott,D., Kidd,T., Goodman,C.S., Henzel,W., and Tessier-Lavigne,M. (1999). Biochemical purification of a mammalian slit protein as a positive regulator of sensory axon elongation and branching. Cell *96*, 771-784.

Wang,X., and Robinson,P.J. (1997). Cyclic GMP-dependent protein kinase and cellular signalling in the nervous system. J. Neurochem. *68*, 443-456.

Watanabe,K., Tamamaki,N., Furuta,T., Ackerman,S.L., Ikenaka,K., and Ono,K. (2006). Dorsally derived netrin 1 provides an inhibitory cue and elaborates the 'waiting period' for primary sensory axons in the developing spinal cord. Development *133*, 1379-1387.

Wegener,J.W., Nawrath,H., Wolfsgruber,W., Kuhbandner,S., Werner,C., Hofmann,F., and Feil,R. (2002). cGMP-dependent protein kinase I mediates the negative inotropic effect of cGMP in the murine myocardium. Circ. Res. *90*, 18-20.

Wessel,D., and Flugge,U.I. (1984). A method for the quantitative recovery of protein in dilute solution in the presence of detergents and lipids. Anal. Biochem. *138*, 141-143.

Wolschin,F., and Weckwerth,W. (2005). Combining metal oxide affinity chromatography (MOAC) and selective mass spectrometry for robust identification of in vivo protein phosphorylation sites. Plant Methods *1*, 9.

Wolschin,F., Wienkoop,S., and Weckwerth,W. (2005). Enrichment of phosphorylated proteins and peptides from complex mixtures using metal oxide/hydroxide affinity chromatography (MOAC). Proteomics. *5*, 4389-4397.

Wu,C., Wu,F., Pan,J., Morser,J., and Wu,Q. (2003). Furin-mediated processing of Pro-C-type natriuretic peptide. J. Biol. Chem. *278*, 25847-25852.

Wu,C.C., and Maccoss,M.J. (2007). Quantitative proteomic analysis of mammalian organisms using metabolically labelled tissues. Methods Mol. Biol. *359*, 191-201.

Wu,C.C., Maccoss,M.J., Howell,K.E., Matthews,D.E., and Yates,J.R., III (2004). Metabolic labeling of mammalian organisms with stable isotopes for quantitative proteomic analysis. Anal. Chem. *76*, 4951-4959.

Wu,K.Y., Hengst,U., Cox,L.J., Macosko,E.Z., Jeromin,A., Urquhart,E.R., and Jaffrey,S.R. (2005). Local translation of RhoA regulates growth cone collapse. Nature *436*, 1020-1024.

Yoder,A.R., Kruse,A.C., Earhart,C.A., Ohlendorf,D.H., and Potter,L.R. (2008). Reduced ability of C-type natriuretic peptide (CNP) to activate natriuretic peptide receptor B (NPR-B) causes dwarfism in lbab -/- mice. Peptides *29*, 1575-1581.

Yoshimura,T., Kawano,Y., Arimura,N., Kawabata,S., Kikuchi,A., and Kaibuchi,K. (2005). GSK-3beta regulates phosphorylation of CRMP-2 and neuronal polarity. Cell *120*, 137-149.

Zaccolo,M., and Movsesian,M.A. (2007). cAMP and cGMP signalling cross-talk: role of phosphodiesterases and implications for cardiac pathophysiology. Circ. Res. *100*, 1569-1578.

Zhao,Z., and Ma,L. (2009). Regulation of axonal development by natriuretic peptide hormones. Proc. Natl. Acad. Sci. U. S. A.

Zhao,Z., Wang,Z., Gu,Y., Feil,R., Hofmann,F., and Ma,L. (2009). Regulate axon branching by the cyclic GMP pathway via inhibition of glycogen synthase kinase 3 in dorsal root ganglion sensory neurons. J. Neurosci. *29*, 1350-1360.

Zhou,F.Q., and Cohan,C.S. (2004). How actin filaments and microtubules steer growth cones to their targets. J. Neurobiol. *58*, 84-91.

Zhou,F.Q., Waterman-Storer,C.M., and Cohan,C.S. (2002). Focal loss of actin bundles causes microtubule redistribution and growth cone turning. J. Cell Biol. *157*, 839-849.

Zhou,F.Q., Zhou,J., Dedhar,S., Wu,Y.H., and Snider,W.D. (2004). NGF-induced axon growth is mediated by localized inactivation of GSK-3beta and functions of the microtubule plus end binding protein APC. Neuron *42*, 897-912.

7 APPENDIX

Table 1: Proteins of cytoplasmatic fraction of F11 cells, detected by mass spectrometry analysis of a one-dimensional SDS-PAGE gel band.

Accession No.	Protein
Q7TMM9	Tubulin beta-2A chain
A7E3N2	Neutrophil cytosol factor 2
O08651	D-3-phosphoglycerate dehydrogenase
P04797	Glyceraldehyde-3-phosphate dehydrogenase
P05213	Tubulin alpha-1B chain
P06745	Glucose-6-phosphate isomerase
P10126	Elongation factor 1-alpha 1
P15429	Beta-enolase
P17182	Alpha-enolase
P18298	S adenosylmethionine synthetase isoform type 2
P18418	Calreticulin precursor
P19324	Serpin H1 precursor
P20673	Argininosuccinate lyase
P34058	Heat shock protein HSP 90 beta
P36269	Actin gamma enteric smooth muscle
P50399	Rab GDP dissociation inhibitor beta
P50503	Hsc70 interacting protein
P50580	Proliferation-associated protein 2G4
P60123	RuvB-like 1
P60711	Actin cytoplasmic 1
P61203	COP9 signalosome complex subunit 2
P62738	Actin aortic smooth muscle
P62960	Nuclease-sensitive element-binding protein 1
P63259	Actin cytoplasmic 2
P68136	Actin alpha sceletal muscle 1
P68369	Tubulin alpha-1A chain
P68372	Tubulin beta-2C chain
P80313	T-complex protein 1 subunit eta
P80315	T-complex protein 1 subunit delta
P85108	Tubulin beta 2A chain
P99024	Tubulin beta-5 chain
Q30A01	Gaba B receptor interacting scaffolding protein
Q32PX5	Smc4I1 protein
Q3B8Q2	Similar to DEAD Asp Glu Ala Asp box polypeptide 48
Q3KRE8	Tubulin beta 2B chain
Q4KM87	Actin like 6A
Q4QRB8	Dead end homolog 1
Q5RKI1	Eukaryotic initiation factor 4A-II
Q5XIC6	Proteasome prosome macropain 26S subunit non ATPase 12
Q5XIF6	Tubulin alpha 4A chain
Q5XIM9	T-complex protein 1 subunit beta
Q63170	Dynein heavy chain 7, axonemal
Q63570	26S protease regulatory subunit 6B
Q641X8	Eukaryotic translation initiation factor 3 subunit E
Q68FR6	Elongation factor 1 gamma

Q68FR8	Tubulin alpha-3 chain
Q6AXS5	Plasminogen activator inhibitor 1 RNA-binding protein
Q6AY56	Tubulin alpha 8 chain
Q6AYT3	UPF0027 protein C22orf28 homolog
Q6AYZ1	Tubulin alpha-1C chain
Q6P3V8	Eukaryotic initiation factor 4A-I
Q6Q0N1	Cytosolic non-specific dipeptidase
Q78ZA7	Nucleosome assembly protein 1-like 1
Q794E4	Heterogeneous nuclear ribonucleoprotein F
Q80TB8	Oxidoreductase KIAA1576
Q91YI0	Argininosuccinate lyase
Q922F4	Tubulin beta-6 chain
Q922R8	Protein disulfide-isomerase A6 precursor
Q99JY9	Actin-related protein 3
Q99K48	Non-POU domain-containing octamer-binding protein
Q9CZ30	Obg-like ATPase 1
Q9D6F9	Tubulin beta-4 chain
Q9D8N0	Elongation factor 1-gamma
Q9DCD0	6-phosphogluconate dehydrogenase, decarboxylating
Q9ERD7	Tubulin beta-3 chain

Table 2: Proteins of postnuclear fraction of F11 cells, detected by mass spectrometry analysis of a two-dimensional SDS-PAGE gel spot.

Accession No.	Protein
A1L113	Keratin 1
A1L317	Keratin, type I cytoskeletal 24
A2A4L8	MCG15366, isoform CRA_c
A2A513	Keratin 10
A2A5N1	Tyrosine 3-monooxygenase/tryptophan 5-monooxygenase activation protein, beta
A2A875	Retinoblastoma binding protein 4 (Retinoblastoma binding protein 4, isoform CRA_a)
A2AFI9	Retinoblastoma binding protein 7
A2AFJ0	Retinoblastoma binding protein 7
A2AFR8	Seryl-aminoacyl-tRNA synthetase
A2AQ07	Tubulin, beta 1 (MCG9966)
A2AWQ3	Regulator of chromosome condensation 2
A2BDV8	MOUSE Heterogeneous nuclear ribonucleoprotein H2
A2RSB1	Nucleosome assembly protein 1-like 4
A3KML3	Tyrosine 3-monooxygenase/tryptophan 5-monooxygenase activation protein, theta polypeptide
A8IP69	14-3-3 protein gamma subtype
B0K024	Aamp protein (Fragment)
B1AQ76	Keratin 13
B1B178	Tubulin, beta 5
B1WBN9	Pyruvate kinase, liver and red blood cell
B2CY77	Laminin receptor (Fragment)
B2MWM9	Calreticulin
B2RQH6	Keratin 75
B2RRE2	Myo18a protein
B2RRT9	Zinc finger, RAN-binding domain containing 2 (Zinc finger, RAN-binding domain containing 2, isoform CRA_a)
B2RRX1	Actin, beta (Actin, beta, cytoplasmic)
B2RSN3	Tubulin, beta 2b

B2RTP7	Krt2 protein
B2RYG4	Kptn protein (Kaptin (Actin binding protein) (Predicted), isoform CRA_a)
B4F7C2	Tubulin, beta 4 (RCG45085)
B5DEI1	Putative uncharacterized protein
O08651	D-3-phosphoglycerate dehydrogenase
P00762	Anionic trypsin-1
P04104	Keratin, type II cytoskeletal 1
P10719	ATP synthase subunit beta, mitochondrial
P11598	Protein disulfide-isomerase A3
P11679	Keratin, type II cytoskeletal 8
P11980	Pyruvate kinase isozymes M1/M2
P12369	cAMP-dependent protein kinase type II-beta regulatory subunit
P15331	Peripherin
P24090	Alpha-2-HS-glycoprotein
P31000	Vimentin
P50396	Rab GDP dissociation inhibitor alpha
P50446	Keratin, type II cytoskeletal 6A
P52480	Pyruvate kinase isozymes M1/M2
P63101	14-3-3 protein zeta/delta
P68372	Tubulin beta-2C chain
Q05CH7	Eif5 protein
Q0VDM9	Krt78 protein (Fragment)
Q32P04	Keratin 5
Q3SYP5	Keratin 16
Q3T984	Putative uncharacterized protein
Q3T9L0	Putative uncharacterized protein
Q3TDF8	Putative uncharacterized protein
Q3TEK2	Putative uncharacterized protein
Q3TEU8	Putative uncharacterized protein
Q3TF41	Putative uncharacterized protein
Q3TF72	Putative uncharacterized protein
Q3TFD9	Putative uncharacterized protein
Q3TFG3	Putative uncharacterized protein
Q3THH8	Putative uncharacterized protein
Q3TIA9	Putative uncharacterized protein
Q3TIH8	Putative uncharacterized protein
Q3TII0	T-complex protein 1, delta subunit
Q3TII3	Elongation factor 1-alpha
Q3TIU3	Putative uncharacterized protein
Q3TIZ0	Putative uncharacterized protein
Q3TJ01	Putative uncharacterized protein
Q3TJ52	Putative uncharacterized protein
Q3TJN2	Putative uncharacterized protein
Q3TKC5	Putative uncharacterized protein
Q3TY03	Putative uncharacterized protein
Q3U224	Putative uncharacterized protein
Q3U6S1	Putative uncharacterized protein
Q3U9U3	Putative uncharacterized protein
Q3UBB0	Putative uncharacterized protein
Q3UDC3	Putative uncharacterized protein
Q3UMG4	Putative uncharacterized protein
Q3UMM1	Putative uncharacterized protein
Q3UMP4	Putative uncharacterized protein
Q3UV17	Putative uncharacterized protein
Q3V1K9	Putative uncharacterized protein
Q4FZU2	Keratin, type II cytoskeletal 6A
Q4QQV0	Tubulin, beta 6
Q4QRB4	Tubulin beta-3 chain

Q4R1A4	TRK-fused gene protein
Q542X7	Putative uncharacterized protein
Q5XI13	Glutamate-rich WD repeat-containing protein
Q5XIM9	T-complex protein 1 subunit beta
Q5XJZ3	Grwd1 protein (Fragment)
Q61553	Fascin
Q62418	Drebrin-like protein
Q6IFU7	Keratin, type I cytoskeletal 42
Q6IFX2	Keratin, type II cytoskeletal 4
Q6IFZ4	Type II keratin Kb15
Q6IG03	Keratin, type II cytoskeletal 73
Q6P7S0	Pyruvate kinase
Q6P9V9	Tubulin alpha-1B chain
Q7TMM9	Tubulin beta-2A chain
Q80VP7	Predicted
Q8BFZ3	Beta-actin-like protein 2
Q8BRD3	Putative uncharacterized protein
Q8C0C7	Phenylalanyl-tRNA synthetase alpha chain
Q8K0G5	Protein TSSC1
Q8K1M3	Protein kinase, cAMP dependent regulatory, type II alpha
Q8K3U8	FK506 binding protein 4 (Fragment)
Q8VE88	Protein FAM114A2
Q8VED5	Keratin, type II cytoskeletal 79
Q8VHV7	Heterogeneous nuclear ribonucleoprotein H
Q9CY29	Putative uncharacterized protein
Q9D828	Putative uncharacterized protein
Q9JHL4	Drebrin-like protein
Q9JJD8	Brain cDNA, clone MNCb-1272, similar to Mus musculus chaperonin subunit 2 (beta) (Cct2), mRNA
Q9QWL7	Keratin, type I cytoskeletal 17
Q9R0H5	Keratin, type II cytoskeletal 71
Q9Z2L7	Cytokine receptor-like factor 3

Table 3: Proteins of postnuclear fraction of F11 cells, detected by mass spectrometry analysis of a two-dimensional Western blot membrane.

Accession No.	Protein
A2AAY5	SH3 and PX domain-containing protein 2B
B1B178	Tubulin beta-5 chain
P00762	Anionic trypsin-1
P11679	Keratin, type II cytoskeletal 8
Q0VDM9	Krt78 protein
Q0VDR7	Krt6b protein
Q3SYP5	Keratin 16
Q3TIZ0	4 days pregnant adult female amnion cDNA, RIKEN full-length enriched library, clone:I530027E06 product:tubulin, alpha 6, fullinsert sequence
Q3UV17	Keratin, type II cytoskeletal 2 oral
Q4FZU2	Keratin, type II cytoskeletal 6A
Q6IFZ4	Type II keratin Kb15
Q8C2C1	2 days neonate thymus thymic cells cDNA, RIKEN full-length enriched library, clone:E430030L01 product:hypothetical protein, full insert sequence
Q8R4G6	Alpha-1,6-mannosylglycoprotein 6-beta-N-acetylglucosaminyltransferase A
Q8VED5	Keratin, type II cytoskeletal 79

8 ABBREVIATION LIST

µl	mikroliter
µM	mikromolar
µm	mikrometer
1D	one dimensional
2D	two dimensional
2H3	neurofilament protein
8-pCPTcGMP	8-para-chlorophenylthio-cGMP
AP	alkaline phosphatase
APC	adenomatosis polyposis coli protein
APS	ammonium persulphate
BSA	bovine serum albumine
cAMP	cyclic adenosine-3',5' monophosphate
cGKI	cGMP dependent kinase
cGMP	cyclic guanosine-3',5' monophosphate
CNP	C-type natriuretic peptide
CRMP2	collapsin response mediator protein-2
Cy3	indocarbocynine
DAB	diaminobenzidine
DiI	1,1'-dioctadecyl-3,3,3',3'-tetramethylindocarbocyanine perchlorate
DMSO	dimethylsulfoxid
dNTP	desoxiribonucleoside triphosphate
DREZ	dorsal root entry zone
DRG	dorsal root ganglion (ganglia)
E	embryonic day
ECL	enhanced chemiluminescence
EGF	epidermal growth factor
Ena	Enabled (protein)
EVL	Ena/VASP like (protein)
FGF	fibroblast growth factor
Fig.	figure
g	gravitation force
GC	guanylyl cyclase
GFP	Green fluorescent protein
GSK3	glycogen synthase kinase 3
h	hour
HRP	horseradish peroxidase
HT	heterozygous
IEF	isoelectric focussing
IP	immunoprecipitation
IP3R	inositol 1,4,5-triphosphate receptor
IPG	immobilised pH gradient
kDa	kilodalton (mol. mass)
KO	knock-out
l	liter
lbab	long bone abnormality
Mena	mammalian ena
min	minute
mM	millimolar

MS	mass spectrometry
MW	molecular weight
NGF	nerve growth factor
NO	nitric oxide
Npr2	natriuretic peptide receptor 2
NS	not stimulated
NT-3	neurotrophin-3
^{o}C	degree Celsius
PBS	phosphate buffered saline
PCR	polymerase chain reaction
PDE	phosphodiesterase
PDGF	platelet derived growth factor
pI	isoelectric point
PKA	cAMP dependent kinase, also called protein kinase A
PMSF	phenylmethylsulfonylfluorid
rpm	revolutions per minute
s	second
SDS	sodium dodecyl sulfate
SDS-PAGE	SDS polyacrilamide gel electrophoresis
TEMED	N,N,N,N – tetramethylethydiamine
Tris	tris(hydroxymethyl)-aminomethan
trkA	tropomyosin related kinase A
V	volt
VASP	vasodilatory stimulated protein
W	watt
WT	wild type
YFP	yellow fluorescent protein

9 ACKNOWLEDGMENTS

I would like to thank Prof. Dr. Fritz G. Rathjen for giving me the opportunity to work with his group at the Max Delbrück Center for Molecular Medicine. The friendly and supportive atmosphere in this group helped me during my PhD work. In this context I would like to thank particularly Dr. Hannes Schmidt. Without his support the completion of this dissertation would not have been possible. I am also grateful to Dr. René Jüttner, who introduced me to DiI labelling and with whom I started my PhD work.

I would like to thank my office (ex)colleagues Christopher Patzke, Jadwiga Cholewa-Schreiber, Susanne Schäffer, Katharina Seiferth and my colleague from neighbour office Rogerio Craveiro for scientific conversations and talks about little nothings of life.

A special thank to our technical assistants, Madlen Driesner and Mechthild Henning, who tought me many methods I used in my PhD work.

Apart from my colleagues, I would like to thank my family and friends who have never lost faith in this long-term project.

This work received financial support from the Max Delbrück-Center and Charite.